Breakdown and rejuvenation of aging brain energy metabolism

Polina Shichkova[1*], Jay S. Coggan[1], Elvis Boci[1], Cyrille Pierre Henri Favreau[1], Stefano Maximiliano Antonel[1], Henry Markram[1,2], Daniel Keller[1]

1 Blue Brain Project, École Polytechnique Fédérale de Lausanne, Geneva, Switzerland,

2 Laboratory of Neural Microcircuitry, Brain Mind Institute, École Polytechnique Fédérale de Lausanne, Lausanne, Switzerland

*Correspondence: Polina Shichkova polinashichkova@gmail.com

Highlights

1. (Comprehensive, data-driven molecular model) The study presents a detailed molecular model of the metabolic system in young and old rodent neocortex, examining over 66,000 molecular interactions within neurons, glia, and blood vessels.
2. (Aging impacts action potential generation) Findings show that the aging brain experiences impaired action potential generation, primarily due to compromised functionality of the Na^+/K^+-ATPase and reduced ATP supply.
3. (Loss of metabolic flexibility) The study reveals that the metabolic system loses flexibility as a consequence of aging, hindering its ability to effectively respond to various stimuli.
4. (Strategies for restoring youthful state) Potential strategies for rejuvenating the aged system include supplying specific factors to the blood, increasing the expression of key elements, and blocking detrimental components.
5. (Importance of transcription factors) The analysis underscores the critical role of transcription factors, such as ESRRA, in affecting the function of enzymes and transporters involved in metabolic processes, providing a foundation for future research on age-related changes in brain function and cognitive health.

Abstract

Cognitive impairments and neurodegeneration in aging are linked to disrupted brain energy metabolism. We address this experimentally challenging problem with a computational molecular model that provides mechanistic insights and therapeutic predictions. This model encompasses key enzymes, transporters, metabolites, and other important factors, enabling the investigation of over 66,000 molecular interactions within and across cellular and subcellular compartments of neurons, glia, and blood vessels. During aging, action potential generation is primarily impaired due to reduced expression of the Na^+/K^+-ATPase pump and diminished ATP supply. The metabolic system loses flexibility, hindering its ability to effectively respond to stimuli or adapt to molecular damage. Astrocytes may defer to neuronal energy stability at their own expense. We identified potential strategies for rejuvenating the aged brain including supplying nutritional factors to the blood, increasing the NADH cytosol-mitochondria shuttle capacity and the expression of Na^+/K^+-ATPase. Transcription factor analysis implicated the estrogen related receptor alpha (ESRRA) as having the highest potential impact on aging, suggesting that dysregulated energy metabolism may be a transitional state between healthy aging and neurodegenerative disorders, rather than a hallmark of aging. This high-fidelity model serves as a foundation for future research on aging and cognitive health.

Main

Brain aging mechanisms

Age is a significant risk factor for numerous disorders, including neurodegenerative diseases (Niccoli and Partridge, 2012; Hou et al., 2019). At the core of brain aging lies energy metabolism (López-Otín et al., 2013, 2023; Mattson and Arumugam, 2018). Neuronal signal transduction is energetically demanding, consuming substantial amounts of ATP. This is reflected in the brain's disproportionate oxygen and glucose consumption compared to the rest of the body (Kety, 1957; Mink et al., 1981; Sokoloff, 1996; Rolfe and Brown, 1997). Moreover, metabolic dynamics and neuronal activity are closely linked (Mann et al., 2021), suggesting that age-related changes in one could potentially influence the other.

We developed and simulated a comprehensive data-driven model of the neuro-glial-vascular (NGV) unit metabolism, integrating neuronal firing and blood flow dynamics (Fig. 1). The NGV unit is a combination of the molecules and processes in neuron, astrocyte, blood and the extracellular space. In the model, concentrations of molecules are specified in molar units (mM) and fluxes of reactions and

transport processes are given in molar concentrations per second (mM/second). Volume ratios of the compartments (given in the supplementary model file) are applied for the scaling of cross-compartment processes (e.g., transports or exchanges). We validated the model against existing literature data (Supplementary Fig. 1, Supplementary Table 1). Consistent with recent evidence (Barros, 2022), our model shows that Na^+/K^+ pump ATP use in the astrocyte is comparable with that of the neuron (Figure 3i). In line with previous studies (Bélanger et al., 2011), our quantitative validation revealed that mitochondrial ATP production is higher in neurons (84%). Cytosolic ATP production is slightly more favored in astrocytes (Supplementary Fig. 2) where only 70% of astrocytic ATP is produced by mitochondria (Supplementary Fig. 2). This observation closely matches experimental estimates of 75% (Bouzier-Sore et al., 2006; Barros, 2022).

Alterations in enzyme expression have recently been shown to actively contribute to tissue aging and serve as potential drug targets (Palla et al., 2021). To model aging of NGV metabolism, we used RNA expression fold changes (RNA FCs) from a mouse cell-type specific study (Schaum et al., 2020; Zhang et al., 2021a) as scaling factors for enzyme and transporter concentrations. These concentrations are crucial components of the corresponding reaction/transport rate equations. Notably, succinate dehydrogenase (SDH) is differentially affected by aging in neurons and astrocytes. SDH is a mitochondrial energy nexus and serves as complex II of the mitochondrial electron transport chain (ETC). SDH connects the tricarboxylic acid cycle (TCA) and the ETC. Pre- and post-SDH enzymes of TCA (fumarase and succinate CoA ligase) display opposite fold changes in aged neurons and astrocytes. SDH itself decreases more in aged neurons than in aged astrocytes. In neurons, aging reduces both succinate CoA ligase and SDH, while increasing fumarase. In astrocytes, succinate CoA ligase levels rise during aging (unlike in neurons), SDH experiences a minor decrease, and fumarase levels decline. Overall, the expression of most enzymes decreases with aging in both neurons and astrocytes.

In addition to changes in enzyme and transporter expression, we used published values to adjust arterial glucose, lactate, β-hydroxybutyrate levels, the total NAD (reduced and oxidized) pool, as well as glutamate concentration changes upon synaptic release events (Dong and Brewer, 2019; Cox et al., 2022). To balance the model, we also reduced the NADH shuttle capacity between the cytosol and mitochondria. These aging input factors are summarized in Fig. 2, with further details available in the Methods section. We then simulated system dynamics driven by either synaptic input or current injection and observed numerous age-specific differences consistent with prior reports (Supplementary Table 1).

Aging affects metabolite levels both at rest and upon stimulation.

The simulated aging phenotype exhibits distinct resting state metabolite concentrations. The response of these concentrations to stimuli (Fig. 3c, d, Supplementary Fig. 3, 4, 5d, 6a) also differs. Interestingly, aging-associated changes in metabolic responses to stimuli of varying amplitudes are not uniform across different metabolites (Supplementary Fig. 6, 7). We performed Uniform Manifold Approximation and Projection for Dimension Reduction (UMAP) dimensionality reduction on relative differences in concentration traces between the two ages, and observed numerous interdependencies between pathways. However, the pentose phosphate pathway (PPP) and TCA tend to form pathway-related clusters (Supplementary Fig. 8). Moreover, pairwise Kendall correlation between metabolic concentration traces is also affected by aging (Supplementary Fig. 9). This effect may be caused by widely described metabolic dysregulation in aging (Mattson and Arumugam, 2018). Consequently, reaction and transport fluxes are impacted as well (Supplementary Fig. 10-12). To sum up, aging effects on metabolite concentrations at rest and in response to neuronal activation are metabolite-specific and largely uncorrelated, reflecting metabolic deregulation in aging.

Lactate transport directionality depends on blood glucose levels in aged, but not young.

In the aged state, neuronal lactate import flux is lower, while astrocyte lactate export flux is slightly higher. This effect can be explained by mitochondrial hypometabolism, which results in increased pyruvate levels and correspondingly higher lactate.

We simulated the effects of varying resting blood glucose levels in a range of 1.6 to 14.6 mM with increments of 1 mM and found a dependence of lactate transport directionality upon glucose levels in aged, but not in young animals (Supplementary Fig. 13). In the young state, we observed an astrocyte-to-neuron lactate shuttle (ANLS) at all tested blood glucose levels. As blood glucose levels increase, lactate export from astrocytes rises while lactate import to neurons decreases. This observation is logical since higher glucose availability reduces the need for neurons to import lactate, and more lactate is available in astrocytes, facilitating its export.

Unexpectedly, in the aged state, we found that both neurons and astrocytes export lactate when blood glucose levels are low (1.6 to 5.6 mM). However, when blood glucose levels are moderate (6.45 to 10.6 mM), ANLS with smaller flux amplitudes occurs, consistent with observations in a recent preprint (Acevedo et al., 2023). At high blood glucose levels (11.6 to 14.6 mM), both types of cells import lactate. This counterintuitive observation may represent a manifestation of metabolic dysregulation in aging. A potential explanation could involve NAD+/NADH and ATP/ADP ratios due to their regulatory role over the entire metabolic network, but a definitive answer would require

experimental investigation. As blood glucose levels increase, lactate export from astrocytes decreases, and neurons switch from export to import of lactate. In summary, lactate transport directionality in aged, but not the young brain, is sensitive to blood glucose levels.

Aging-associated changes in metabolism alter electrophysiological characteristics.

Interestingly, aging metabolism leads to changes in neuronal firing characteristics for both presynaptic input (Fig. 3) and current injection-driven simulations (Supplementary Fig. 5). Age-related differences in neuronal firing characteristics evoked by current injection are particularly important because we have excluded glutamate release effects from the simulation. This was done to mitigate the possibility of synaptic activity reduction becoming a confounding factor. Observations are consistent between synaptic input and current injection-driven responses (Supplementary Fig. 14), indicating that the effects on neuronal firing characteristics result from changes in metabolism rather than just synaptic glutamate release scaling. The primary driving factor is the reduction in Na^+/K^+-ATPase expression in the aged brain. If Na^+/K^+-ATPase expression remains at its young level, neuronal firing characteristics only slightly differ between young and old under conditions of high-frequency firing (78-79 Hz). However, no significant differences are observed for firing at lower frequencies such as 4-8 Hz. Altogether, age-related change in Na^+/K^+-ATPase expression rather than ATP-level reduction is the key factor defining the differences in characteristics of neuronal firing and the shape of an action potential in aging, consistent with a recently suggested theory of non-canonical control of neuronal energy status (Baeza-Lehnert et al., 2019).

Less energy is available and consumed by neuronal signaling in the aged state.

Energy deficiency is a prominent feature of brain aging (Bonvento and Bolaños, 2021), but cell-type specific changes remain poorly understood. Adenylate energy charge (AEC), a widely used proxy for cellular energy status (Atkinson, 1968), is higher in the young compared to the old state (Fig. 3e), indicating a decrease in energy availability with aging. The total ATP cost of firing at approximately 8 Hz is 2e9 (young) and 1.8e9 (old) molecules of ATP per second per NGV unit, which aligns with literature estimates (Howarth et al., 2012; Yi and Grill, 2019; Zhu et al., 2019). The primary energy-demanding functions in the brain are mediated by the Na^+/K^+-ATPase (Niven, 2016; Meyer et al., 2022). We observed reduced ATP consumption by the neuronal Na^+/K^+-ATPase in aging (Fig. 3f), which could be attributed to a decrease in neuronal firing frequency. Conversely, astrocytic Na^+/K^+-ATPase ATP usage slightly increased in the aged state (Fig. 3f). The ratio of the astrocyte-to-neuron Na^+/K^+-ATPase flux is around 2 to 3 (Fig. 3g), and this value is marginally higher in the aged compared to the young state. In summary, aging is accompanied by the decline in energy

status of both neuron and astrocyte, but changes in ATP use of the Na^+/K^+ pump are cell-type dependent.

Aging brain metabolism is more fragile and susceptible to molecular damage.

Protein dysfunction is associated with several aging hallmarks, including loss of proteostasis, oxidative damage, and impaired DNA repair (Mattson and Arumugam, 2018; Schaum et al., 2020). Moreover, reduced protein translation fidelity leads to a phenotype resembling an early stage of Alzheimer's disease (Brilkova et al., 2022). To model the impact of molecular damage on enzyme and transporter functions, we conducted simulations with one perturbation at a time for each protein's kinetic parameter, adjusting its value by 20% (increasing and decreasing in separate simulation runs). We then calculated sensitivities by comparing 2,264 simulation runs with perturbed parameters to the baseline in young and aged state simulations (see formula in Fig. 4b). From the difference of sensitivities during stimulus response and at rest normalized by rest state sensitivities, we calculated responsivity (Fig. 4d), which reveals cell-type specific differences between neuron and astrocyte (Fig. 4d). Neuronal responsivity mostly decreases with age, while responsivity of the astrocyte mostly increases. This observation is in line with the literature on astrocyte reactivity (Weber and Barros, 2015). However, in contrast to the “selfish” astrocyte hypothesis (Weber and Barros, 2015), we suggest that the increase in astrocytic responsivity is a manifestation of its self-sacrifice in an attempt to support the declining neuron. Overall, this observation suggests a dysregulation of intercellular communication.

We visualized the responsivity of the entire metabolic network in the two age groups by positioning the nodes of both metabolites and enzymes using the Fruchterman-Reingold force-directed algorithm (Hagberg et al., 2008). The lengths of edges were weighted reciprocally to metabolic responsivity (Fig. 4e). More details are available from Supplementary File 2. These networks displayed clustering of nodes by function, which is better separated in young than in old states.

We then performed a quantitative comparison of the networks. For both age states we calculated the closeness centrality of nodes, which is the reciprocal of the sum of shortest path distances between each node and all other nodes. The aged state showed on average longer distances than the young state (Fig. 4f).

To evaluate the fragility of metabolism at the two ages, we quantified the aging-associated fragmentation of the network into "islands" by calculating the number of connected components in young and old networks after removal of edges with responsivities below a given percentile threshold

(Fig. 4g). Between a 76% and a 93% threshold, we observed a higher number of connected components in the age state. Both networks are fully connected at lower than 76% threshold values and fully disconnected at 100%. Therefore, aging brain metabolism is more fragile and susceptible to damage, while metabolic responsivity moves in opposite directions for neurons (down) and astrocytes (up) in the aged state.

Molecular responsivity based anti-aging targets are consistent with aging mechanisms. Enzyme-metabolite pairs exhibiting the highest differences in metabolic responsivity (Supplementary Fig. 16) can potentially be considered as anti-aging targets (Fig. 5a). To broaden the set of potential drug targets and narrow down the number of simultaneous therapeutic interventions, we performed transcription factor (TF) enrichment analysis using ChEA3 (Keenan et al., 2019). ChEA3 is a tool that prioritizes TFs based on the overlap between a given list of genes and a TF targets database. This analysis aimed to identify common TFs that could serve as potential anti-aging targets regulating several target enzymes (Fig. 5b). We then consider the ten highest priority targets.

The top-scoring TF was ESRRA (estrogen-related receptor alpha). This TF regulates expression of multiple metabolism-related genes, including those of mitochondrial function, biogenesis and turnover, as well as lipid catabolism (Tripathi et al., 2020). It is also linked to autophagy and NF-kB inflammatory response via Sirt1 signaling (Cantó et al., 2009; Yuk et al., 2015; Kim et al., 2018; Suresh et al., 2018). Mitochondrial dysfunction and autophagy impairments are consistently among the hallmarks of aging (López-Otín et al., 2013, 2023; Mattson and Arumugam, 2018). Notably, ESRRA expression is downregulated in aging according to various studies (Schaum et al., 2020; Tripathi et al., 2020). Altogether, ESRRA acts as a regulatory hub of multiple aging-associated pathways as outlined in **Supplementary Fig. 19**. The additional transcription factors identified have strong links in the literature to aging and neurodegeneration (see **Supplementary Information File 3**).

We further searched the STRING database (Szklarczyk et al., 2019) for the protein-protein associations of the top TF ESRRA (Fig. 5c) and identified these proteins: Hif1a, Sirt1, Hdac8, Ppargc1a, Ppargc1b, Mef2c, Nrip1, Ncoa1, Tfam, Perm1. Interestingly, numerous reports attribute roles in aging and neurodegeneration to these proteins as detailed in the **Supplementary Information File 3**.

Our identified anti-aging targets largely align with the literature data on therapeutics for healthy aging (Campisi et al., 2019). Furthermore, these targets suggest a role for less studied TFs in aging brain

energy metabolism and provide insights into the links between molecular mechanisms implicated in aging and neurodegeneration.

Rejuvenation by targeted interventions and a combination of diet, NAD supplementation and Na^+/K^+-ATPase activation.

We investigated whether key features of the aged brain phenotype, such as energy deficiency and altered neuronal firing, could be rejuvenated through targeted interventions. We conducted constrained optimization on 20 combinations of parameter sets. These parameter sets included: 1) the enzymatic targets identified by the differences in metabolic responsivity (same as the input for transcription factor enrichment analysis above), 2) the enzymatic targets regulated by top transcription factor from the enrichment results mentioned earlier, 3) parameters corresponding to arterial blood glucose and ketone levels (mimicking diet), 4) parameters corresponding to arterial blood lactate levels (attributed to the effects of exercise), and 5) total NAD-pool parameter in neuron and astrocyte (NAD supplementation). Surprisingly, optimization using a combination of diet (lower blood glucose and higher blood b-hydroxybutyrate), exercise (higher blood lactate), NAD supplementation, and modulation of the cytosol-mitochondria NAD-associated reducing equivalents shuttle (hereafter referred to as DEN-therapy) resulted in ATP levels increase of both neurons and astrocytes towards young state values.

To restore neuronal firing characteristics, we supplemented each intervention by reversing the Na+/K+ pump age-related downregulation. For each intervention, observed neuronal firing characteristics were similar to those of a young state. The energy status of both cell types was intermediate between young and old states (**Fig. 5**). Insulin is a common biological factor that activates the Na^+/K^+-ATPase and also lowers blood glucose. In conclusion, we computationally demonstrated restoration of ATP levels and neuronal firing characteristics in response to identified therapies.

Discussion

This study presents the most detailed dynamic simulation of age-specific NGV metabolism coupled to neuronal firing and blood flow. Our model specifically emphasizes the key brain energy metabolism pathways and processes involved in neuronal signal transduction. In building our model, we strove to be as biologically detailed and unbiased as possible, but due to limited available data, we had to refine weakly constrained parameters and focus on the most relevant pathways and processes rather than simulating dynamics at the whole genome-scale. Additionally, due to data sparsity, differences

between *in vitro* and *in vivo* conditions as well as natural biological variability complicate development of computational models.

In spite of these challenges, our results in both young and aged states align well with various published experimental reports on metabolite levels and neuronal firing. For example, we discovered aging-associated changes in metabolism affect neuronal firing patterns and characteristics that are consistent with literature (Power et al., 2002; Disterhoft and Oh, 2007; Kumar and Foster, 2007; Smithers et al., 2017; Vitale et al., 2021). In addition, our sensitivity analysis, which mimics the effects of conditions such as phosphorylation levels, transcription and translation errors, as well as molecular damage to enzyme and transporter kinetic properties, revealed cell-type specific differences in the aged brain. It also predicted diminished flexibility in distributing the burden of ATP supply to adapt to fluctuating energy needs in the aged brain.

With sensitivity and transcription factor enrichment analyses, we were able to pinpoint potential anti-aging targets. Through constrained optimization, we identified a combinatorial therapy that rejuvenates key features of the aging brain phenotype. This therapy involves maintaining specific levels of blood glucose, lactate, and β-hydroxybutyrate achievable through diet and exercise, coupled with redox state maintenance via NAD-supplementation, modulation of the cytosol-mitochondria reducing equivalent shuttle (related to NADH), and Na^+/K^+-ATPase activation. For instance, aging phenotype reversal can be achieved in part by regulating insulin signaling, which concurrently addresses blood glucose and Na^+/K^+-ATPase.

More complex interventions, which act on the top potential targets identified earlier in conjunction with elements of DEN-therapy, also managed to restore ATP levels in cells while maintaining blood glucose levels at 5-5.5 mM. However, it is important to consider the translational perspective of these complex interventions. Given that they act on multiple enzymatic targets at the same time, their development and implementation would require a significantly more extensive and thorough investigation before they can be considered for practical application in treating aging-related issues. Notably, the outcomes of these complex therapies appear to be comparable to those achieved with the simpler DEN-therapy, raising the question of whether the additional complexity of such therapies is necessary for effective treatment.

The promising combination therapy identified in this study, which includes diet, exercise, NAD supplementation, NAD shuttle and Na^+/K^+-ATPase modulation, shares similarities with proposed anti-aging interventions such as caloric restriction, ketogenic diet, and exercise. The suggested

anti-aging mechanisms of metformin (Kulkarni et al., 2020) and resveratrol (Park et al., 2012; Santos et al., 2021) also target some of the pathways involved in this combination therapy. However, there are numerous other processes that are not included in the model, and the most studied anti-aging therapies remain incompletely characterized. Our data-driven and optimization model construction approach was remarkably successful in simulating very complex conditions and stimuli, as well as the emulation of aging phenotypes.

We observed that even with significant modifications attributable to aging, the model remained viable and produced simulation results consistent with published literature. Importantly, random modifications of kinetic parameters and enzyme concentrations led to worse simulation outcomes compared to the data-driven aging version of the model. This result suggests a coordinated response in the expression changes of enzymes and transporters in response to changes in blood nutrients and total NAD pool. If the expression changes represent an adaptive response to molecular damage accumulation, then dysregulated energy metabolism may be a transitional state between healthy aging and neurodegenerative disorders rather than a distinct aging hallmark.

The model and methods developed in this study open up new avenues for addressing the fundamental questions of brain aging, disease-associated genetic variants, enzymatic deficiencies, and the effects of different diets. The fact that the model is able to simulate a variety of stimuli and conditions, including aging and changes in blood nutrients, suggests that it has the potential to be a valuable tool for future research. As such, it is most appropriate to treat the mathematical formulation of a biological system as a tool, which is suitable to address a number of questions in a given context. For this tool to be of wider use, it needs to be easy to modify so that it can support simulations of different conditions or even serve in personalized medicine applications. Additionally, the methods used in this study could be applied to other complex systems, further advancing our understanding of the biological world.

Figures.

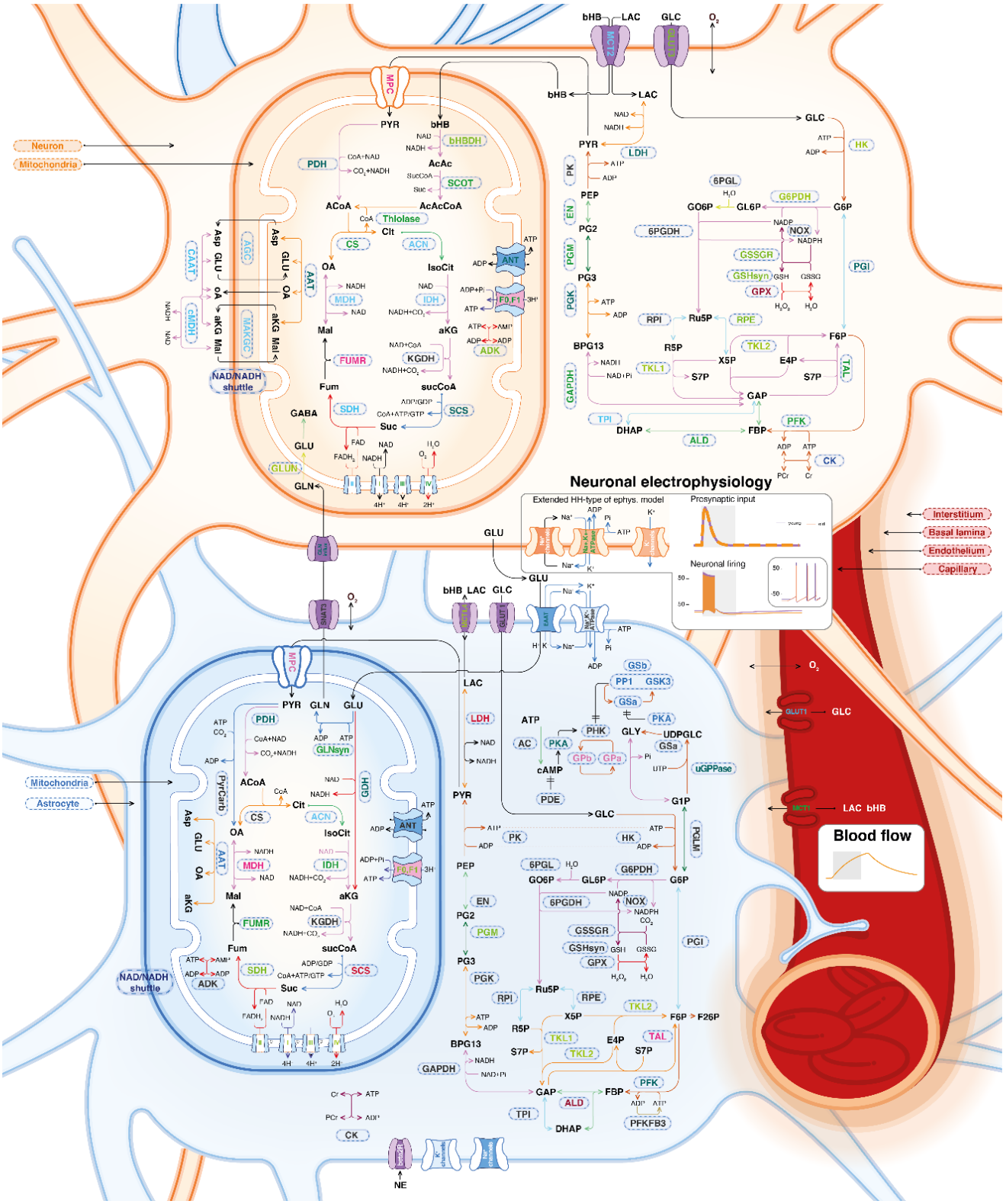

Fig. 1. Model overview. The model consists of three connected sub-systems: metabolism, neuronal electrophysiology and the blood flow. Compartments of the model include the neuronal and astrocytic cytosol, mitochondrial matrix and intermembrane space, interstitium, basal lamina, endothelium, capillary, artery (only with fixed arterial concentrations of nutrients and oxygen), and endoplasmic

reticulum (only with Ca^{2+} fixed pool). Enzymes and transporters shown in the figure correspond to the rate equations in the model which govern the dynamics of metabolite concentration changes. Neuronal electrophysiology is modeled in a slightly extended Hodgkin-Huxley type of model. Blood flow activation is described by a simple function dependent on the stimulus onset and duration according to the literature models.

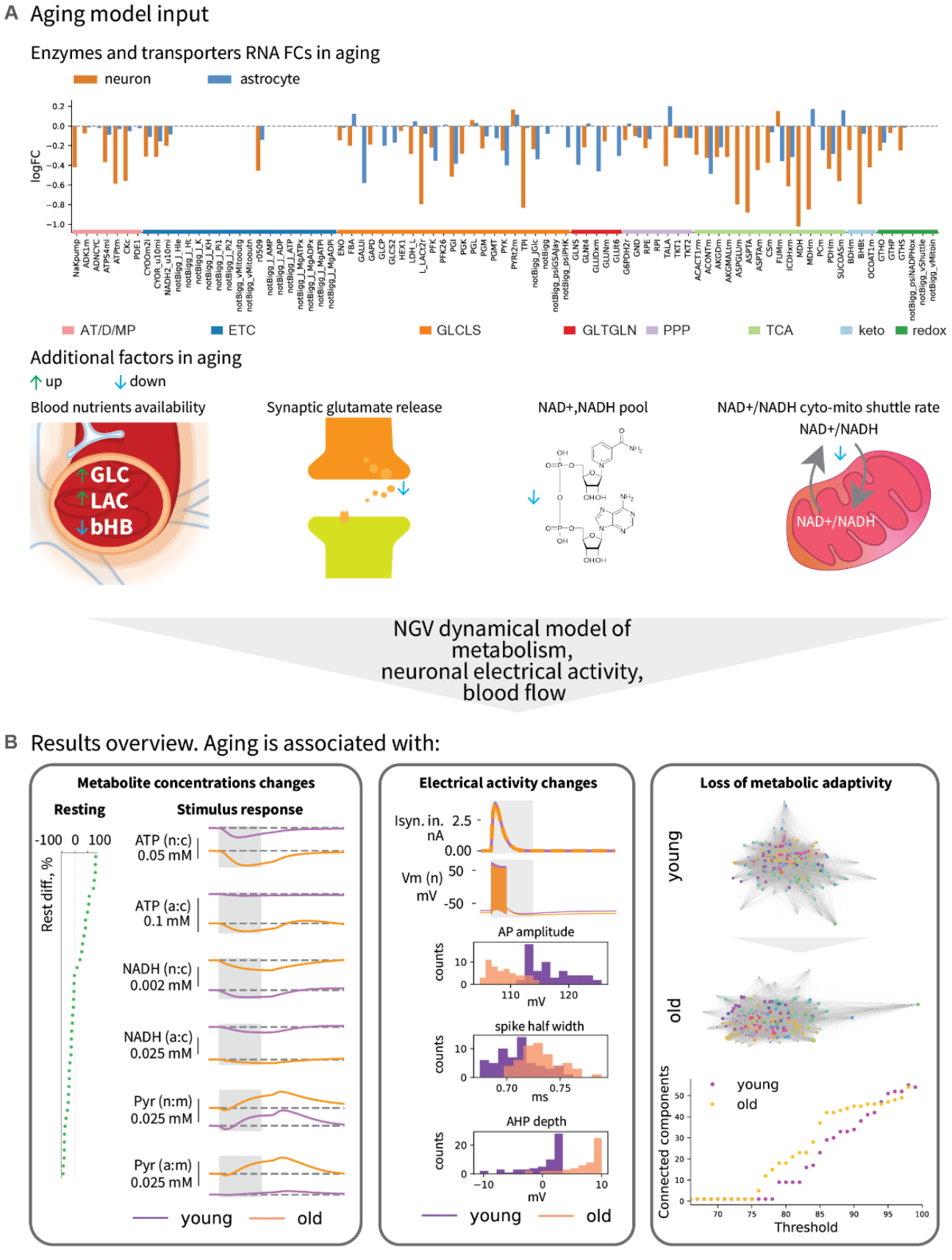

Fig. 2. Aging model input (a) and results overview (b). a, Aging input is modeled with RNA expression fold changes of enzymes and transporters, scaling of arterial glucose, lactate and b-hydroxybutyrate, as well as the total NAD (reduced and oxidized) pool, synaptic effects of glutamate concentration changes upon release events, and the reducing equivalents (NADH-related) shuttle

between cytosol and mitochondria. **b,** The key results include aging effects on metabolite levels, electrical activity of the neurons, and changes in adaptivity of the system in response to kinetic parameter perturbations (mimicking molecular damage and other conditions affecting enzyme and transporter functions).

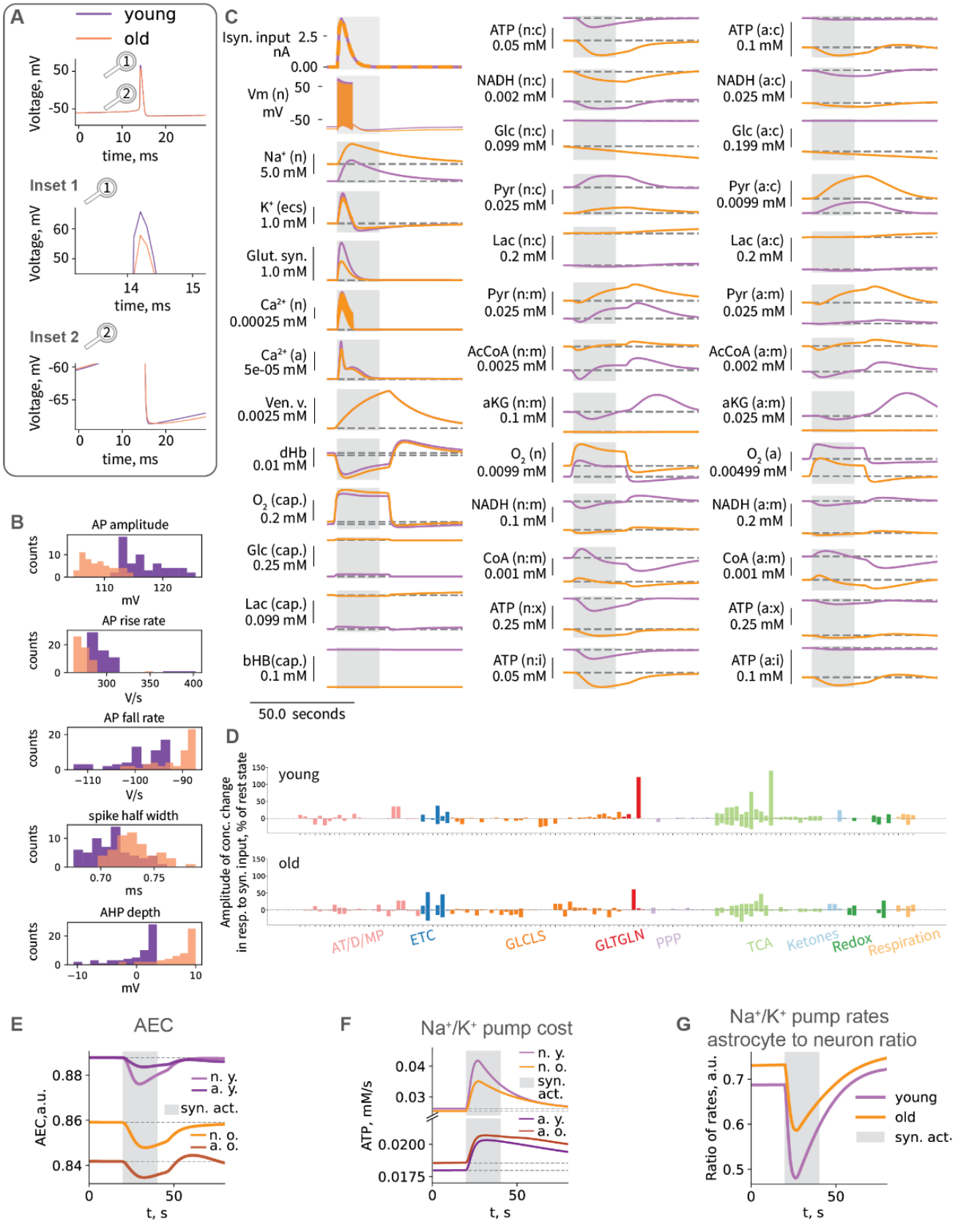

Fig. 3. Simulation results. a, Example AP in voltage traces in simulations of young and aged neurons with insets providing a closer view. **b,** Characteristics of neuronal firing in young and old ages upon synaptic activation. **c,** Dynamics of metabolism in response to synaptic activation at different ages (only a selection of the most important variables is shown). Compartment names abbreviations: n - neuron, a - astrocyte, c - cytosol, m - mitochondria, x - mitochondrial matrix, i - mitochondrial IMS, cap. - capillary. **d,** Amplitude of concentration changes in response to synaptic activation in young (top) and old (bottom), individual metabolites labels are available in **Supplementary Fig. 18**. **e,** AEC: Adenylate Energy Charge in young and old neurons and astrocytes. **f,** Main energy consumption: Na^+/K^+-ATPase rate of ATP use. **g,** Ratio of astrocyte to neuron Na^+/K^+ pump rate.

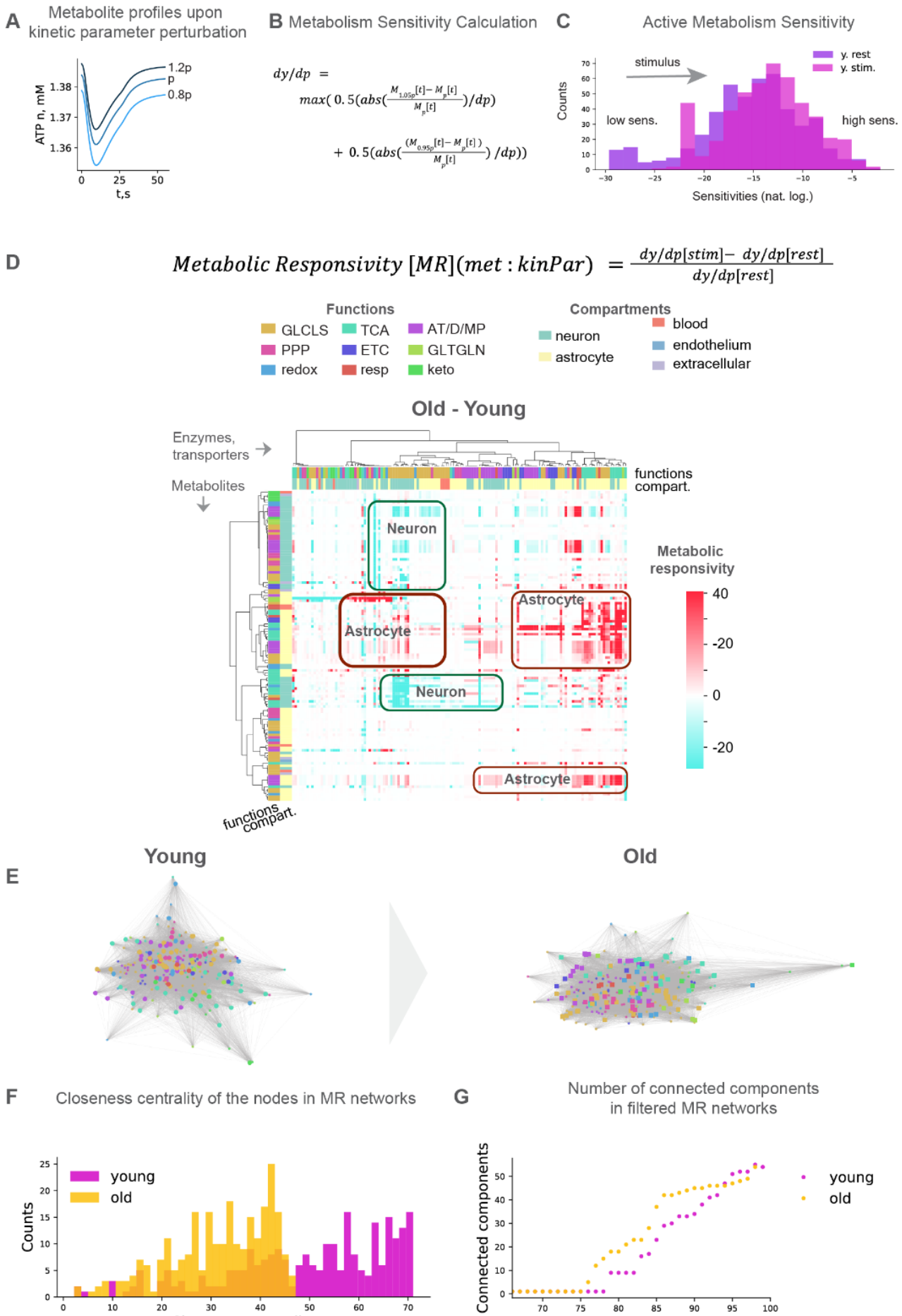

Fig. 4. Metabolic response to kinetic perturbations changes with age. a, Example metabolite level profiles in response to kinetic parameter perturbation. **b,** Calculation of metabolic sensitivity to kinetic parameter perturbations. **c,** Active metabolism sensitivity. **d,** Metabolic responsivity to kinetic parameter perturbations. **e,** Metabolic responsivity networks in young and aged (same function-color relation as in **d**). **f,** Closeness centrality of the nodes in the networks of metabolic responsivity aggregated by enzymes. **g,** Number of connected components in filtered networks of metabolic responsivity aggregated by enzymes. Ions, membrane potential, gating variables, mitochondrial membrane potential, and metabolites with fixed concentrations are removed from the analysis for all figures in this panel.

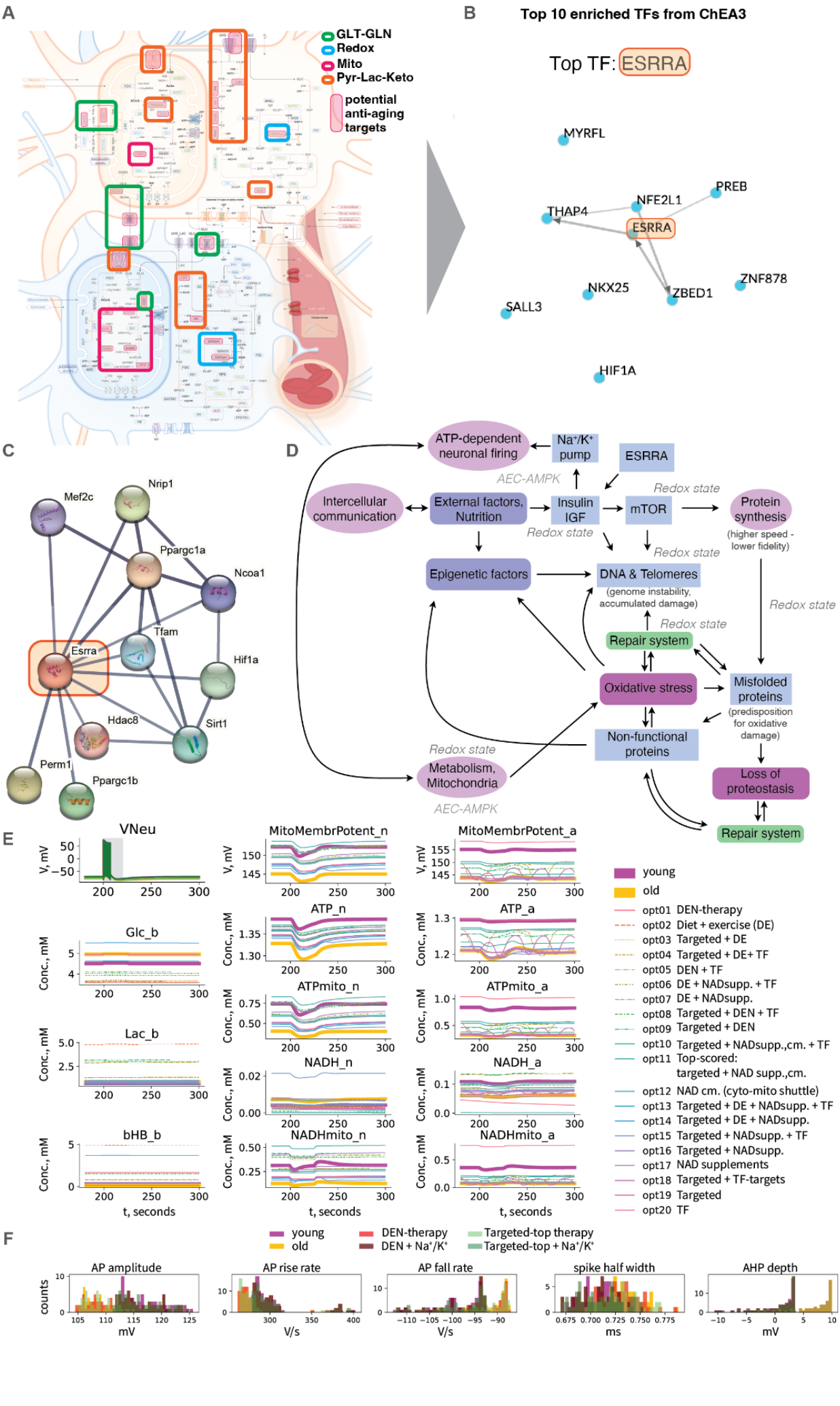

Fig. 5. Reversing aging via targeted metabolism interventions. a, Sensitivity analysis-based potential targets are outlined by pink boxes and grouped by function in thick line boxes in the modeled system. **b,** Transcription factor enrichment results obtained from ChEA3 analysis (the top 10 TFs are shown). **c,** Results of the STRING-database search for ESRRA (the top TF from ChEA3 analysis). **d,** The interplay of molecular mechanisms in brain aging. **e,** Time series traces of selected variables in young, aged, and treated aged states. The treatments were 20 different therapies based on combinations of different factors. These factors were top enzymes and transporters selected by metabolic responsivity, as well as top enzymes and transporters regulated by ESRRA. Additional factors included common interventions as diet, exercise, NAD supplementation and NAD cytosol-mitochondria shuttle modulation. **f,** Characteristics of neuronal firing in young, aged, and treated aged with selected therapies. In addition to selected top-performing and top-translatable therapies, we restored Na^+/K^+ pump expression to the young state. Application of the Na^+/K^+ pump expression restoration and each of the treatments restored characteristics of neuronal firing.

Methods

Baseline model building

We reconstructed and simulated a model of NGV metabolism coupled to a simple blood flow model and a Hodgkin-Huxley (HH) type of neuron model. The main concepts of electro-metabo-vascular coupling, as well as blood flow and neuronal electrophysiology model are based on the models available from the literature (Aubert et al., 2001; Jolivet et al., 2015; Calvetti et al., 2018; Winter et al., 2018). Our model specifically emphasizes the key brain energy metabolism pathways and processes involved in neuronal signal transduction. However, to gain a more comprehensive understanding of the various complementary molecular mechanisms and pathways involved in aging and disease, it is desirable to further expand the model to a whole-cell scale and incorporate more regulatory processes. At present, this task is hindered by data sparsity. As more data becomes available, the model can be iteratively refined and expanded.

Compared to the more generalized phenomenological metabolism models, our metabolism model features 183 processes (95 enzymatic reactions, 19 processes of transport of molecules across the cell and mitochondrial membranes, and 69 other processes related to ionic currents, blood flow dynamics and some miscellaneous non-enzymatic processes, e.g. Mg2+ binding to mitochondrial adenine

nucleotides). Every reaction, transport or other process is represented by its rate equation, which is literature-derived. Changes of molecular concentrations are described by a system of 151 differential equations and additionally cytosolic ADP, creatine, NAD, NADP are calculated from the conservation law and total pool of relevant molecules.

The model is based on the combination of literature data for enzyme kinetics and molecular concentrations. We have meticulously collected all parameters and equations from the literature sources, as referenced in Supplementary Table 2 and throughout the model code, and programmatically queried databases BRENDA (Chang et al., 2021), SabioRK (Wittig et al., 2018). However, observed discrepancies in the parameters reported by different sources define the need for the optimization procedure, to derive plausible biological middle-ground. The parameters with uncertainties observed in the literature were constrained by their lower and upper bounds taking into account the type of the parameter (Michaelis constant of reaction, inhibition/activation constant, maximal rate of reaction, equilibrium constant, Hill coefficient) and optimized as described in the Optimization part of the Methods.

To have the most realistic biological average for the initial values of all variables (concentrations, membrane potential, mitochondria membrane potential, venous volume, gating variables) according to the literature, we considered not only measured and modeled literature data on the absolute values themselves, but also additional constraints, such as known ratios of NADH to NAD^+ in the neuron (Neves, 2011; Dienel, 2012; Berndt et al., 2015; Mongeon et al., 2016) and astrocyte (Mongeon et al., 2016). One of the most important variables in the model, ATP concentration, was reported at 2 mM level in many experimental and modeling studies (Erecińska and Silver, 1989; Cloutier et al., 2009; Jolivet et al., 2015; Calvetti et al., 2018; Winter et al., 2018). However, some more recent data report it at 1 to 1.5 mM scale (Baeza-Lehnert et al., 2019; Köhler et al., 2020). Assuming that more recent measurement technologies can provide more precise data, we set cytosolic ATP in the neuron to approximately 1.4 mM according to Baeza-Lehnert et al. (Baeza-Lehnert et al., 2019) and to approximately 1.3 mM in astrocyte according to Kohler et al. (Köhler et al., 2020) where it was reported in a range of 0.7 to 1.3 mM (acutely isolated cortical slices) and 1.5 mM (primary cultures of cortical astrocytes).

Mammalian ATP to ADP ratios are reported in a very wide range of values from 1 to more than 100 (Tantama et al., 2013). Ratio of ATP to AMP is around 100 (Erecińska and Silver, 1989). Further, metabolite ratios from (Erecińska and Silver, 1989) were used to adjust initial concentrations of phosphocreatine and phosphate to the ATP levels. Lactate concentrations in different compartments,

which is central to the ANLS debate, was set according to the recent Mächler et al. paper (Mächler et al., 2016). We also tested the model with all alternative literature concentrations for the metabolites mentioned above.

Glucose supply from blood is of key importance to brain energy metabolism (Benton et al., 1996). For this reason we approached it particularly meticulously. In our model, glucose concentrations are assigned to detailed compartments, such as arterial, capillary, endothelial, basal lamina, interstitium, neuronal cytosol and astrocytic cytosol (Barros et al., 2017). According to the literature, hexokinase flux is split approximately equally between neuron and astrocyte (Barros et al., 2007, 2017; Jolivet et al., 2010), so that we adjusted Vmax of hexokinase in a way for fluxes to match the literature data at rest. Upon activation, the ratio of glucose influx to astrocyte versus neuron increases, consistently with the literature knowledge (Jolivet et al., 2010).

Implementation and simulation.

This metabolism model is implemented and simulated in Julia programming language (Bezanson et al., 2017). We used the DifferentialEquations.jl package (Rackauckas and Nie, 2017) to solve the differential equations system using order 2/3 L-stable Rosenbrock-W method (autodifferentiation disabled, both absolute and relative tolerances set to 1e-8). The choice of Julia language is defined by the combination of its high performance, extensively developed mathematical methods ecosystem, and the readability of the code, which supports its future use. Most of the analysis and figures-making code is written in Python programming language.

The model is built in a modular way, so that every molecular process has a dedicated rate function, and combination of relevant rate functions defines the dynamics of variables. This supports convenient testing of various enzymatic mechanisms, parameters and initial values of concentrations, as well as easier model subsetting and expansion.

Once the manuscript is accepted for publication, we will provide the GitHub repository with the code for model simulation, optimization, validation and analysis. These scripts are aimed to facilitate the model's reuse in future studies.

Optimization.

Time series data on the dynamics of specific metabolites in neurons and astrocytes is very sparse and sometimes contradictory. To avoid favoring one data source over the other, we only performed

optimizations for the steady state (minimizing derivatives). We built and optimized the model bottom-up in multiple iterations, gradually expanding it with more details. We started with the model of neuronal electrophysiology (Pospischil et al., 2008; Øyehaug et al., 2012; Jolivet et al., 2015; Krishnan et al., 2015; Calvetti et al., 2018). We included detailed astrocytic ion management based on the existing literature model (Witthoft et al., 2013). Then for the metabolism model, we started with capillary dynamics, oxygen and glucose transport, and hexokinase, because they are very well studied and CMR of glucose is widely measured, which sets a strong constraint on hexokinase rate. Then we proceeded to add reaction by reaction and evaluate rates in simulations, each time adding a new reaction, first if needed roughly manually refining underconstrained parameters. Then after several reactions were added, we ran optimization (with an objective to minimize derivatives) for a selected small set of parameters which are the least constraint by the literature. Then we modeled lactate transport and connected it to glycolysis. We separately optimized PPP for steady state (with an objective to minimize derivatives). For the mitochondria, we started from the electron transport chain, which is mitochondrial-membrane potential dependent and extremely sensitive to parameter variations. We mostly used the ETC model from Theurey and the colleagues (Theurey et al., 2019), and then we carefully selected a small number of parameters to optimize them (with an objective to minimize derivatives) to make the ETC model compatible with ATP and ADP concentrations from more recent experimental evidence. Then we added one-by-one TCA reactions to ETC, the same way as described above for other pathways. And we also added ketones metabolism, part of MAS, glutamate-glutamine cycle (after having both neuron and astrocyte together in the system).

The optimization procedure referenced above is single objective optimization performed using BlackBoxOptim.jl [https://github.com/robertfeldt/BlackBoxOptim.jl of Robert Feldt] with the default algorithm (adaptive differential evolution optimizer) iteratively selecting different sets of processes to reduce the parameter space.

To avoid non-physiological molecular concentrations (negative or too high values), we used Julia-callbacks and the “isoutofdomain” mechanism in solving the differential equations system during optimization. For these biological plausibility reasons, we utilized “isoutofdomain” to control the solution of the differential equations system to stay non-negative, so that the solver takes smaller time steps if the solution leaves the domain, unless the minimum step size is reached and integration is terminated. The same methods were applied for the anti-aging optimization, but the selection of neuronal firing related variables from the young state simulated time series data were used for the objective function.

Computational models are often optimized by fitting parameters to the data using a selected algorithm. Indeed, some time series data are available for various aspects of brain metabolism, including for concentrations of glucose, lactate, pyruvate, NADH and ATP, the BOLD signal, and cerebral metabolic rates of oxygen and glucose. However, to our knowledge these usually come from different experiments rather than simultaneous measurements of multiple metabolite concentrations and other characteristics. It has been demonstrated by numerous studies that one can fit system dynamics to selected data given a sufficient number of weakly constrained parameters and nonlinear rate equations (Dyson, 2004). An interesting case is when measurements with similar metadata from different studies produce significantly different dynamics of metabolite concentrations, such as in the example of extracellular brain glucose from Kiyatkin and Lenoir (Kiyatkin and Lenoir, 2012) as compared to Fillenz and Lowry (Fillenz and Lowry, 1998), which was further used in one of the early integrative NGV models (Cloutier et al., 2009). We therefore aimed to avoid the global optimization of fitting parameters to selected time series, and instead followed laborious iterative refinements in bottom-up model building with parameter estimation targeting the steady state (minimization of derivatives at rest). However, this approach has a downside: it does not guarantee exact matching of the experimentally recorded dynamics of any selected experiment. It is only possible to get close enough to the time series observed experimentally and in other models if the underlying model has a sufficient level of detail, uses relevant kinetic data for initial parameterization and employs applicable constraints (e.g., physiological range of metabolite concentrations, typical range of values for kinetic parameters of a given type). While many time series produced by our model are close to the literature reports, glucose concentration traces and cerebral metabolic rate of glucose consumption have only modest stimulus responses as compared to the literature. This can be explained by our decision to follow the most detailed (to our knowledge) approach to glucose transport in the brain available in the literature (Barros et al., 2007; Simpson et al., 2007). This approach takes into account compartmentalisation into arterial, capillary, basal lamina, interstitial space, astrocytes and neurons, with glucose transfer between these compartments described by rates that consider intracellular/extracellular concentration-dependent trans-acceleration and asymmetry of transporters.

Workflow and the key aspects of the bottom-up model building and optimization.

In order to build the model in a bottom-up data-driven way and avoid unreasonable preference for any particular data source, we developed a workflow, which resulted in the model performing surprisingly well for different setups. It produced quality simulation outcomes which are largely consistent with various literature. The only drawbacks are that the workflow is largely iterative, time-demanding, and requires manual intervention.. Here are the steps and the key considerations.

Step 1. Collect as much reliable data as available. In our case of building a model which combines the metabolism, electrophysiology and the blood flow, the following data were needed: molar concentrations of molecules (metabolites, proteins, ions), enzymes and transporters kinetic parameters, electrophysiology and blood flow dynamics parameters, rate equations of all processes, mechanisms of reactions and the data on their inhibitors and activators with corresponding mechanisms of action, existing models of pathways and their combinations. In most cases, reaction rate is modeled in the literature with at least a few different equations. This is due to the use of different formalisms in the literature. For example, the same reaction can be described in a precise mechanistic way considering multiple transition states of complexes formed by enzyme with substrates, products, regulators, or it can be described in a more simplified form of modular rate law or Michaelis-Menten kinetics, when assumptions about the reaction mechanism are met. It is important to keep collected models of reactions and how they are used in the existing models of pathways and systems, because for practical applications the scale of the model needs to be balanced with how many parameters are used for each equation in the model. For example, detailed mechanistic rate equations can be parameterized well for small models when there is enough consistent reliable data, but for cases with high uncertainty in the data, it is often hard to optimize and not overfit such models.

Step 2. Next, we model individual reactions. In some cases (most of which are relatively old biochemistry studies), time series data on individual enzymes are available. These can be used to optimize the parameters of enzymatic rate equations, especially if they are underconstrained, coming from different species or tissues. This step also allows us to evaluate how fast individual reactions are, how significant are the effects of inhibitors and activators and whether to include them in the model or not, and how problematic each particular reaction is in terms of the steady state and response to changing inputs.

Step 3. Once the data is collected, we bring together reactions one-at-a-time according to the reconstructed pathways networks. This process is highly iterative and needs to be repeated multiple times starting from different data. We need to try multiple combinations to see in which cases the optimization needed to bring the combination close to steady state is minimal. It is also important to combine those small subsets of reactions with pseudo-reactions of substrates source flux and products sink flux, to have an estimate of how this unit will perform once it is plugged into a bigger system. Iterating on this step, one can grow the system up to the models of pathways in individual cells, and existing models of those pathways are very helpful for initial choice of the most promising combinations of reaction rates and parameters. It is also useful to keep approximately the same level of

detail for the equations of all reactions in the pathway to prevent the emergence of some artificial bottlenecks. For the refinement of the parameters when connecting reactions in a pathway, instead of just following commonly used list of reactions of the pathway in order the metabolites enter it, it is useful to start from different steps of the pathway, especially with the reactions which are either known key regulators of the overall pathway flux (bottlenecks) or close to connection points to other pathways, or those with the most complicated mechanisms. The key aspects to decide on the performance of selected parameters set in the model are the concentrations at the steady state (or pseudo-steady state if the formal one cannot be achieved in a reasonable time), their response to stimuli (at least qualitatively in which direction and approximately how fast do they change, when no data is available), reaction and transport fluxes. It is important to keep several best performing models for all subsystems/pathways, because once they are plugged into a bigger system, performance ranking can change.

Step 4. Once small units/pathways are built in at least a few variations, they can be connected into bigger systems. For the optimization of connecting reactions, it is important to start from different entry points, compare overall fluxes of the pathways, and consider volumetric scaling aspects. In some cases temporary use of pseudo-reactions for source and sink of some metabolites for the optimization significantly improves the performance.

Step 5. Large metabolic system can further be connected (using the same strategy as in Step 4) to the electrophysiology and blood flow models. Electrophysiology and blood flow models can be found in the literature in a number variations and need to be optimized separately if needed.

Step 6. Then models of the neuron and the astrocyte can be connected in the same way as described above. Simulations and sensitivity analysis can further be used to select the parameters optimization of which has the highest effects and can efficiently improve the model according to available data. If no consistently reliable data is available, the objective function can be set to minimization of derivatives at rest state for the system to be at the steady state.

Validation.

First, we tested the response of the key metabolites (ATP, NADH, lactate, glucose) to the stimuli. All concentration related variables were ensured to stay in the range of biologically plausible values by the callbacks and the “isoutofdomain” parameter to a solver as described in the Optimization part of Methods. Next, we calculated the BOLD signal (Supplementary Figure 1d) and OGI (in range of 4.5-5 depending on stimulus, while literature data is in range of 4-5.5) using equations from Jolivet et al.

2015 to compare them with the literature (Jolivet et al., 2015; Winter et al., 2018; Jung et al., 2021). These two high-level phenomena are commonly used as benchmarks in NGV metabolism modeling papers (Jolivet et al., 2015; Calvetti et al., 2018; Winter et al., 2018). We also qualitatively compared dynamics of some key metabolites and reaction and transport fluxes to their expected response to stimuli. Then we estimated energy use from the components of the Na^+/K^+-ATPase rate equation (calculated from sum of neuron and astrocyte Na^+/K^+ pump ATP consumption flux in mM concentration per second with the volume of 17.8 um3 and the literature estimate of ionic gradients sharing 31% of total energy use) and compared it to the literature estimates (Howarth et al., 2012). We further validated aging-associated effects against the literature data shown in Supplementary Table 1.

Implementing aging effects in the model

Aging is a multifactor phenomenon which affects metabolism at different levels: transcriptome, proteome, metabolome, and potentially even kinetic properties of enzymes and transporters due to accumulated genetic damage, lower protein synthesis fidelity and higher chances of protein misfolding. To implement the aging effect in our model in a fully data driven way, the data on neuron and astrocyte specific proteomics, metabolomics and kinetics of enzymes are needed. However, to the best of our knowledge, most of such data is not yet publicly available.

We modeled the aging effects as following:

1. enzymes and transporters expression fold changes from TMS dataset (Schaum et al., 2020; Zhang et al., 2021a) applied as scaling factors to levels of corresponding enzymes and transporters
2. scaled initial concentrations of blood glucose, lactate, beta-hydroxybutyrate according to the literature data on difference in their levels in aging (approximation, because effect size depends on the literature source)
3. total NAD+ and NADH concentration pool scaling, because it decreases in aging according to qualitative literature (approximation)
4. synaptic glutamate release pool (approximation, but synaptic input is set the same for comparability of the results)
5. scaling of reducing equivalents shuttles between cytosol and mitochondria: NADH shuttle is a generalized rate equation based on activity of multiple enzymes of malate-aspartate and glycerol-phosphate shuttles, for which we followed literature to model it (Jolivet et al., 2015).

For the above factors, which mention “approximative/approximation”, the direction of change is according to the literature, but the absolute number of scaling factors (not known/contradictory in the literature) is set with an objective for the model to be steady at rest.

We implemented the aging effects on enzyme and transporter levels in two parallel ways: 1) using cell-type specific transcriptomics data (Schaum et al., 2020; Zhang et al., 2021a) and 2) using integrated proteomics data from the metaanalysis we performed earlier (Shichkova et al., 2021). The first approach featured higher coverage depth for the astrocyte-specific data. So that, to reduce bias from inferring missing data in the second method, we decided to rely on RNA data for implementing aging effects into simulation, while we used the second data source as a part of validation.

RNA fold changes for modeling aging effects

The extensive single-cell transcriptomics mouse data has recently become available (Schaum et al., 2020; Zhang et al., 2021a), providing the insights into the aging patterns of various cells, including neurons and astrocytes. However, RNA needs to be translated into proteins. As the changes in protein synthesis are reported in aging, RNA data need to be used with caution when inferring age-dependent protein concentrations. Even though, using RNA fold changes to scale enzyme and transporter levels results in metabolite concentration changes consistent with the literature (Supplementary Table 1).

We mapped reaction IDs to gene names using the gene-reaction-rules from publicly available metabolism reconstruction Recon 3D (Brunk et al., 2018). Then for the cases of multiple genes per reaction (i.e. enzymes built of several protein subunits or different isoforms present at the same time) we calculated age-scaling in two ways: 1) by using geometric mean of all fold changes, and 2) taking fold changes which results in lowest levels of RNA in aging, i.e. using the assumption that each protein subunit or isoform can be rate limiting if it's concentration is not sufficient to build fully-functional protein. Each of these methods we applied twice: for all genes and only for those with significant changes (significance defined by the source data paper). Next, we manually went through the mapping of all genes to reactions to make sure to keep only those that are enzyme subunits/isoforms and not regulatory factors and refine by subcellular location.

Protein levels for modeling aging effects.

Several studies measured brain protein levels in different ages, but they provided mostly brain tissue/regions data, rather than single neuron and astrocyte age-specific protein levels. The other studies provided neuron and astrocyte specific protein levels, but they were either using cultured cells, or young/adult rodents. For these reasons even a combination of proteomics data sets remains sparse for the goal of cell-type and age specific protein quantification. Even though using protein levels

directly to scale Vmax of the enzymes and transporters would allow to take into account posttranscriptional effects of protein synthesis and degradation, to reduce potential bias, we decided to rely only on the RNAseq data for age-associated changes in enzyme and transporter levels.

Other necessary aging factors

Arterial glucose, lactate and b-hydroxybutyrate, as well as total NAD (reduced and oxidized) pool are fixed in the model, but multiple studies report their changes in aging. For this reason we scaled them according to the literature. The resulting model was far from steady state, which could be explained by some missing age-associated changes. Indeed, we then scaled NADH exchange between mitochondria and cytosol, as it is also known to be affected by the aging process, and it resulted in a well-functioning model producing biologically meaningful observations. Further, for a more realistic setup, we also scaled synaptic effects of glutamate concentration changes upon release events, but it had less effect and the age-associated changes in electric features extracted from simulations with only current injection are consistent with those driven synaptically.

Data Availability

All the data used in this study are publicly available from referenced sources. The model is available on the web portal [this information will be available after peer-reviewed publication].

Funding

This study was supported by funding to the Blue Brain Project, a research center of the École Polytechnique Fédérale de Lausanne, from the Swiss government's ETH Board of the Swiss Federal Institutes of Technology.

Acknowledgements

The authors thank Judit Planas Carbonell, Claudia Savoia, and Jean-Denis Courcol for organizing web portal development and visualization, and Matthias Wolf for software support. We thank Karin Holm for writing assistance and Ayima Okeeva for the model notebook evaluation.

Author contributions.

PS: model, analyses, figures, writing, conceptualization. JSC: writing, conceptualization. EB: figures. CF: movie on the portal. SA: web portal. HM: writing, conceptualization. DK: writing, conceptualization.

Declaration of interests.

The authors declare no competing interests.

Supplementary Information

Supplementary Table 1. Observed aging effects and their comparison to the literature.

Decrease in aging is highlighted by blue background, increase in aging is highlighted by red; consistency with literature is highlighted by green background, inconsistency is highlighted by orange background; literature data from different sources providing contradictory evidence is highlighted by purple background.

Observation from simulation	Changes in aging	Literature data, reference, agrees or not
Energy budget characteristics		
Total energy use (neuron + astrocyte)	At rest: approximately the same 1.5e9 molecules ATP/second in both young and old. During neuronal firing in response to synaptic activation: decrease from 2e9 molecules ATP/second (young) to 1.8e9 molecules ATP/second (old). Energy use for neuronal firing in response to synaptic input is more affected by aging than the baseline rest state metabolism.	
Adenylate energy charge (AEC)	AEC slightly decreases in aging in both neuron and astrocyte. Amplitude of AEC response to stimulation decreases very slightly in the aging neuron and astrocyte. Surprisingly, there is a small overshoot of AEC in the astrocyte right after the approx. 7 seconds interval of neuronal firing in response to synaptic activation in aging, but not in the young state.	
Total Na+/K+-ATPase ATP	Na+/K+-ATPase ATP consumption in response to neuronal firing is slightly lower in aging. It is at least	“Activity decreases with aging” (Fraser and Arieff, 2001)

consumption in response to synaptic activation	partially related to the lower mean firing frequency in aging.	
ATP cost of AP	Lower in aging. It may be the result of limited ATP availability, i.e. metabolic aging serves as a cause for aging-associated changes in neuronal firing characteristics.	
Astrocyte to neuron ratio of Na/K ATPase rate	Increases with aging.	
Neuronal firing characteristics		
Voltage base (the average voltage during the last 10% of time before the stimulus)	From approx. -72 mV in young to approx. -78.5 mV in aged.	"Aged Type I neurons exhibited a hyperpolarized resting membrane potential (RMP) of circa -80 mV compared to circa -70 mV in the Young" (Smithers et al., 2017)
Mean firing frequency	Lower in the aged than in young.	Different reports (increase, decrease, no change) in different cell types and species (Rizzo et al., 2015)
AP amplitude, height, and peak voltage	Lower in the aged than in young.	Different reports (increase, decrease, no change) in different cell types and species (Rizzo et al., 2015)
AP rise rate and maximum of rise rate of spike (AP peak upstroke)	Lower in the aged than in young.	
AP fall rate and minimum of fall rate from spike (AP peak downstroke)	Absolute values are lower in the aged than in young.	
Spike width	Wider spikes in the aged than in young.	Slightly increases from 1 month to 10 months [Fig. 4 in (Vitale et al., 2021)]
AHP depth	Higher amplitude. Mostly positive in the aged while mostly negative in young.	"Enhanced AHP in aging" (Power et al., 2002) "Age-enhanced AHP" (Disterhoft and Oh, 2007)

		"The amplitude of the AHP increases during aging" [(Riddle, 2007), especially fig. 10.1] Increase or no change depending on cell type and species (Rizzo et al., 2015)
AHP depth from peak	Lower in the aged than in young.	
Difference of the amplitude of the first and the last peak	Lower in the aged than in young.	
Difference in amplitude of the first and the second peak, and difference in peak voltage of the second to first spike	Lower in the aged than in young.	
The decay time constant of the voltage right after the stimulus	Lower in the aged than in young.	
Irregularity index (Mean of the absolute difference of all ISIs, except the first one (see LibV1: ISI_values feature for more details.))	Higher in the aged than in young.	
Maximum difference of the height of two subsequent peaks	Lower in the aged than in young.	
Na+	Up in both neuron and astrocyte	
Metabolism characteristics		
Mitochondrial membrane potential	From approx. 155 mV in young to approx. 145 mV in aged (observed from sim.)	"Decreased mitochondrial membrane potential (DeltaPsi(M)) has been found in a variety of aging cell types from several mammalian species."

		(Sugrue and Tatton, 2001)
ATP	Down in all compartments (observed from sim.)	"Decreased ATP concentration in the neuronal somata of aged flies" (Oka et al., 2021) "The neuronal metabolism of glucose declines steadily, resulting in a growing deficit of adenosine triphosphate (ATP) production - which, in turn, limits glucose access." (Błaszczyk, 2020) "Decrease in mitochondrial energy transducing capacity" (Ivanisevic et al., 2016) Down in Fig 5. of (Ivanisevic et al., 2016)
Mg^{2+}	Down in the mitochondrial matrix (observed from sim.)	"Aging is very often associated with magnesium (Mg) deficit." (Barbagallo et al., 2009) "Elevation of brain magnesium prevents synaptic loss and reverses cognitive deficits in Alzheimer's disease mouse model" (Li et al., 2014) "Diminished Mg intake, impaired intestinal Mg absorption and renal Mg wasting" (Barbagallo et al., 2021) "The magnesium status of aging subjects is likely to be marginal, if not frankly deficient" (Seelig and Preuss, 1994) "The most common cause of Mg deficit in the elderly population is dietary Mg deficiency, although secondary Mg deficit in aging may also results from many different mechanisms" (Barbagallo and Dominguez, 2010)
NAD pool (ox. + red.)	Down (implemented into the model)	"Its depletion has emerged as a fundamental feature of aging" (Fang et al., 2017)

		"A significant decline in intracellular NAD+ levels and NAD:NADH ratio with ageing in the CNS" (Braidy et al., 2014) Down in Fig 5. of (Ivanisevic et al., 2016)
NAD^+/NADH cytosol	Down in the cytosol of both the neuron and astrocyte (observed from simulations). Limitation: cytosol and mitochondria NAD pools are connected by poorly constrained NAD shuttles, which may influence this observation.	"A significant decline in intracellular NAD^+ levels and NAD:NADH ratio with ageing in the CNS" (Braidy et al., 2014) "An increased ratio of NAD+/NADH indicating an oxidative shift" (Dong and Brewer, 2019)
NAD^+/NADH mitochondria	Up in mitochondria of both the neuron and astrocyte (observed from simulations). Observed increase in this ratio may be a compensatory mechanism for the decreased total NAD pool (ox. + red.) Limitation: cytosol and mitochondria NAD pools are connected by poorly constrained NAD shuttles, which may influence this observation.	"A significant decline in intracellular NAD^+ levels and NAD:NADH ratio with ageing in the CNS" (Braidy et al., 2014) "An increased ratio of NAD+/NADH indicating an oxidative shift" (Dong and Brewer, 2019)
Glucose in blood	Increases (implemented into the model)	"Circulating glucose concentrations generally increase during aging" (Mattson and Arumugam, 2018)
Glucose in neuron, astrocyte, basal lamina, interstitium	Decreases (observed from sim.)	"The neuronal metabolism of glucose declines steadily" (Błaszczyk, 2020) "Glucose metabolism is impaired in cells; reduced glucose utilization" (Mattson and Arumugam, 2018)
Lactate	Up in all compartments (in blood: implemented into the model, other compartments: observed from sim.)	"High brain lactate" (Ross et al., 2010) "Rise of lactate" (Datta and Chakrabarti, 2018)
Pyruvate in cytosol of neuron	Down	Down in aged (home cage and enriched environment) (Ge et al., 2021)
Pyruvate in	Up	

cytosol of astrocyte		
Pyruvate in mitochondria	Up in both neuron and astrocyte	
AcCoA in mitochondria	Up in both neuron and astrocyte	Up in aged (home cage and enriched environment) (Ge et al., 2021) Down in Fig 5. of (Ivanisevic et al., 2016)
CoA in mitochondria	Down in both neuron and astrocyte	
Fumarate in mitochondria	Down in both neuron and astrocyte	Down in aged (home cage and enriched environment) (Ge et al., 2021)
Malate in mitochondria	Down in both neuron and astrocyte	Not significant in (Ge et al., 2021)
Oxaloacetate in mitochondria	Down in both neuron and astrocyte	
aKG in mitochondria	Down in both neuron and astrocyte	Down in aged rats (Curtis et al., 2022) Not significant (Ge et al., 2021)
Succinate in mitochondria	Up in both neuron and astrocyte	Down in aged home cage, up in aged enriched environment (Ge et al., 2021)
Succinate-CoA	Down in both neuron and astrocyte	
Isocitrate	Down in both neuron and astrocyte	
Citrate	Down in both neuron and astrocyte	Down in aged rats (Curtis et al., 2022) Not significant (Ge et al., 2021)
Acetoacetate	Up in neuron	
AcAcCoA	Down in neuron	
bHB cells and extracellular	Down in neuron (observed from sim.), extracellular space	Up in aged enriched environment, comparable to young in home cage (Ge et al., 2021)
bHB blood	Down in blood (implemented into the model)	Down in blood (Eap et al., 2022)
QH2 in mitochondria	Down in astrocyte; almost no difference in neuron at rest, but lower response to stimulus	Down (Mantle et al., 2021; Hosseini et al., 2022)

Cytochrome C in mitochondria	Down in astrocyte; almost no difference in neuron at rest, but lower response to stimulus	Down (Jones and Brewer, 2009)
(Jones and Brewer, 2009)IP3 astrocyte	Lower amplitude of response to synaptic activation	
G1P astrocyte	Up	
F26BP astrocyte	Up	
G6P	Up in both neuron and astrocyte	Up in aged with enriched environment (Ge et al., 2021)
F6P	Up in both neuron and astrocyte	
FBP neuron	Up	Up in Fig 5. of (Ivanisevic et al., 2016)
FBP astrocyte	Down	
GAP neuron	Up	
GAP astrocyte	Down	
DHAP neuron	Up	Up in aged (home cage) (Ge et al., 2021)
DHAP astrocyte	Down	
BPG13	Down in both neuron and astrocyte	
PG3	Down in both neuron and astrocyte	Not significant in (Ge et al., 2021) Up in Fig 5. of (Ivanisevic et al., 2016)
PG2	Down in both neuron and astrocyte	
PEP	Down in both neuron and astrocyte	Not significant in (Ge et al., 2021) Up in Fig 5. of (Ivanisevic et al., 2016)
NADPH neuron	Down	“age-related declines in NAD(P)H” (Ghosh et al., 2014)
NADPH astrocyte	Up	
PPP except E4P	All metabolite concentrations increase in both neuron and astrocyte	R5P, R1P up in Fig 5. of (Ivanisevic et al., 2016)

E4P neuron	Up	
E4P astrocyte	Down in both neuron and astrocyte	
GSH	Down in both neuron and astrocyte	Comparable to young in human aging (Tong et al., 2016), but down in various neurodegenerative diseases (Iskusnykh et al., 2022) Up (Hupfeld et al., 2021)
PCr	Down in both neuron and astrocyte	"Aging is associated with lower levels of creatine and phosphocreatine" (Smith et al., 2014)
cAMP	Down in astrocyte (not implemented in the neuron model)	Down (Kelly, 2018)
Glutamate	Lower amplitude of glutamate concentration change in response to synaptic input in neuron (observed from sim.) and synaptic compartment (implemented into the model), down in astrocyte	Down (Kaiser et al., 2005; Hädel et al., 2013; Cox et al., 2022)
Glutamine neuron	Up in neuron	Up (Kaiser et al., 2005)
Glutamine astrocyte, ecs	Down in astrocyte and ecs	
Derived properties		
CMR glucose	Down	"The neuronal metabolism of glucose declines steadily" (Błaszczyk, 2020) "Glucose metabolism is impaired in cells; reduced glucose utilization" (Mattson and Arumugam, 2018)

Supplementary Table 2. Data sources.

Data	References
Electrophysiology model data	(Takahashi et al., 1981; Pospischil et al., 2008; Witthoft et al., 2013; Jolivet et al., 2015; Calvetti et al., 2018)
Blood flow dynamics	(Jolivet et al., 2015; Winter et al., 2018)
Glucose transport	(Simpson et al., 2007; DiNuzzo et al., 2010; Barros et al., 2017)

Lactate transport	(Simpson et al., 2007; Jolivet et al., 2015; Calvetti et al., 2018)
bHB transport	(Halestrap and Denton, 1974; Roeder et al., 1982; Neves et al., 2012; Pérez-Escuredo et al., 2016; Calvetti et al., 2018)
Oxygen transport	(Jolivet et al., 2015)
Hexokinase	(Barros et al., 2007, 2017; DiNuzzo et al., 2010; Jolivet et al., 2010, 2015)
PGLM (astrocyte only)	(Lambeth and Kushmerick, 2002)
Glycogen phosphorylase	(Lambeth and Kushmerick, 2002; DiNuzzo et al., 2010; Xu et al., 2011; Coggan et al., 2020)
Glycogen synthase	(Lambeth and Kushmerick, 2002; DiNuzzo et al., 2010; Xu et al., 2011; Coggan et al., 2020)
Glycogen metabolism regulation	(Lambeth and Kushmerick, 2002; Xu et al., 2011; Coggan et al., 2020)
PDE	(Rybalkin et al., 2013)
PGI	(Gaitonde et al., 1989; Mulukutla et al., 2014; Berndt et al., 2015; Bouzier-Sore and Bolaños, 2015)
PFK	(Mulukutla et al., 2014; Berndt et al., 2015; Bouzier-Sore and Bolaños, 2015; Jolivet et al., 2015)
PFKFB3 (astrocyte only)	(Mulukutla et al., 2014; Berndt et al., 2015)
Aldolase	(Mulukutla et al., 2014; Berndt et al., 2015)
TPI	(Mulukutla et al., 2014; Berndt et al., 2015)
GAPDH	(Mulukutla et al., 2014; Berndt et al., 2015)
PGK	(Sharma and Rothstein, 1984; Mulukutla et al., 2014; Berndt et al., 2015)
PGM	(Mulukutla et al., 2014; Berndt et al., 2015)
Enolase	(Mulukutla et al., 2014; Berndt et al., 2015)
Pyruvate kinase	(Mulukutla et al., 2014; Berndt et al., 2015)
LDH	(Jolivet et al., 2015)
PPP	(Winter et al., 2018)
Pyruvate transport to mitochondria	(Berndt et al., 2015)
PDH	(Berndt et al., 2015; Mulukutla et al., 2015; Zhang et al., 2018)

Pyruvate carboxylase (astrocyte only)	(Barden et al., 1972; Mahan et al., 1975; Schousboe et al., 2019)
Thiolase	(Gilbert et al., 1981; Huth and Menke, 1982; Yang et al., 1987; Antonenkov et al., 2000)
SCOT	(Hersh and Jencks, 1967; White and Jencks, 1976)
bHBDH	(Nielsen et al., 1973; Dombrowski et al., 1977)
Citrate synthase	(Berndt et al., 2015; Mulukutla et al., 2015)
Aconitase	(Berndt et al., 2015; Mulukutla et al., 2015)
IDH	(Wu et al., 2007; Berndt et al., 2012; Mulukutla et al., 2015)
aKGDH	(Smith et al., 1974; McCormack and Denton, 1979; Luder et al., 1990; Mogilevskaya et al., 2006; Berndt et al., 2012)
SCS	(Berndt et al., 2015)
SDH (Complex II ETC)	(Theurey et al., 2019)
Fumarase	(Berndt et al., 2015)
MDH	(Berndt et al., 2015)
MAS	(Wilcock et al., 1973; Huynh et al., 1980; Recasens et al., 1980; Berndt et al., 2015; Mulukutla et al., 2015; Borst, 2020)
GLT-GLN	(Pamiljans et al., 1962; Listrom et al., 1997; Chaudhry et al., 1999; Calvetti and Somersalo, 2011; Botman et al., 2014; Mulukutla et al., 2015; Flanagan et al., 2018)
Creatine kinase	(Jolivet et al., 2015)
$NADH/NAD^+$ shuttles	(Jolivet et al., 2015)
ETC	(Theurey et al., 2019)
C_H_mitomatr_n	(Theurey et al., 2019)
K_x_n	(Theurey et al., 2019)
Mg_x_n	(Theurey et al., 2019)
NADHmito_n	(Jolivet et al., 2015)
QH2mito_n	(Theurey et al., 2019)
CytCredmito_n	(Theurey et al., 2019)
O2_n	(Jolivet et al., 2015; Calvetti et al., 2018)
ATPmito_n	(Theurey et al., 2019)
ADPmito_n	(Theurey et al., 2019)
ATP_mx_n	(Theurey et al., 2019)
ADP_mx_n	(Theurey et al., 2019)

Pimito_n	(Theurey et al., 2019)
ATP_i_n	(Theurey et al., 2019)
ADP_i_n	(Theurey et al., 2019)
AMP_i_n	(Theurey et al., 2019)
ATP_mi_n	(Theurey et al., 2019)
ADP_mi_n	(Theurey et al., 2019)
Pi_i_n	(Theurey et al., 2019)
MitoMembrPotent_n	(Theurey et al., 2019)
Ctot_n	(Theurey et al., 2019)
Qtot_n	(Theurey et al., 2019)
C_H_ims_n	(Theurey et al., 2019)
ATP_n	(Baeza-Lehnert et al., 2019)
ADP_n	(Erecińska and Silver, 1989; Mironov, 2007; Tantama et al., 2013; Jolivet et al., 2015; Calvetti et al., 2018)
FUMmito_n	(Fink et al., 2018)
MALmito_n	(Garrett and Grisham, 2013; Fink et al., 2018)
OXAmito_n	(Williamson et al., 1967; Nazaret et al., 2009; Choi and Gruetter, 2012; Byrne et al., 2014; Fink et al., 2018)
SUCmito_n	(Byrne et al., 2014; Tretter et al., 2016; Fink et al., 2018)
SUCCOAmito_n	(Park et al., 2016)
CoAmito_n	(Rock et al., 2000; Mogilevskaya et al., 2006; Poliquin et al., 2013)
AKGmito_n	(Nazaret et al., 2009; Byrne et al., 2014; Park et al., 2016)
CaMito_n	(Brocard et al., 2001; Mogilevskaya et al., 2006)
ISOCITmito_n	(Frezza, 2017)
CITmito_n	(Ronowska et al., 2018)
AcCoAmito_n	(Cai et al., 2011; Lee et al., 2014; Park et al., 2016; Ronowska et al., 2018)
AcAc_n	(Nehlig, 2004)
AcAcCoA_n	(Menahan et al., 1981; Berndt et al., 2018)
PYRmito_n	(Nazaret et al., 2009; Arce-Molina et al., 2020)
bHB_n	(Chowdhury et al., 2014)

bHB_ecs	(Nehlig, 2004; Chowdhury et al., 2014; Achanta and Rae, 2017)
bHB_a	(Chowdhury et al., 2014)
bHB_b	(Nehlig, 2004; Chowdhury et al., 2014; Achanta and Rae, 2017)
ASPmito_n	(Maletic-Savatic et al., 2008)
ASP_n	(Maletic-Savatic et al., 2008)
GLUmito_n	(Roberg et al., 1999; Nazaret et al., 2009; Featherstone, 2010)
MAL_n	(Mueggler and Wolfe, 1978)
OXA_n	(Williamson et al., 1967; Choi and Gruetter, 2012)
AKG_n	(Pritchard, 1995)
GLU_n	(Shestov et al., 2007; Byrne et al., 2014)
NADH_n	(Neves et al., 2012; Jolivet et al., 2015; Park et al., 2016; Calvetti et al., 2018)
C_H_mitomatr_a	(Theurey et al., 2019)
K_x_a	(Theurey et al., 2019)
Mg_x_a	(Theurey et al., 2019)
NADHmito_a	(Jolivet et al., 2015)
QH2mito_a	(Theurey et al., 2019)
CytCredmito_a	(Theurey et al., 2019)
O2_a	(Jolivet et al., 2015; Calvetti et al., 2018)
ATPmito_a	(Theurey et al., 2019)
ADPmito_a	(Theurey et al., 2019)
ATP_mx_a	(Theurey et al., 2019)
ADP_mx_a	(Theurey et al., 2019)
Pimito_a	(Theurey et al., 2019)
ATP_i_a	(Theurey et al., 2019)
ADP_i_a	(Theurey et al., 2019)
AMP_i_a	(Theurey et al., 2019)
ATP_mi_a	(Theurey et al., 2019)
ADP_mi_a	(Theurey et al., 2019)
Pi_i_a	(Theurey et al., 2019)
MitoMembrPotent_a	(Theurey et al., 2019)

Ctot_a	(Theurey et al., 2019)
Qtot_a	(Theurey et al., 2019)
C_H_ims_a	(Theurey et al., 2019)
ATP_a	(Köhler et al., 2020)
ADP_a	(Erecińska and Silver, 1989; Tantama et al., 2013; Jolivet et al., 2015; Calvetti et al., 2018)
FUMmito_a	(Fink et al., 2018)
MALmito_a	(Garrett and Grisham, 2013; Fink et al., 2018)
OXAmito_a	(Byrne et al., 2014)
SUCmito_a	(Byrne et al., 2014)
SUCCOAmito_a	(Park et al., 2016)
CoAmito_a	(Rock et al., 2000; Poliquin et al., 2013)
AKGmito_a	(Byrne et al., 2014)
CaMito_a	(Brocard et al., 2001; Mogilevskaya et al., 2006)
ISOCITmito_a	(Frezza, 2017)
CITmito_a	(Ronowska et al., 2018)
AcCoAmito_a	(Cai et al., 2011; Lee et al., 2014; Park et al., 2016; Ronowska et al., 2018)
AcAc_a	(Nehlig, 2004)
AcAcCoA_a	(Menahan et al., 1981; Berndt et al., 2018)
PYRmito_a	(Arce-Molina et al., 2020)
GLN_n	(Shestov et al., 2007)
GLN_out	(Bröer and Brookes, 2001; Pochini et al., 2014)
GLN_a	(Hertz and Rothman, 2017)
GLUT_a	(Savtchenko et al., 2018; Verkhratsky and Nedergaard, 2018)
Va	(Breslin et al., 2018)
Na_a	(Witthoft et al., 2013)
K_a	(Witthoft et al., 2013; Flanagan et al., 2018)
K_out	(Takahashi et al., 1981)
GLUT_syn	(Robinson and Jackson, 2016; Hertz and Rothman, 2017; Verkhratsky and Nedergaard, 2018; Mahmoud et al., 2019)
VNeu	(Jolivet et al., 2015; Calvetti et al., 2018; Coggan et al., 2020)
Na_n	(Jolivet et al., 2015; Calvetti et al., 2018; Coggan

	et al., 2020)
h	(Jolivet et al., 2015)
n	(Jolivet et al., 2015)
Ca_n	(Jolivet et al., 2015)
pgate	(Pospischil et al., 2008)
nBK_a	(Witthoft et al., 2013)
mGluRboundRatio_a	(Witthoft et al., 2013)
IP3_a	(Witthoft et al., 2013)
hIP3Ca_a	(Witthoft et al., 2013)
Ca_a	(Witthoft et al., 2013; Verkhratsky and Nedergaard, 2018; Coggan et al., 2020)
Ca_r_a	(Bennett et al., 2008; Witthoft et al., 2013)
sTRP_a	(Witthoft et al., 2013)
vV	(Cloutier et al., 2009; Jolivet et al., 2015; Winter et al., 2018)
EET_a	(Witthoft et al., 2013)
ddHb	(Cloutier et al., 2009; Jolivet et al., 2015; Winter et al., 2018)
O2cap	(Jolivet et al., 2015; Calvetti et al., 2018)
Glc_b	(Jolivet et al., 2015)
Glc_t_t	(Barros et al., 2017)
Glc_ecsBA	(Pathak et al., 2015; Barros et al., 2017)
Glc_a	(Jolivet et al., 2015; Barros et al., 2017; Calvetti et al., 2018)
Glc_ecsAN	(Pathak et al., 2015; Barros et al., 2017)
Glc_n	(Jolivet et al., 2015; Barros et al., 2017; Calvetti et al., 2018)
G6P_n	(Kauffman et al., 1969; Anderson and Wright, 1980; Orosz et al., 2003; Cloutier et al., 2009; Park et al., 2016; Winter et al., 2018)
G6P_a	(Kauffman et al., 1969; Anderson and Wright, 1980; Orosz et al., 2003; Cloutier et al., 2009; Park et al., 2016; Winter et al., 2018)
F6P_n	(Kauffman et al., 1969; Cloutier et al., 2009; Winter et al., 2018)
F6P_a	(Kauffman et al., 1969; Cloutier et al., 2009;

	Winter et al., 2018)
FBP_n	(Byrne et al., 2014)
FBP_a	(Byrne et al., 2014)
f26bp_a	(Erecińska and Silver, 1994; Mulukutla et al., 2015)
GLY_a	(Cloutier et al., 2009; DiNuzzo et al., 2010; Waitt et al., 2017)
AMP_n	(Erecińska and Silver, 1989; Theurey et al., 2019)
AMP_a	(Erecińska and Silver, 1989; Theurey et al., 2019)
G1P_a	(Byrne et al., 2014)
GAP_n	(Tiveci et al., 2005; Cloutier et al., 2009; Jolivet et al., 2015)
GAP_a	(Tiveci et al., 2005; Cloutier et al., 2009; Jolivet et al., 2015)
DHAP_n	(Kauffman et al., 1969; Byrne et al., 2014)
DHAP_a	(Kauffman et al., 1969; Byrne et al., 2014)
BPG13_n	(Lambeth and Kushmerick, 2002; Shestov et al., 2007)
BPG13_a	(Lambeth and Kushmerick, 2002; Shestov et al., 2007)
NADH_a	(Jolivet et al., 2015; Park et al., 2016; Calvetti et al., 2018)
Pi_n	(Theurey et al., 2019)
Pi_a	(Theurey et al., 2019)
PG3_n	(Lambeth and Kushmerick, 2002; Berndt et al., 2015; Park et al., 2016)
PG3_a	(Lambeth and Kushmerick, 2002; Berndt et al., 2015; Park et al., 2016)
PG2_n	(Lambeth and Kushmerick, 2002; Berndt et al., 2015; Park et al., 2016)
PG2_a	(Lambeth and Kushmerick, 2002; Berndt et al., 2015; Park et al., 2016)
PEP_n	(Cloutier et al., 2009; Byrne et al., 2014; Jolivet et al., 2015)
PEP_a	(Cloutier et al., 2009; Byrne et al., 2014; Jolivet et al., 2015)
Pyr_n	(Lajtha and Reith, 2007; Byrne et al., 2014; Lerchundi et al., 2015; Calvetti et al., 2018;

	Muraleedharan et al., 2020)
Pyr_a	(Lajtha and Reith, 2007; Byrne et al., 2014; Lerchundi et al., 2015; Calvetti et al., 2018; Muraleedharan et al., 2020)
Lac_b	(Mächler et al., 2016; Calvetti et al., 2018)
Lac_ecs	(Mächler et al., 2016; Calvetti et al., 2018)
Lac_a	(Shestov et al., 2007; Calvetti et al., 2018)
Lac_n	(Shestov et al., 2007; Calvetti et al., 2018)
NADPH_n	(Winter et al., 2018; Bradshaw, 2019)
NADPH_a	(Winter et al., 2018; Bradshaw, 2019)
GL6P_n	(Winter et al., 2018)
GL6P_a	(Winter et al., 2018)
GO6P_n	(Gaitonde et al., 1989; Winter et al., 2018)
GO6P_a	(Winter et al., 2018)
RU5P_n	(Winter et al., 2018)
RU5P_a	(Winter et al., 2018)
R5P_n	(Winter et al., 2018)
R5P_a	(Winter et al., 2018)
X5P_n	(Winter et al., 2018)
X5P_a	(Winter et al., 2018)
S7P_n	(Winter et al., 2018)
S7P_a	(Winter et al., 2018)
E4P_n	(Winter et al., 2018)
E4P_a	(Winter et al., 2018)
GSH_n	(Vali et al., 2007; Koga et al., 2011; Duarte and Gruetter, 2013; Sedlak et al., 2019)
GSH_a	(Koga et al., 2011; McBean, 2017)
GSSG_n	(McBean, 2017)
GSSG_a	(McBean, 2017)
Cr_n	(Cloutier et al., 2009; Jolivet et al., 2015; Baeza-Lehnert et al., 2019)
PCr_n	(Cloutier et al., 2009; Jolivet et al., 2015; Baeza-Lehnert et al., 2019)
Cr_a	(Cloutier et al., 2009; Jolivet et al., 2015)
PCr_a	(Cloutier et al., 2009; Jolivet et al., 2015)
cAMP_a	(Coggan et al., 2018, 2020)

NE_neuromod	(Coggan et al., 2018, 2020)
UDPgluco_a	(Tsuboi et al., 1969; Park et al., 2016)
UTP_a	(Anderson and Wright, 1980; Park et al., 2016)
GS_a	(Xu et al., 2011; Coggan et al., 2020)
GPa_a	(Xu et al., 2011; Coggan et al., 2020)
GPb_a	(Xu et al., 2011; Coggan et al., 2020)

Supplementary Figures.

Supplementary Fig. 1. Validation, predicted energy budget. a, Simulated concentrations and the literature data. **b,** Comparison of ratios of model K_M to average mammalian data K_M for the same pairs enzyme-metabolite to min/mean and max/mean ratios of that mammalian data for the same pairs enzyme-metabolite, **c,** Lactate dynamics compared to simulation of the other model from the literature (Jolivet et al., 2015). **d,** BOLD dynamics (Jolivet et al., 2015; Winter et al., 2018; Jung et al., 2021). **e,** NADH dynamics in neuronal mitochondria compared to literature (Jolivet et al., 2015). **f,** NADH dynamics in astrocyte cytosol compared to literature (Jolivet et al., 2015). **g,** ATP consumption per AP in young and old ages.

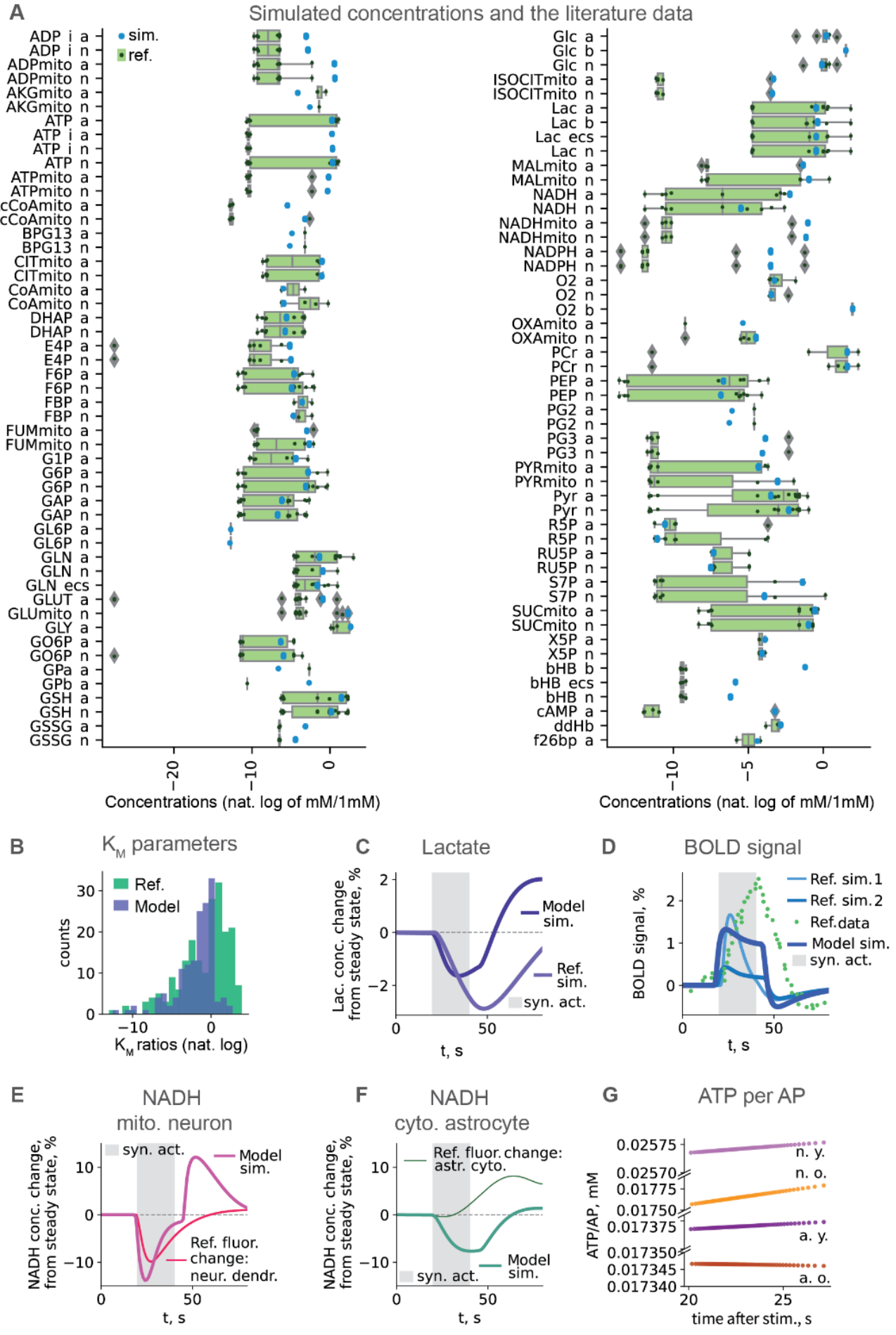

Supplementary Fig. 2. ATP production, glucose and lactate transport fluxes.

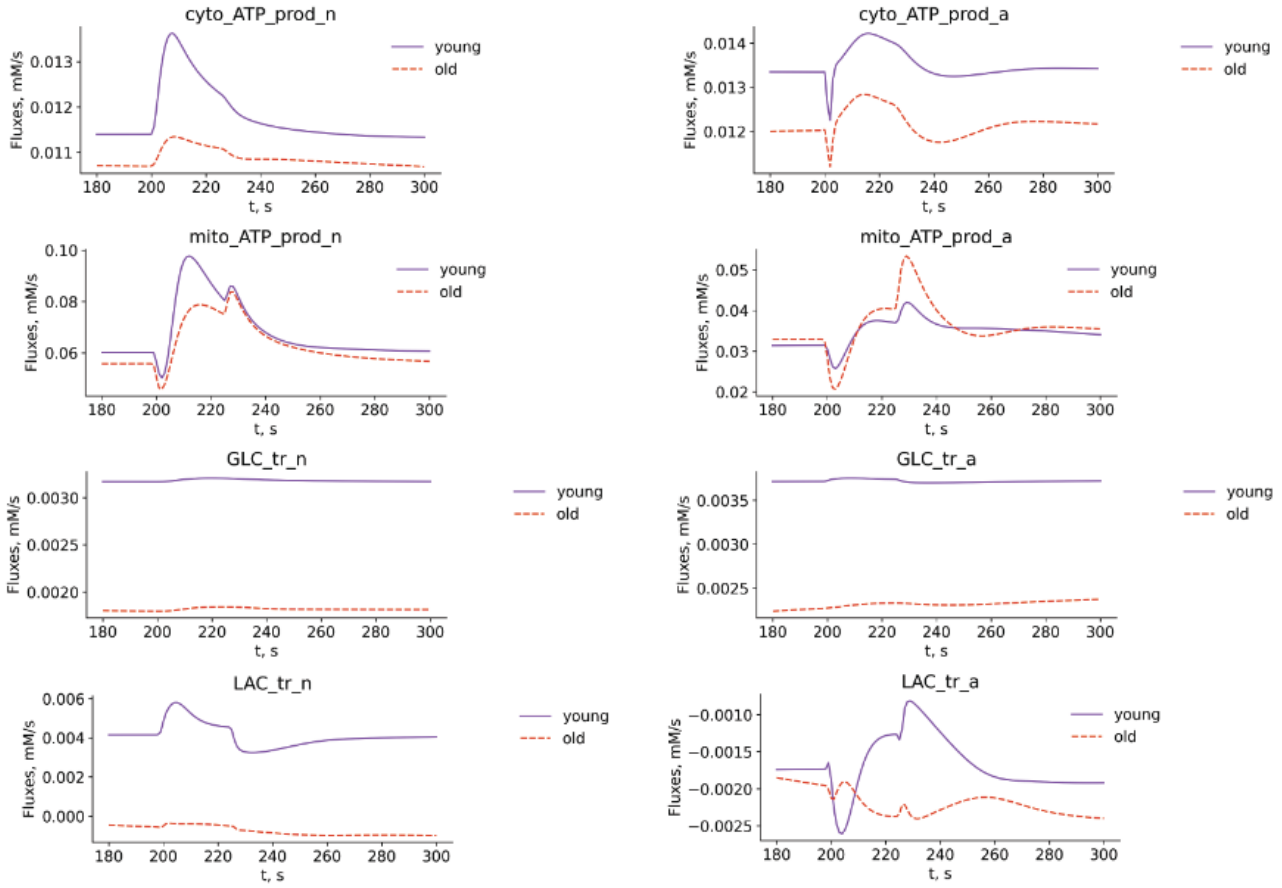

Supplementary Fig. 3. Differences between young and old in rest state concentrations (top) and in sum of relative deviations of concentration from rest (normalized by rest state) upon synaptic activation (bottom), both ranked by rest state differences (top), only top ranked are shown.

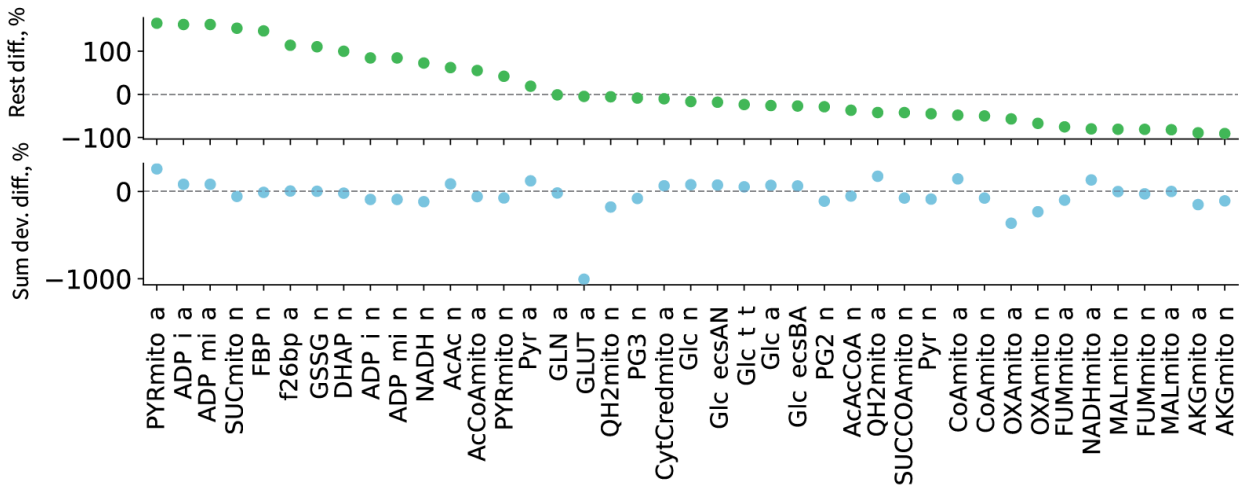

Supplementary Fig. 4. Comparison of amplitudes of metabolic response to synaptic activation in young and old ages (filtered by absolute values of deviations and difference in deviations of higher than 1%).

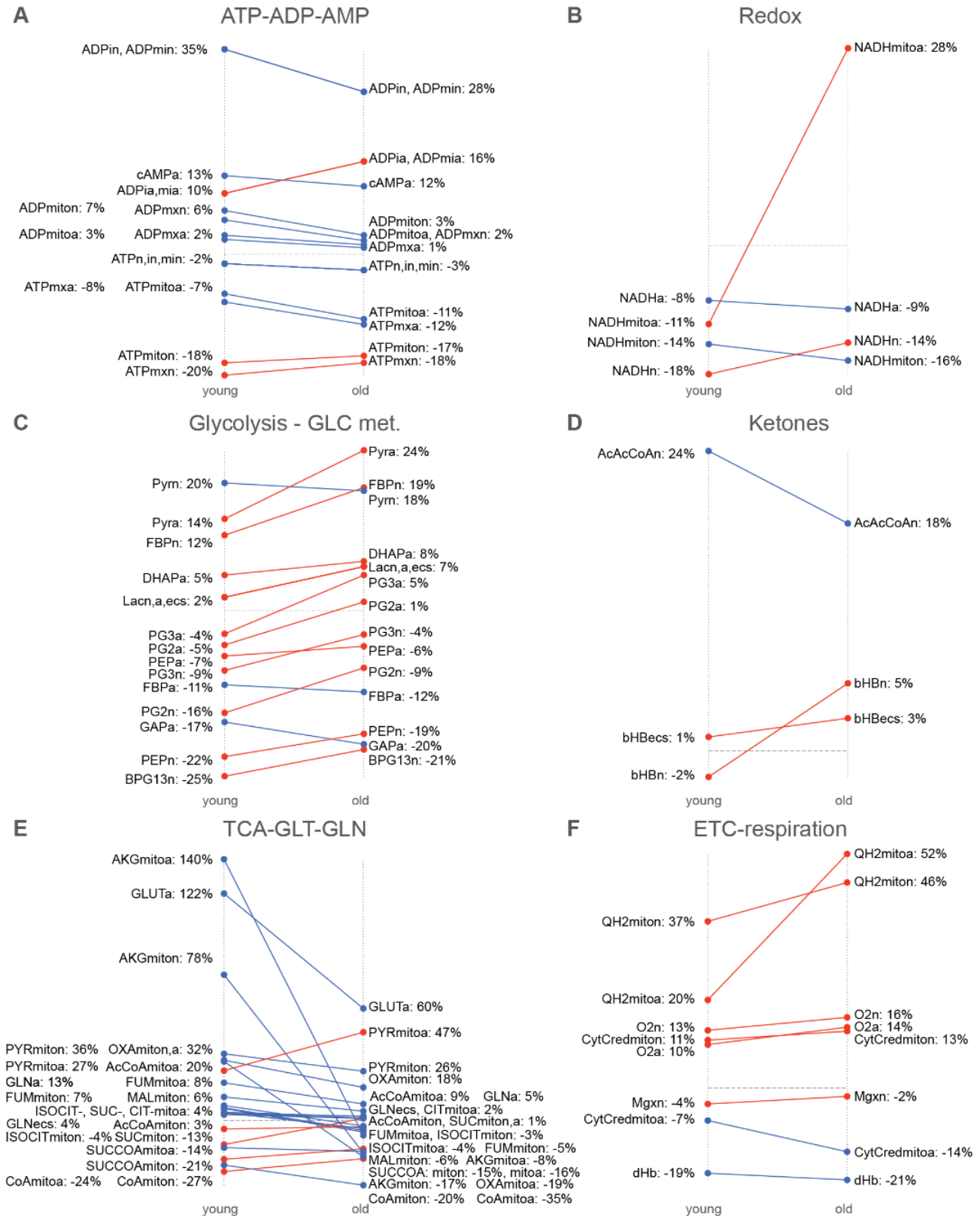

Supplementary Fig. 5. Train of APs evoked by 1 nA current injection simulations. **a,** Dynamics of metabolism in response to a train of APs evoked by current injection in different ages. **b,** Characteristics of neuronal firing in young and old ages evoked by current injection.

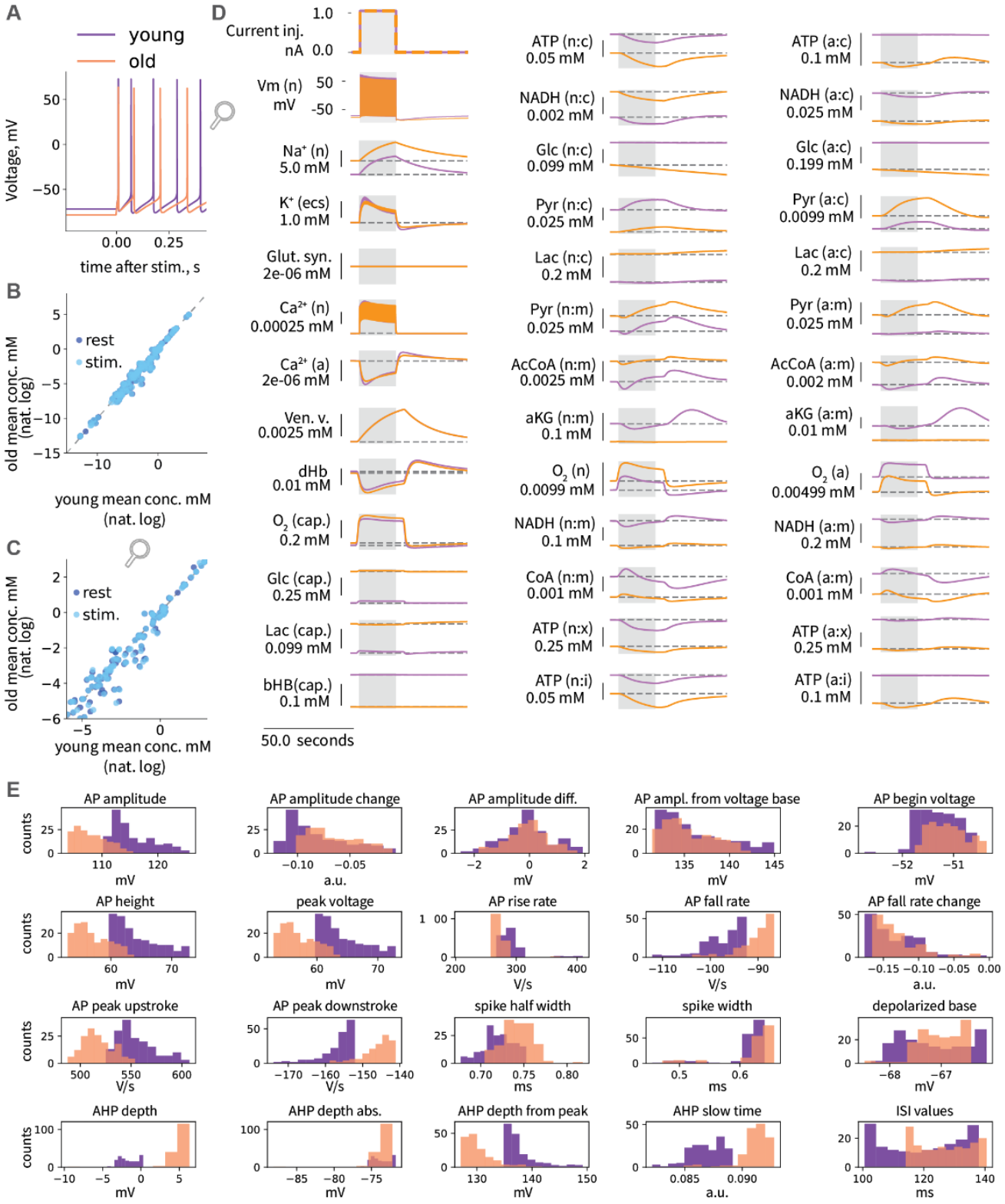

Supplementary Fig. 6. Aging-associated differences in range of response to the current injections of different amplitudes.

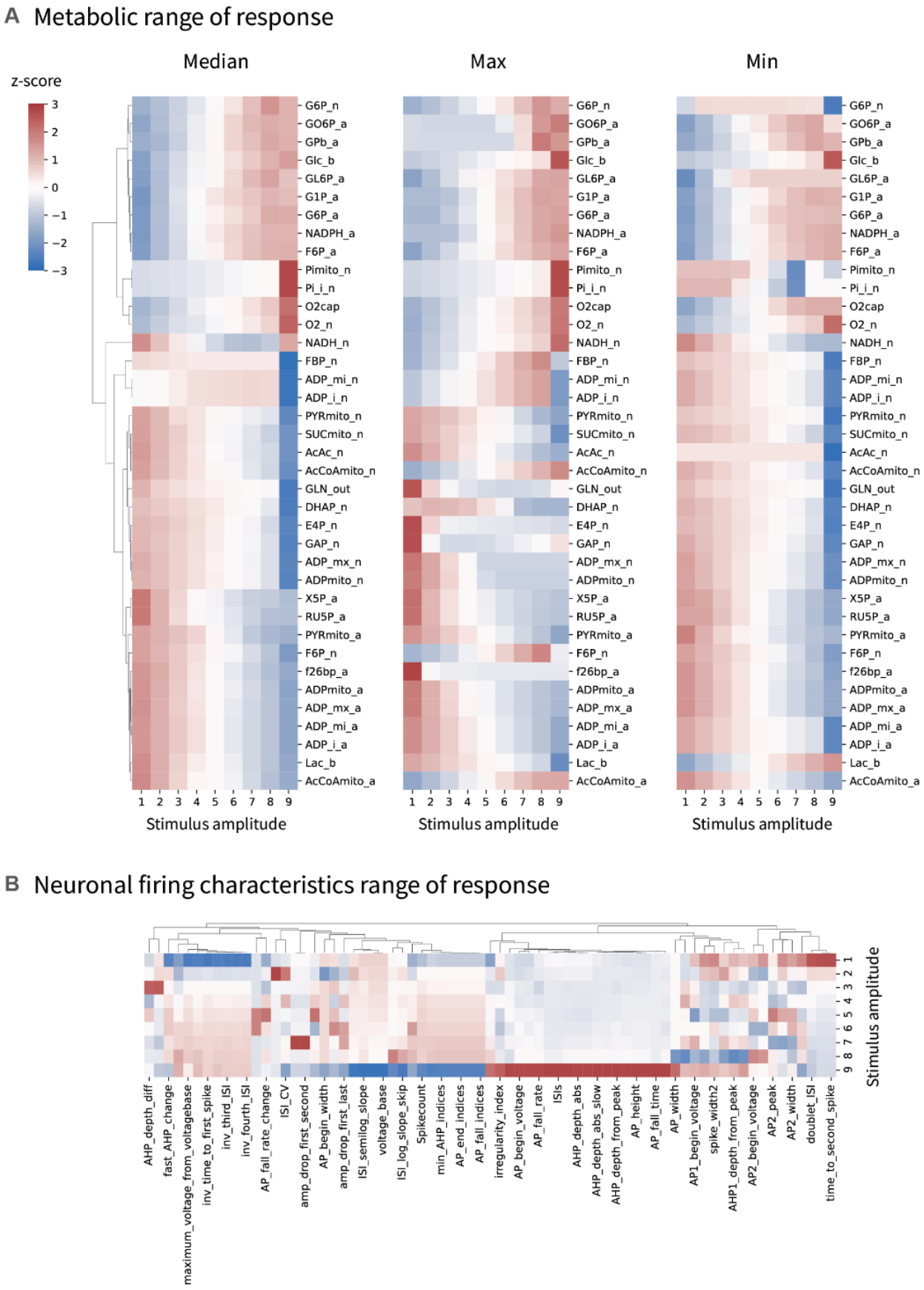

Supplementary Fig. 7. Dependence of metabolism and electrophysiology responses on the current injection amplitude in young and old ages. **a,** Young and old age responses to current injections of two different amplitudes: input current (top left in A), firing traces (left on second row in A), percent difference in metabolic response: 100*(m_IinjHigh - m_IinjLow)/m_IinjLow (all other figures in A). **b,** Characteristics of neuronal firing in young and old ages upon current injections of two different amplitudes.

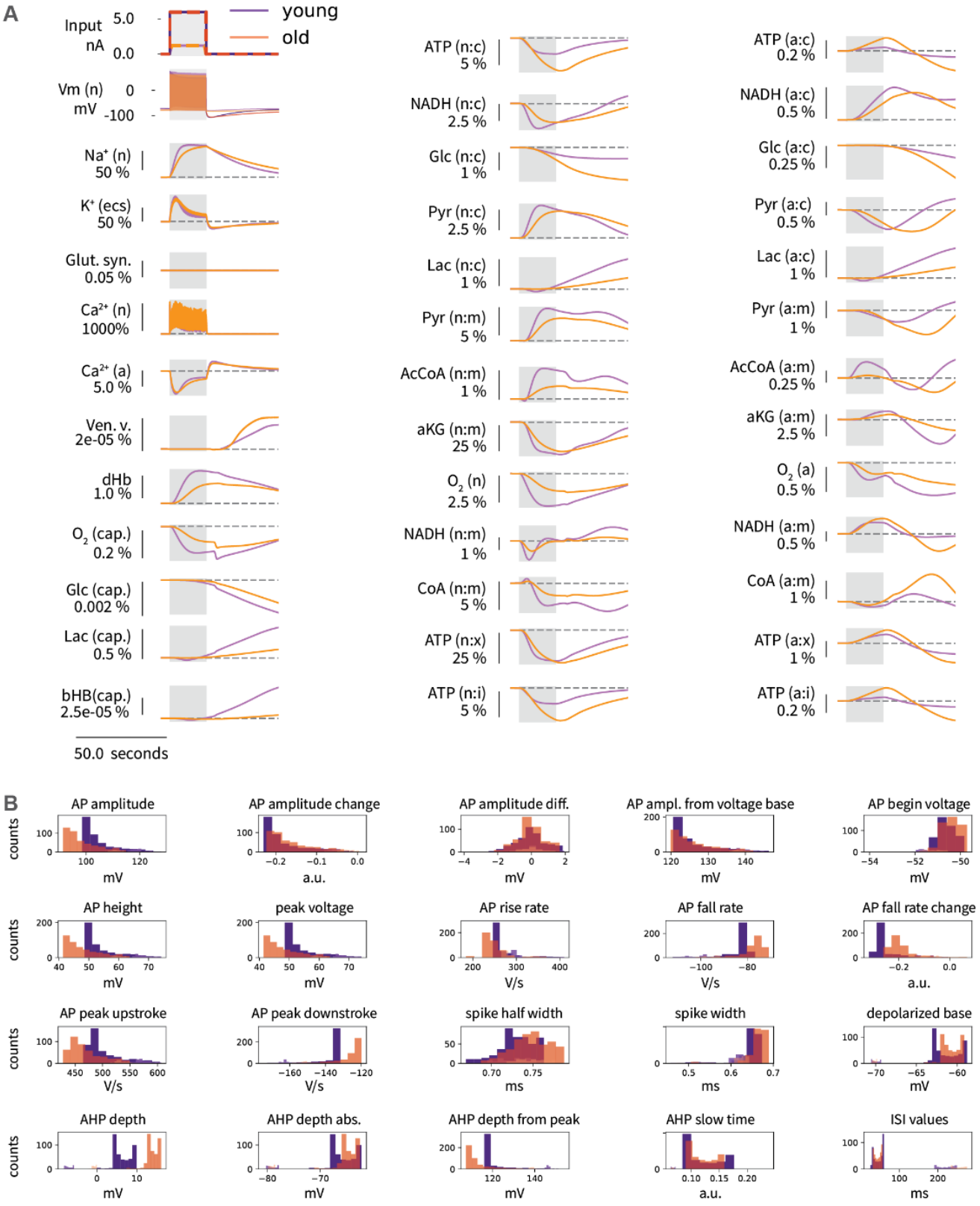

Supplementary Fig. 8. UMAP of relative differences in concentration traces in old compared to young.

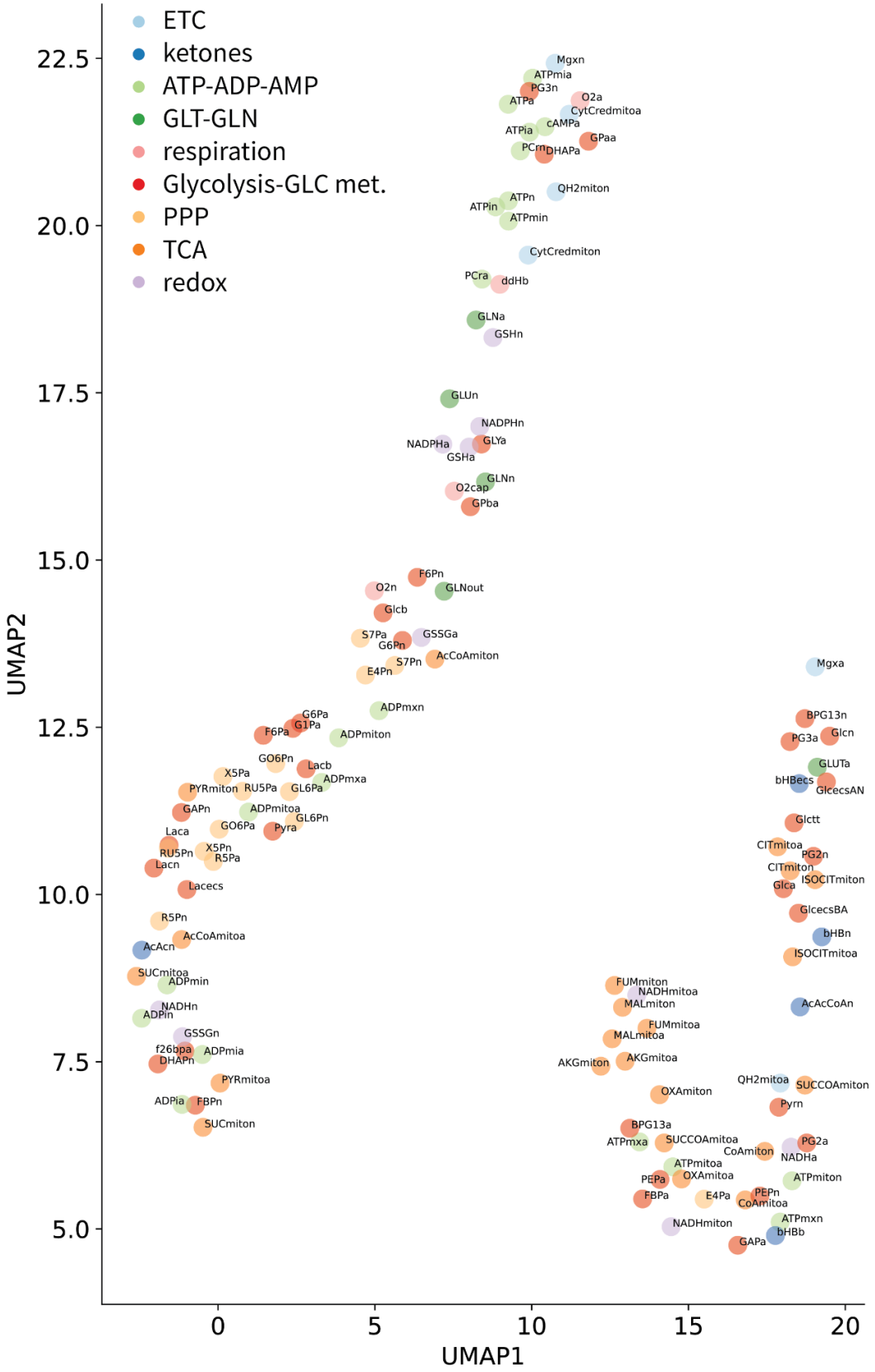

Supplementary Fig. 9. Kendall correlation of metabolite concentrations time series data in aging.

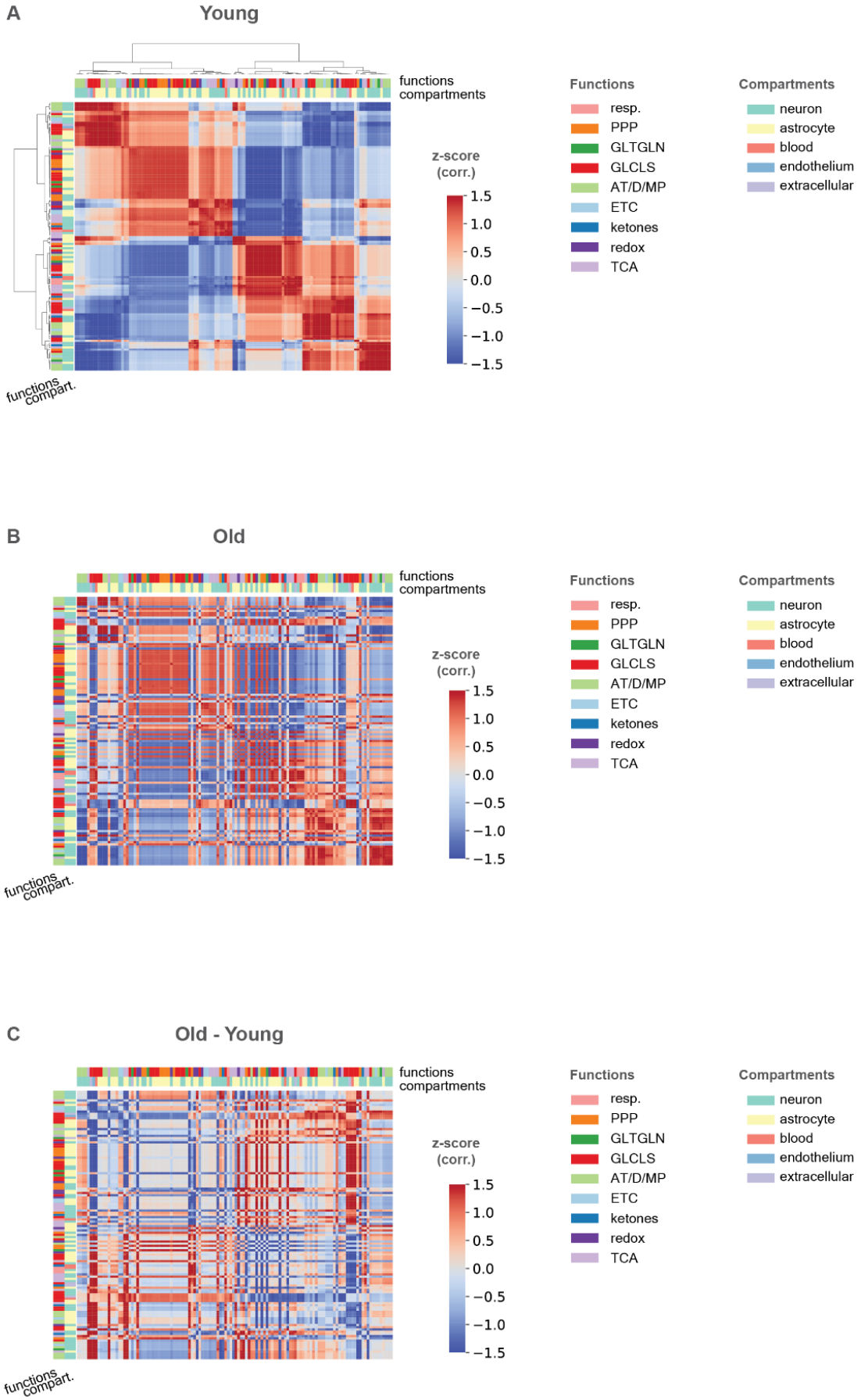

Supplementary Fig. 10. Cytosolic NADH fluxes.

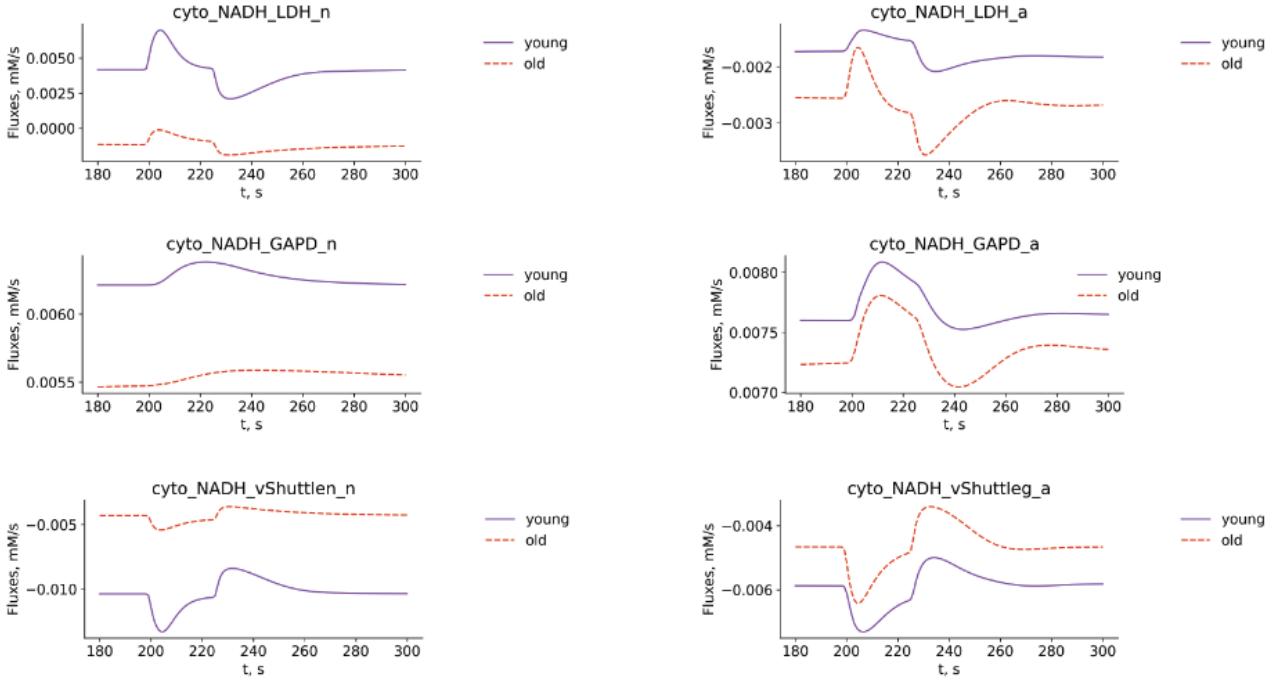

Supplementary Fig. 11. Cytosolic NADPH fluxes.

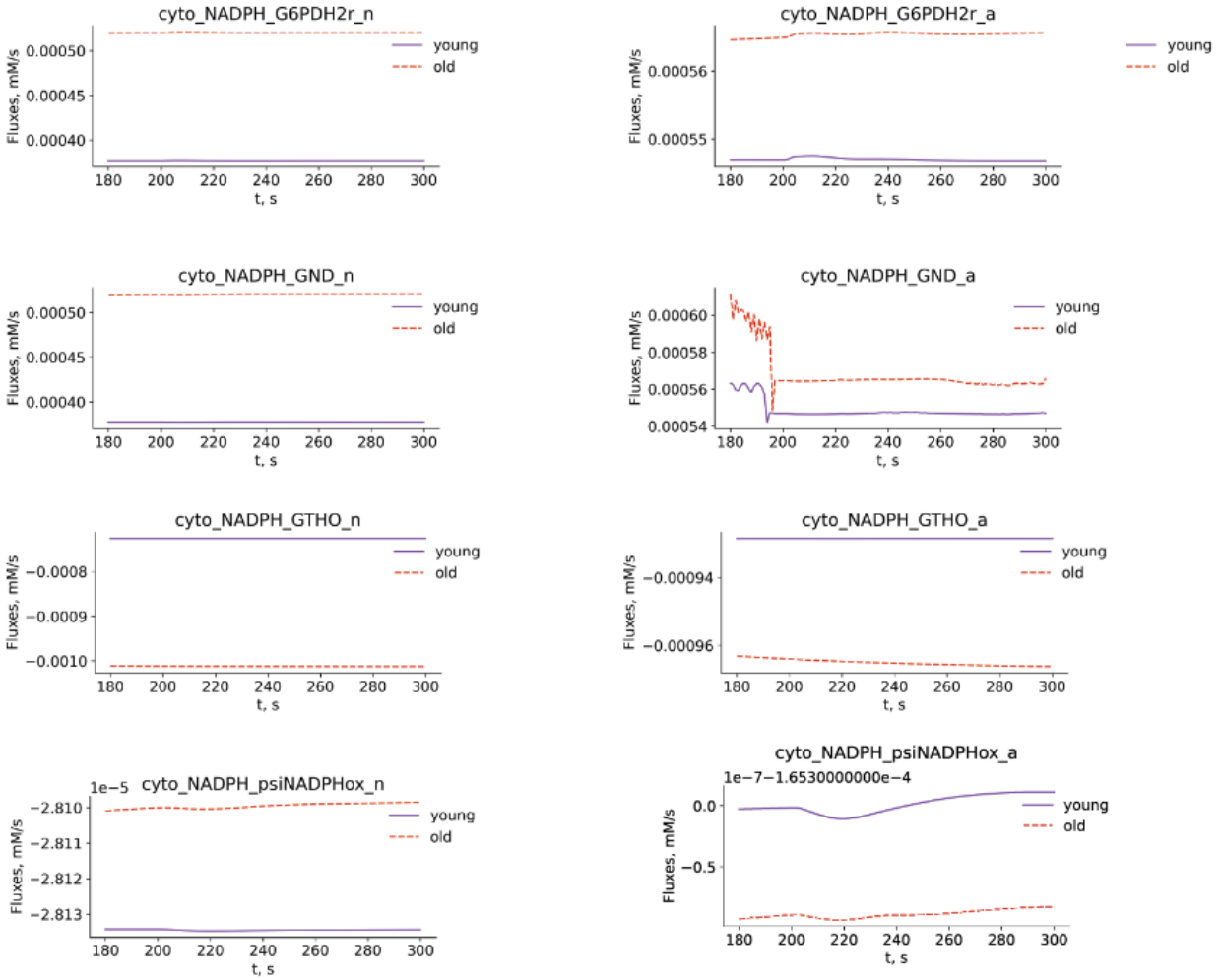

Supplementary Fig. 12. Mitochondrial NADH fluxes.

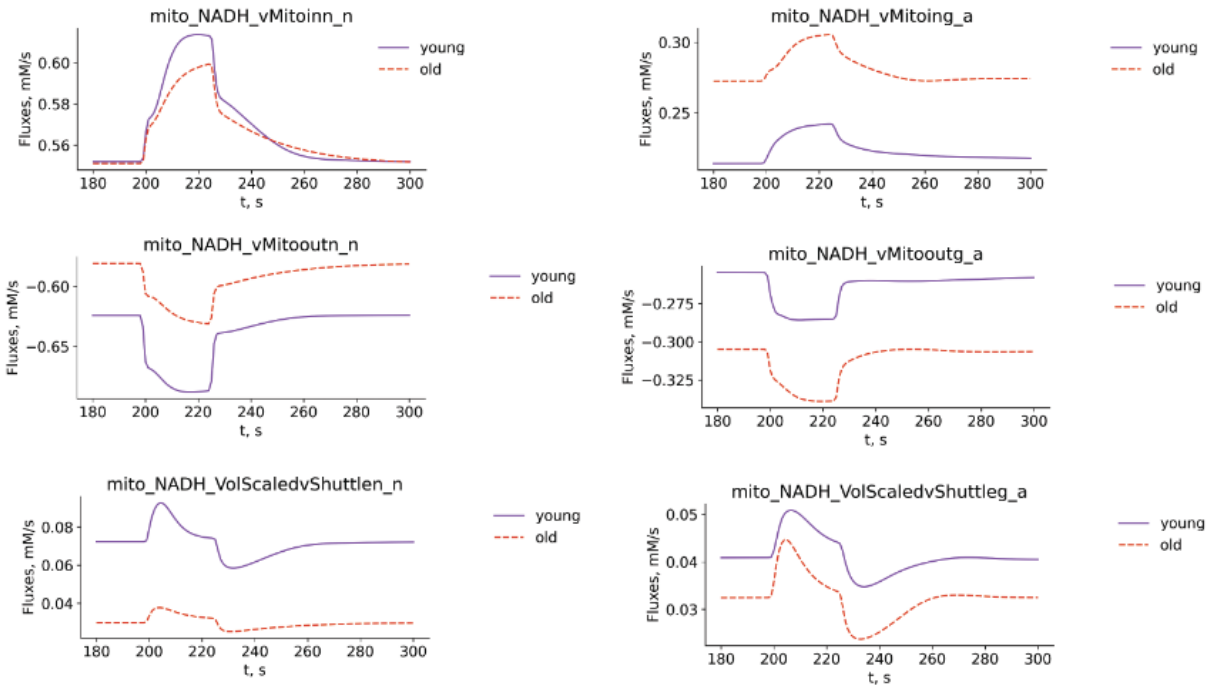

Supplementary Fig. 13. Lactate shuttle in conditions with different blood glucose levels.

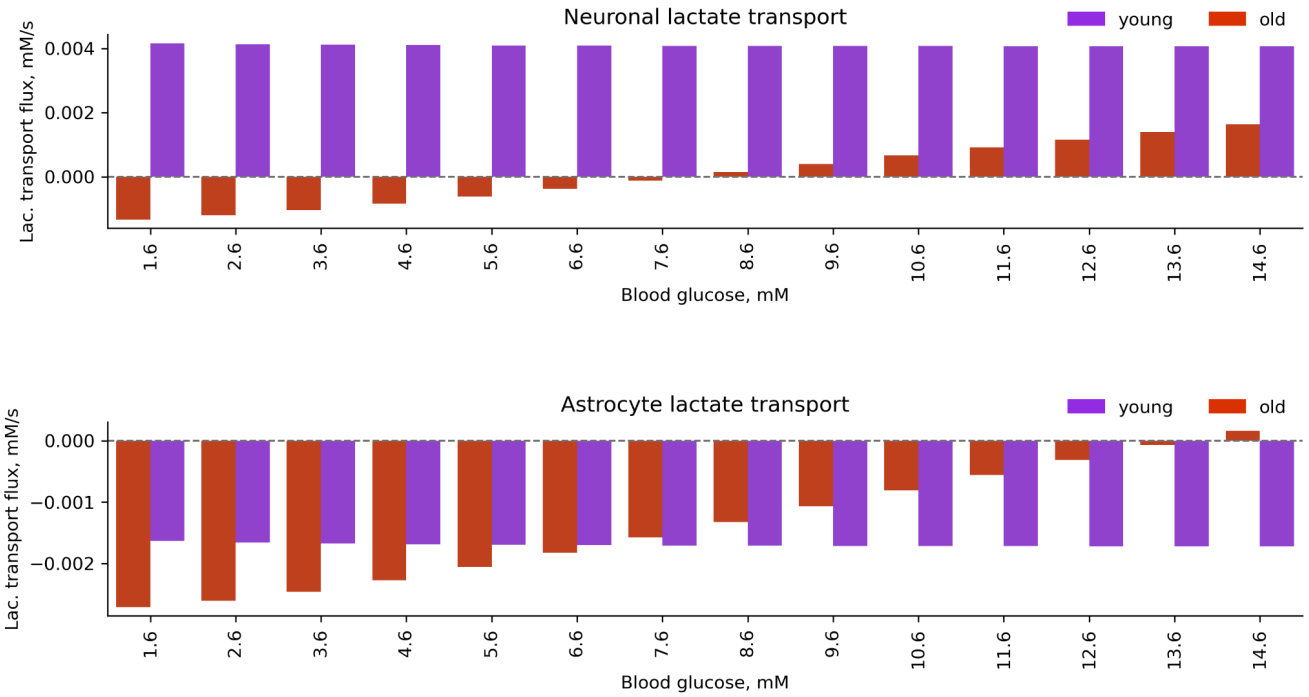

Supplementary Fig. 14. Comparison of synaptic activation and current injection evoked metabolic responses. **a,** Young and old age responses to synaptic input and current injection (approximately the same firing frequency): input current (top left in A), firing traces (left on second row in A), percent difference in metabolic response: 100*(m_Iinj - m_syn)/m_syn (all other figures in A). **b,** Characteristics of neuronal firing in young and old ages upon synaptic activation and current injection (approximately the same firing frequency).

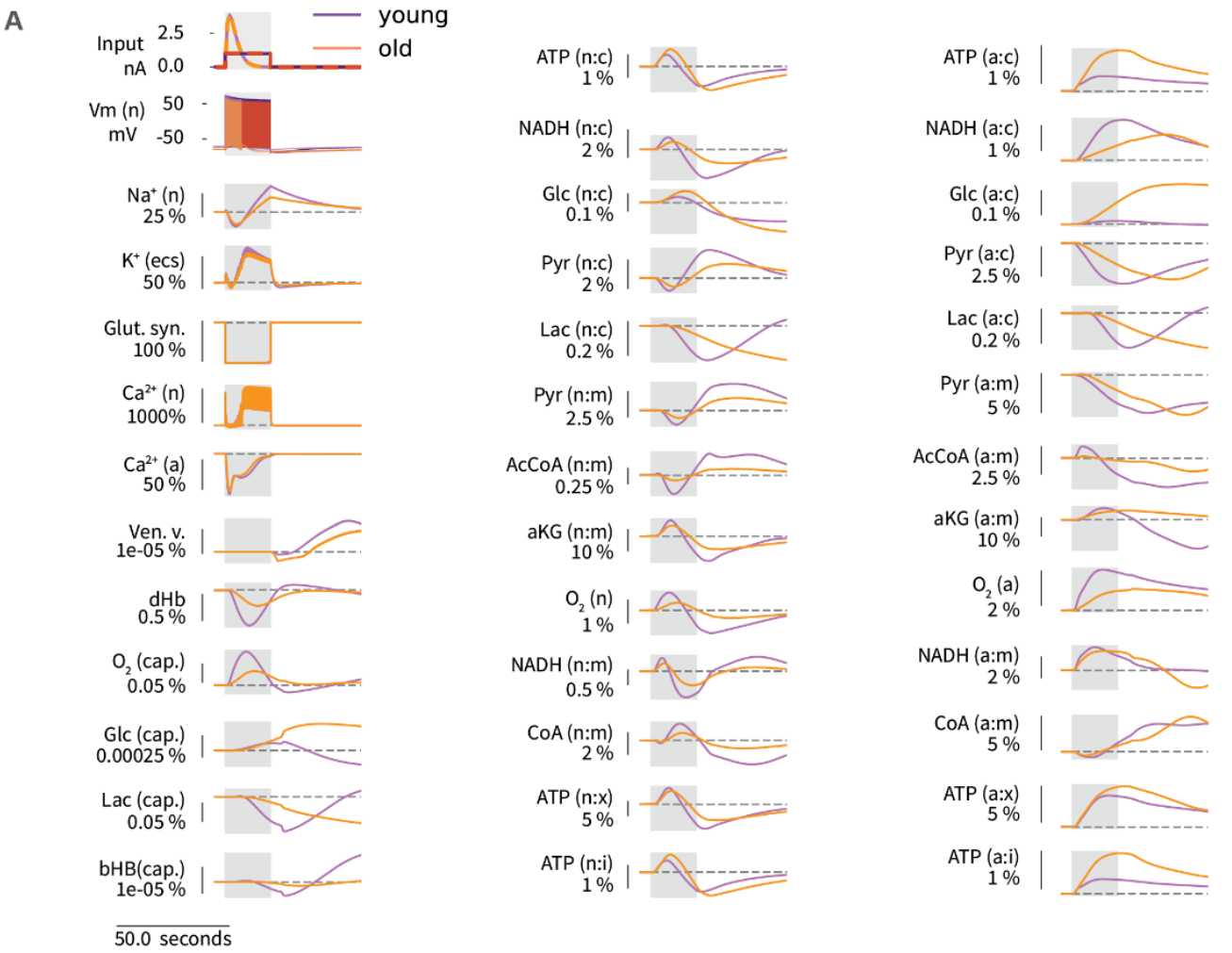

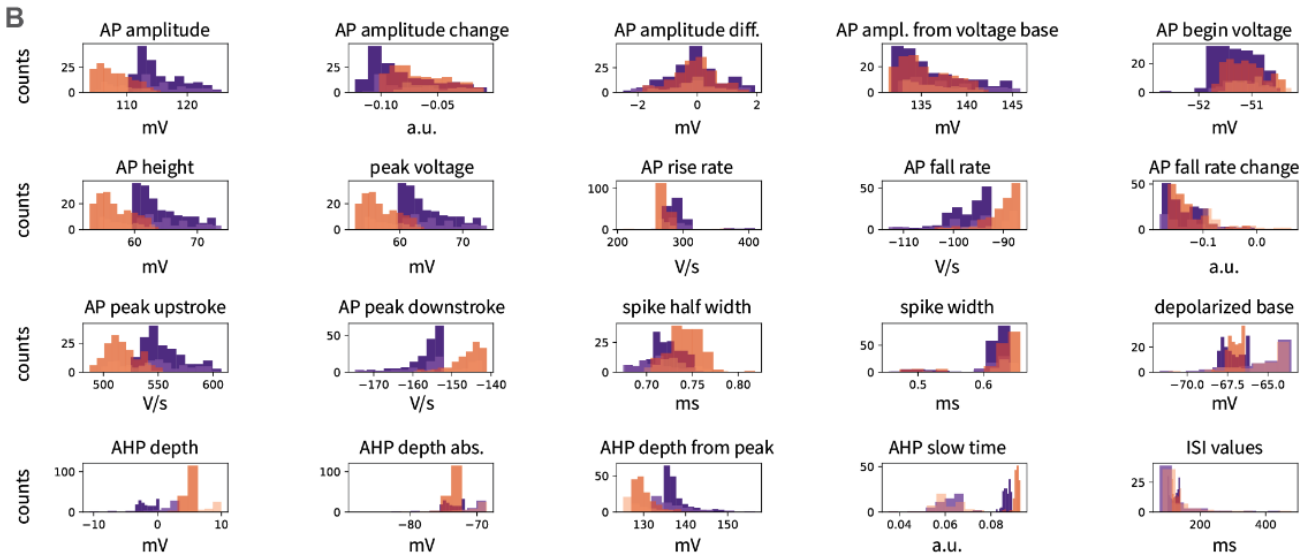

Supplementary Fig. 15. Sensitivities curve fit.

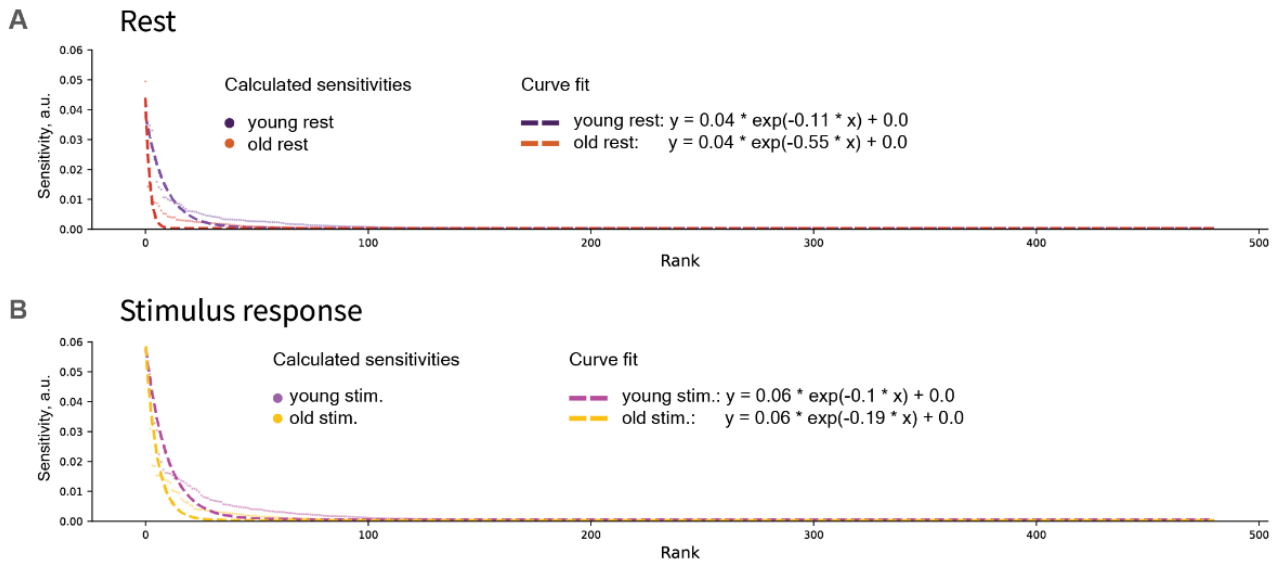

Supplementary Fig. 16. Metabolic responsivity difference.

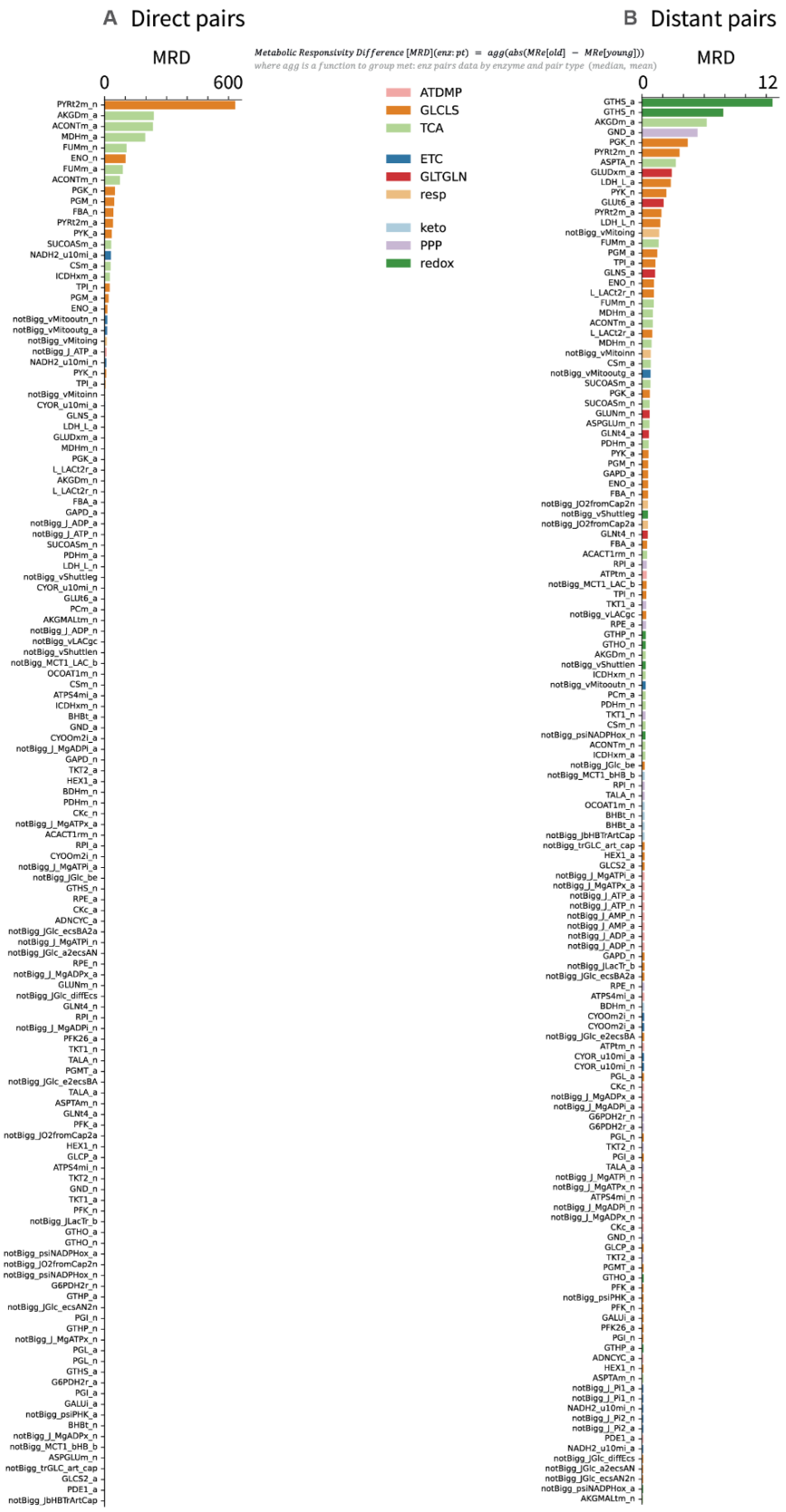

Supplementary Fig. 17. Bottom-up iterative model building workflow and the key considerations.

Supplementary Fig. 18. Labels of individual metabolites for **Fig. 3d**.

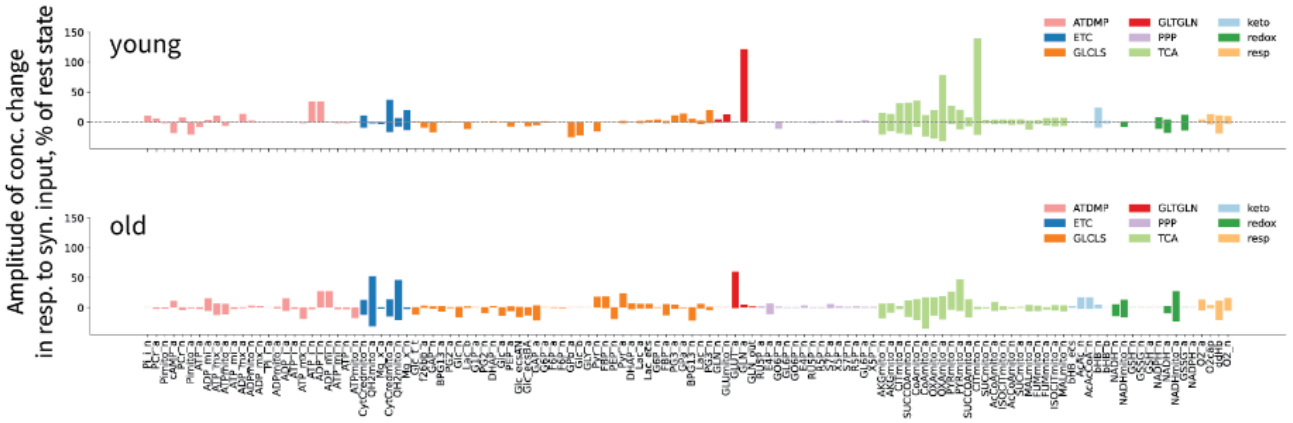

Supplementary Fig. 19. Literature evidence for ESRRA being a regulatory hub of aging-associated pathways (colored by reference).

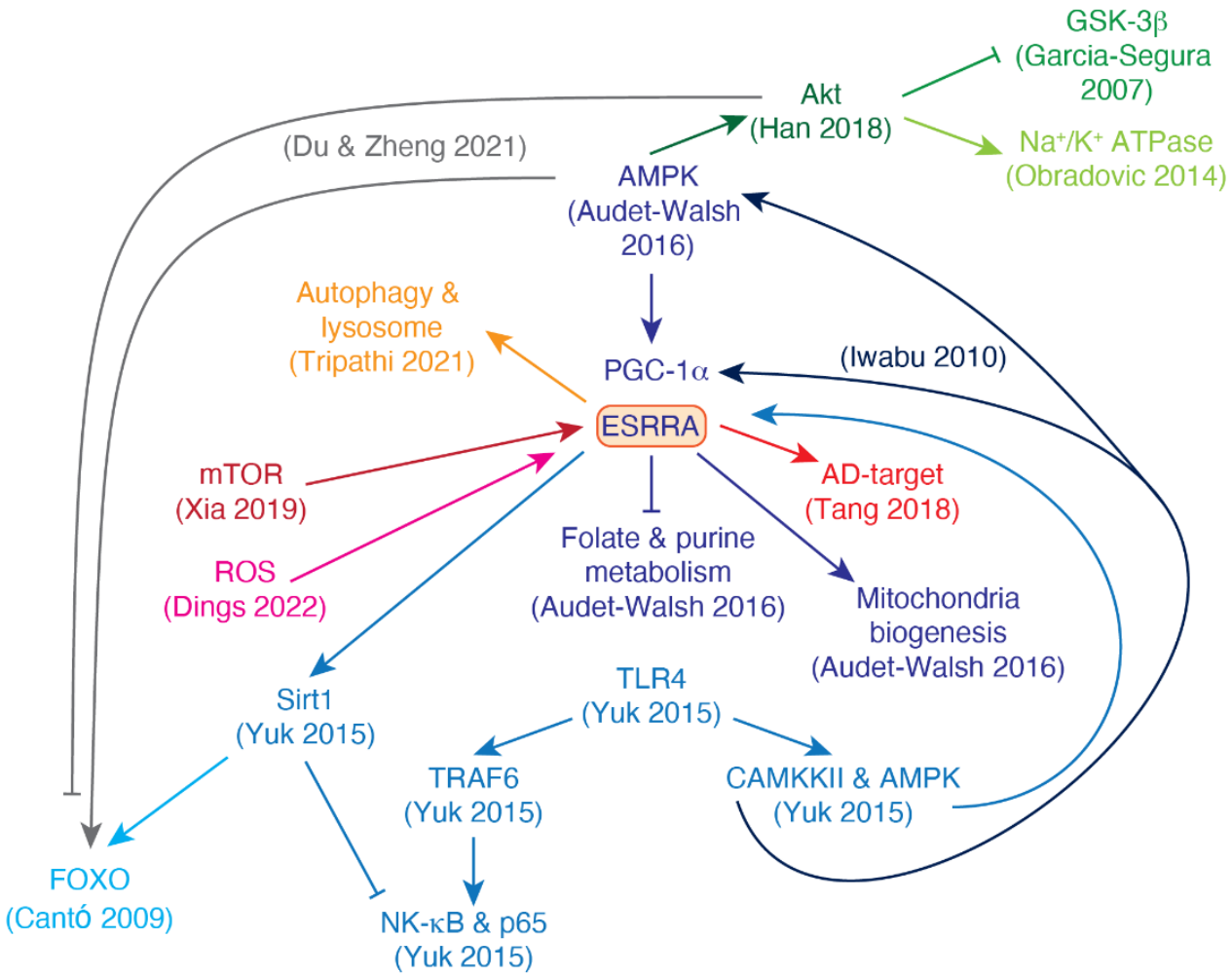

Supplementary Information File 1.

Explanation of the Fruchterman-Reingold force-directed algorithm to position nodes

The Fruchterman-Reingold force-directed algorithm is used for a representation of the network. Edges correspond to springs which are holding nodes close, and nodes correspond to repelling objects. There are two types of forces which define the position of nodes as described below.

1. Attractive force, which acts between nodes that are connected by an edge. It is stronger for nodes connected by higher-weight edges, so these nodes are pulled closer together by the attractive force.
2. Repulsive force, which acts between all pairs of nodes (regardless of connecting edge presence). This force pushes nodes away from each other.

So the resulting edge lengths are not directly proportional to the weights. Instead, the edge weight affects the strength of the attractive force between connected nodes, where larger weight of edge (which in our case corresponds to smaller metabolic responsivity) means a stronger attractive force, and nodes being pulled together.

Closeness centrality in context of metabolic responsivity

Closeness centrality (CC) is calculated as a reciprocal of the sum of shortest path distances between the node and all other nodes. Higher centrality means smaller metabolic responsivity: CC is reciprocal to distance, while distance is reciprocal to weight, which makes CC proportional to the weight, while weight is defined as reciprocal of metabolic responsivity, which makes CC reciprocal of metabolic responsivity (Equation 1).

$$CC \sim \frac{1}{distance} = \frac{1}{\frac{1}{weight}} = weight = 1/MR \quad \text{(Equation 1)}$$

Supplementary Information File 2.

Changes in other characteristics of neuronal firing (related to Fig.3):

AHP1_depth_from_peak: -7.42%, old: 144.86, young: 156.48

AHP2_depth_from_peak: -7.23%, old: 140.48, young: 151.42

AP1_amp: -8.5%, old: 114.94, young: 125.62

AP1_begin_voltage: -0.35%, old: -51.64, young: -51.82

AP1_begin_width: 0.0%, old: 1.3, young: 1.3

AP1_peak: -14.23%, old: 63.3, young: 73.81

AP1_width: 3.59%, old: 0.76, young: 0.73

AP2_AP1_begin_width_diff: nan%, old: 0.0, young: 0.0

AP2_AP1_diff: -31.37%, old: -1.04, young: -1.52

AP2_AP1_peak_diff: -53.87%, old: -0.49, young: -1.05

AP2_amp: -8.22%, old: 113.9, young: 124.1

AP2_begin_voltage: -0.53%, old: -51.08, young: -51.35

AP2_begin_width: 0.0%, old: 1.3, young: 1.3

AP2_peak: -13.66%, old: 62.82, young: 72.75

AP2_width: 3.46%, old: 0.72, young: 0.7

APlast_amp: -6.17%, old: 105.99, young: 112.96

APlast_width: 3.5%, old: 0.79, young: 0.76

ISI_CV: -2.13%, old: 0.57, young: 0.58

ISI_log_slope: -0.57%, old: 0.16, young: 0.17

ISI_log_slope_skip: 0.24%, old: 0.22, young: 0.22

ISI_semilog_slope: 6.44%, old: 0.02, young: 0.02

Spikecount: -8.47%, old: 54, young: 59

Spikecount_stimint: -8.47%, old: 54, young: 59

adaptation_index: 11.23%, old: 0.01, young: 0.01

adaptation_index2: 11.31%, old: 0.01, young: 0.01

amp_drop_first_last: -29.32%, old: 8.64, young: 12.23

amp_drop_first_second: -53.87%, old: 0.49, young: 1.05

amp_drop_second_last: -27.0%, old: 8.16, young: 11.17

decay_time_constant_after_stim: -91.66%, old: 1603.71, young: 19220.41

doublet_ISI: 5.9%, old: 195.7, young: 184.8

inv_fifth_ISI: -6.26%, old: 8.94, young: 9.53

inv_first_ISI: -5.57%, old: 5.11, young: 5.41

inv_fourth_ISI: -6.06%, old: 8.31, young: 8.84

inv_last_ISI: -7.22%, old: 2.09, young: 2.26

inv_second_ISI: -5.68%, old: 6.53, young: 6.92

inv_third_ISI: -5.8%, old: 7.53, young: 7.99

inv_time_to_first_spike: -33.47%, old: 6.0, young: 9.02

irregularity_index: 16.38%, old: 8.87, young: 7.62

max_amp_difference: -16.07%, old: 1.14, young: 1.35

maximum_voltage: -14.23%, old: 63.3, young: 73.81

maximum_voltage_from_voltagebase: -2.75%, old: 141.84, young: 145.86

mean_AP_amplitude: -6.7%, old: 108.94, young: 116.76

mean_frequency: -8.46%, old: 7.55, young: 8.25

minimum_voltage: 3.33%, old: -85.43, young: -82.68

number_initial_spikes: -10.0%, old: 18, young: 20

steady_state_hyper: 6.37%, old: -85.14, young: -80.05

steady_state_voltage: 8.57%, old: -83.27, young: -76.7

time_to_first_spike: 50.32%, old: 166.7, young: 110.9

time_to_last_spike: -0.02%, old: 7150.2, young: 7151.4

time_to_second_spike: 22.56%, old: 362.4, young: 295.7

trace_check: nan%, old: 0, young: 0

voltage_base: 9.0%, old: -78.54, young: -72.05

Statistical tests for comparison of characteristics of neuronal firing (Figure 3).

AP_amplitude

Levene statistic: 6.605499030481687 p-value: 0.011491236053743635

Levene: different variances (reject H0)

Fligner statistic: 6.630869011027655 p-value: 0.01002263560239055

Fligner: different variances (reject H0)

Wilcoxon-Mann-Whitney U test statistic: 3057.0 p-value: 4.0249411168018834e-17

Wilcoxon-Mann-Whitney U test: different distributions (reject H0)

Kolmogorov-Smirnov statistic: 0.834902699309479 p-value: 6.661338147750939e-16

Kolmogorov-Smirnov: different distributions (reject H0)

AP_amplitude_change

Levene statistic: 3.8760940845777174 p-value: 0.051516931692045034

Levene: same variances (fail to reject H0)

Fligner statistic: 4.545621778929398 p-value: 0.033003033701898096

Fligner: different variances (reject H0)

Wilcoxon-Mann-Whitney U test statistic: 920.0 p-value: 0.0002729809833335603

Wilcoxon-Mann-Whitney U test: different distributions (reject H0)

Kolmogorov-Smirnov statistic: 0.42940793754066364 p-value: 3.8705542437011964e-05

Kolmogorov-Smirnov: different distributions (reject H0)

AP_amplitude_diff

Levene statistic: 6.152257861376695 p-value: 0.014653671953606095

Levene: different variances (reject H0)

Fligner statistic: 5.75689520557301 p-value: 0.016424069262576897

Fligner: different variances (reject H0)

Wilcoxon-Mann-Whitney U test statistic: 1491.0 p-value: 0.7882208195357832

Wilcoxon-Mann-Whitney U test: same distribution (fail to reject H0)

Kolmogorov-Smirnov statistic: 0.1486662329212752 p-value: 0.5084641118074855

Kolmogorov-Smirnov: same distribution (fail to reject H0)

AP_amplitude_from_voltagebase

Levene statistic: 7.459710428818111 p-value: 0.007341447281952335

Levene: different variances (reject H0)

Fligner statistic: 7.391190337972734 p-value: 0.006554409829916771

Fligner: different variances (reject H0)

Wilcoxon-Mann-Whitney U test statistic: 1862.0 p-value: 0.12275003593521057

Wilcoxon-Mann-Whitney U test: same distribution (fail to reject H0)

Kolmogorov-Smirnov statistic: 0.1864406779661017 p-value: 0.23771345375057895

Kolmogorov-Smirnov: same distribution (fail to reject H0)

AP_begin_voltage

Levene statistic: 0.3716334196659708 p-value: 0.5433611341543954

Levene: same variances (fail to reject H0)

Fligner statistic: 0.3123751596228548 p-value: 0.5762263366963747

Fligner: same variances (fail to reject H0)

Wilcoxon-Mann-Whitney U test statistic: 1226.0 p-value: 0.03514923245426359

Wilcoxon-Mann-Whitney U test: different distributions (reject H0)

Kolmogorov-Smirnov statistic: 0.21876961707470183 p-value: 0.1096654688128944

Kolmogorov-Smirnov: same distribution (fail to reject H0)

AP_height

Levene statistic: 7.459710428818096 p-value: 0.007341447281952389

Levene: different variances (reject H0)

Fligner statistic: 7.391190337972734 p-value: 0.006554409829916771

Fligner: different variances (reject H0)

Wilcoxon-Mann-Whitney U test statistic: 3079.0 p-value: 1.3582777666804203e-17

Wilcoxon-Mann-Whitney U test: different distributions (reject H0)

Kolmogorov-Smirnov statistic: 0.8549905838041432 p-value: 6.661338147750939e-16

Kolmogorov-Smirnov: different distributions (reject H0)

peak_voltage

Levene statistic: 7.459710428818096 p-value: 0.007341447281952389

Levene: different variances (reject H0)

Fligner statistic: 7.391190337972734 p-value: 0.006554409829916771

Fligner: different variances (reject H0)

Wilcoxon-Mann-Whitney U test statistic: 3079.0 p-value: 1.3582777666804203e-17

Wilcoxon-Mann-Whitney U test: different distributions (reject H0)

Kolmogorov-Smirnov statistic: 0.8549905838041432 p-value: 6.661338147750939e-16

Kolmogorov-Smirnov: different distributions (reject H0)

AP_rise_rate

Levene statistic: 3.2120282887999094 p-value: 0.07582303196261797

Levene: same variances (fail to reject H0)

Fligner statistic: 8.500912633404996 p-value: 0.003549683927627355

Fligner: different variances (reject H0)

Wilcoxon-Mann-Whitney U test statistic: 3008.0 p-value: 4.274566678078413e-16

Wilcoxon-Mann-Whitney U test: different distributions (reject H0)

Kolmogorov-Smirnov statistic: 0.8163841807909604 p-value: 6.661338147750939e-16

Kolmogorov-Smirnov: different distributions (reject H0)

AP_fall_rate

Levene statistic: 3.066184321429485 p-value: 0.08269937892109969

Levene: same variances (fail to reject H0)

Fligner statistic: 6.71176089244189 p-value: 0.0095779100160061

Fligner: different variances (reject H0)

Wilcoxon-Mann-Whitney U test statistic: 442.0 p-value: 3.7647624938176844e-11

Wilcoxon-Mann-Whitney U test: different distributions (reject H0)

Kolmogorov-Smirnov statistic: 0.7052730696798494 p-value: 3.952393967665557e-14

Kolmogorov-Smirnov: different distributions (reject H0)

AP_fall_rate_change

Levene statistic: 0.6190034404678872 p-value: 0.433125124634122

Levene: same variances (fail to reject H0)

Fligner statistic: 3.187363730600531 p-value: 0.0742095978425819

Fligner: same variances (fail to reject H0)

Wilcoxon-Mann-Whitney U test statistic: 351.0 p-value: 2.5793688476458548e-12

Wilcoxon-Mann-Whitney U test: different distributions (reject H0)

Kolmogorov-Smirnov statistic: 0.8103448275862069 p-value: 1.775156606426841e-20

Kolmogorov-Smirnov: different distributions (reject H0)

AP_peak_upstroke

Levene statistic: 4.408526533521235 p-value: 0.038025854014361024

Levene: different variances (reject H0)

Fligner statistic: 4.601321053363534 p-value: 0.03194732985273627

Fligner: different variances (reject H0)

Wilcoxon-Mann-Whitney U test statistic: 3064.0 p-value: 2.853607187168821e-17

Wilcoxon-Mann-Whitney U test: different distributions (reject H0)

Kolmogorov-Smirnov statistic: 0.7919020715630886 p-value: 6.661338147750939e-16

Kolmogorov-Smirnov: different distributions (reject H0)

AP_peak_downstroke

Levene statistic: 1.2715834062751352 p-value: 0.2619014544184533

Levene: same variances (fail to reject H0)

Fligner statistic: 1.6194972442709932 p-value: 0.2031619039342202

Fligner: same variances (fail to reject H0)

Wilcoxon-Mann-Whitney U test statistic: 239.0 p-value: 7.258645224012553e-15

Wilcoxon-Mann-Whitney U test: different distributions (reject H0)

Kolmogorov-Smirnov statistic: 0.834902699309479 p-value: 6.661338147750939e-16

Kolmogorov-Smirnov: different distributions (reject H0)

spike_half_width

Levene statistic: 0.8356847163178224 p-value: 0.36261535212273177

Levene: same variances (fail to reject H0)

Fligner statistic: 0.9340883843599507 p-value: 0.3338028095263355

Fligner: same variances (fail to reject H0)

Wilcoxon-Mann-Whitney U test statistic: 716.0 p-value: 4.7016301099113494e-07

Wilcoxon-Mann-Whitney U test: different distributions (reject H0)

Kolmogorov-Smirnov statistic: 0.5266792215944758 p-value: 1.0318489573890588e-07

Kolmogorov-Smirnov: different distributions (reject H0)

spike_width2

Levene statistic: 0.4059195398968852 p-value: 0.5253838004179687

Levene: same variances (fail to reject H0)

Fligner statistic: 0.8000585301188278 p-value: 0.3710758705566992

Fligner: same variances (fail to reject H0)

Wilcoxon-Mann-Whitney U test statistic: 728.0 p-value: 1.8132084872745687e-06

Wilcoxon-Mann-Whitney U test: different distributions (reject H0)

Kolmogorov-Smirnov statistic: 0.4362394274560833 p-value: 2.7784173407874313e-05

Kolmogorov-Smirnov: different distributions (reject H0)

depolarized_base

Levene statistic: 0.21330792406056287 p-value: 0.6451074156436485

Levene: same variances (fail to reject H0)

Fligner statistic: 0.5099912340048506 p-value: 0.47514265083983753

Fligner: same variances (fail to reject H0)

Wilcoxon-Mann-Whitney U test statistic: 1622.0 p-value: 0.617871778194361

Wilcoxon-Mann-Whitney U test: same distribution (fail to reject H0)

Kolmogorov-Smirnov statistic: 0.1724137931034483 p-value: 0.3298788555460255

Kolmogorov-Smirnov: same distribution (fail to reject H0)

AHP_depth

Levene statistic: 0.08022401294287185 p-value: 0.7775216314033404

Levene: same variances (fail to reject H0)

Fligner statistic: 0.10770161746045517 p-value: 0.7427761389915951

Fligner: same variances (fail to reject H0)

Wilcoxon-Mann-Whitney U test statistic: 271.0 p-value: 3.055267399749676e-14

Wilcoxon-Mann-Whitney U test: different distributions (reject H0)

Kolmogorov-Smirnov statistic: 0.8518518518518519 p-value: 6.661338147750939e-16

Kolmogorov-Smirnov: different distributions (reject H0)

AHP_depth_abs

Levene statistic: 0.08022401294287124 p-value: 0.7775216314033404

Levene: same variances (fail to reject H0)

Fligner statistic: 0.10770132317169079 p-value: 0.7427764779807888

Fligner: same variances (fail to reject H0)

Wilcoxon-Mann-Whitney U test statistic: 1510.0 p-value: 0.6353512902776368

Wilcoxon-Mann-Whitney U test: same distribution (fail to reject H0)

Kolmogorov-Smirnov statistic: 0.12962962962962962 p-value: 0.6655913571840438

Kolmogorov-Smirnov: same distribution (fail to reject H0)

AHP_depth_from_peak

Levene statistic: 1.3399447901571637 p-value: 0.24952849723117262

Levene: same variances (fail to reject H0)

Fligner statistic: 2.424339978036405 p-value: 0.1194635491567324

Fligner: same variances (fail to reject H0)

Wilcoxon-Mann-Whitney U test statistic: 2893.0 p-value: 8.049943715324859e-14

Wilcoxon-Mann-Whitney U test: different distributions (reject H0)

Kolmogorov-Smirnov statistic: 0.7777777777777778 p-value: 6.661338147750939e-16

Kolmogorov-Smirnov: different distributions (reject H0)

AHP_slow_time

Levene statistic: 0.2773733483050493 p-value: 0.5995181094433077

Levene: same variances (fail to reject H0)

Fligner statistic: 0.3607862611307999 p-value: 0.5480698901731853

Fligner: same variances (fail to reject H0)

Wilcoxon-Mann-Whitney U test statistic: 1598.0 p-value: 0.48348010610693026

Wilcoxon-Mann-Whitney U test: same distribution (fail to reject H0)

Kolmogorov-Smirnov statistic: 0.22604588394062078 p-value: 0.10176313080703958

Kolmogorov-Smirnov: same distribution (fail to reject H0)

ISI_values

Levene statistic: 0.02132078025677348 p-value: 0.8841831976486665

Levene: same variances (fail to reject H0)

Fligner statistic: 0.07623370008066287 p-value: 0.7824677972955265

Fligner: same variances (fail to reject H0)

Wilcoxon-Mann-Whitney U test statistic: 1117.0 p-value: 0.027011518317369983

Wilcoxon-Mann-Whitney U test: different distributions (reject H0)

Kolmogorov-Smirnov statistic: 0.3684210526315789 p-value: 0.0007881130606729458
Kolmogorov-Smirnov: different distributions (reject H0)

Supplementary Information File 3.

The top-scoring TF was ESRRA (estrogen-related receptor alpha). This TF regulates expression of multiple metabolism-related genes, including those of mitochondrial function, biogenesis and turnover, as well as lipid catabolism (Tripathi et al., 2020). It is also linked to autophagy and NF-kB inflammatory response via Sirt1 signaling (Cantó et al., 2009; Yuk et al., 2015; Kim et al., 2018; Suresh et al., 2018). Mitochondrial dysfunction and autophagy impairments are consistently among the hallmarks of aging (López-Otín et al., 2013, 2023; Mattson and Arumugam, 2018). Notably, ESRRA expression is downregulated in aging according to various studies (Schaum et al., 2020; Tripathi et al., 2020).

The second-scoring TF was Nkx2-5 (NK2 homeobox 5), which is highly conserved among species and mostly studied in development and cardiac function (Takeda et al., 2009). Reduction of Nkx2-5 cardiac expression has been reported in aging (Volkova et al., 2005).

The third-ranked TF was the evolutionary conserved energy sensor NFE2L1 (nuclear factor erythroid 2-related factor 1, also called Nrf1 or nuclear respiratory factor 1). It is one of the key regulators of redox signaling and homeostasis. Dysfunction of this TF is associated with glucose metabolism reprogramming via AMPK signaling (Yang et al., 2021). NFE2L1 also upregulates expression of proteasomal genes in an ERK-signaling dependent manner (Zhang et al., 2021b), which is suggested to contribute to the development of neurodegenerative diseases (Lee et al., 2011).

The next TF was ZBED1 (zinc finger BED domain-containing protein 1). It acts as a small ubiquitin-like modifier (SUMO) ligase by SUMOylating Mi2-alpha during nucleosome remodeling and deacetylation (Yamashita et al., 2016).

The fifth TF, THAP4 (nitrobindin), detoxifies reactive nitrogen and oxygen species and scavenges peroxynitrite (De Simone et al., 2018).

The next TF was PREB (prolactin regulatory element binding). Interestingly, it has been reported as one of the links between aging and Alzheimer's disease (Zhou et al., 2019).

The next TF was HIF1A (hypoxia inducible factor 1), which serves as a key regulator of the hypoxia response at both cellular and system scale. The role of HIF1a in brain aging and neurodegenerative diseases is convoluted, multifaceted and incompletely understood. On one hand, HIF1a promotes erythropoiesis, angiogenesis and exerts neuroprotection (Majmundar et al., 2010; Burtscher et al., 2021). On the other hand, there are contradictory reports on either the detrimental (Sun et al., 2006; March-Diaz et al., 2021; Lee et al., 2023) or protective (Ashok et al., 2017) role of HIF1a in neurodegeneration, Alzheimer's disease in particular. To add the complexity, HIF1a is involved in inflammatory response and metabolism regulation (McGettrick and O'Neill, 2020; Taylor and Scholz, 2022). Even though mechanisms of HIF1a are so multifaceted, therapeutic potential of this TF has been recognized (Lee et al., 2019; Luo et al., 2022).

The next TF was MYRFL (myelin regulatory factor-like protein). Its biological function (and that of some other myelin regulatory factors, such as MYRF) is poorly understood, which is surprising given the importance of myelin for neuronal health (Huang et al., 2021).

The next TF was ZNF878 (zinc finger protein 878), which is one of the hundreds in the rapidly evolved KRAB-domain containing family (Shen et al., 2021).

The last out of top-10 TFs was SALL3 (spalt-like transcription factor 3). It modulates DNA methyltransferase activity and influences human induced pluripotent stem cell differentiation (Kuroda et al., 2019).

We further searched the STRING database (Szklarczyk et al., 2019) for the protein-protein associations of the top TF ESRRA (Fig. 5c), following which we performed a literature search for the top-10 proteins from this search: Hif1a, Sirt1, Hdac8, Ppargc1a, Ppargc1b, Mef2c, Nrip1, Ncoa1, Tfam, Perm1. Interestingly, numerous reports attribute roles in aging and neurodegeneration to these proteins as detailed below.

Hif1a is a common hit in the top-10 of STRING associations and ChEA3 enrichment with its implications in brain aging and neurodegeneration described above.

Sirt1 is a NAD+-dependent deacetylase, a member of the sirtuin family of proteins. It is largely studied for its role in aging, longevity, apoptosis, stress resistance, inflammation, linking nutrition and chromatin regulation, energy homeostasis and caloric restriction (Rodgers et al., 2005; Guarente, 2006;

Milne et al., 2007; Cantó et al., 2009; Finkel et al., 2009; Bishop et al., 2010; Ledford, 2010; Gut and Verdin, 2013; O'Neill and Hardie, 2013; Ng et al., 2015; Shin et al., 2016; Satoh et al., 2017; Katsyuba et al., 2018; Yang et al., 2018).

Another protein found in STRING associations of ESRRA is HDAC8 (histone deacetylase 8), closely related to the sirtuins signaling. It is largely recognised as a promising drug target in several disorders (Chakrabarti et al., 2015; Mormino et al., 2021; Zhao et al., 2021; Emmons et al., 2022).

Another protein in our list, Ppargc1a (peroxisome proliferator-activated receptor gamma coactivator 1-alpha, also called PGC-1alpha), is an important regulator of energy metabolism and is implicated in aging (Rodgers et al., 2005; Anderson and Prolla, 2009; Garcia et al., 2018). It is associated with Parkinson's (Li et al., 2022) and Huntington's diseases (Cui et al., 2006).

Closely related to PGC-1alpha is the other protein on our list, Ppargc1b (peroxisome proliferator-activated receptor gamma coactivator 1-alpha, also called PGC-1beta), which is also involved in energy metabolism regulation, but less well studied and is an active area of research (Thiepold et al., 2017; Thibonnier et al., 2020).

The next protein on our list is Tfam (mitochondrial transcription factor 1), which is regulated by PGC-1alpha and is implicated in brain aging and neurodegeneration (Grimm and Eckert, 2017; Kang et al., 2018).

Another protein on the list is Perm1 (PGC-1 And ERR-Induced Regulator In Muscle Protein 1) is mostly studied in cardiac mitochondrial metabolism regulation (Huang et al., 2022).

The next on the list is Nrip1 (nuclear receptor interacting protein 1). It is an oxidative metabolism regulator and a potential therapeutic target in Down syndrome (Izzo et al., 2014).

The other protein on the list is Ncoa1 (nuclear receptor coactivator 1), which is involved in hormonal regulation, learning, memory and neurogenesis (Nishihara et al., 2007; Sun and Xu, 2020).

Next, brain-expressed Mef2c (myocyte enhancer factor 2C) is a TF downregulated in aging in an interferon signaling-dependent way (Deczkowska et al., 2017). Furthermore, therapeutic potential of this TF in neurodegeneration and aging has been recently shown with its effects in promoting cognitive resilience (Barker et al., 2021).

To sum up, our identified anti-aging targets largely align with the literature data on therapeutics for healthy aging (Campisi et al., 2019), but also suggest a role of a few poorly studied TFs in the brain energy metabolism aging and provide the insights on the links between molecular mechanisms implicated in aging and neurodegeneration.

Supplementary Information File 4.

This information will be available after peer-reviewed publication.

Supplementary Information File 5.

This information will be available after peer-reviewed publication.

Supplementary Information File 6.

This information will be available after peer-reviewed publication.

Supplementary Information File 7.

Mapping of model variables indexes to descriptive names and Bigg nomenclature (King et al., 2016) (where available).

#idx	id	u_ + bigg_id (if available) + compartment_id	descriptive name
1	K_x_n	u_k_m_n	Potassium ion in neuronal mito. matrix
2	Mg_x_n	u_mg2_m_n	Magnesium ion in neuronal mito. matrix
3	NADHmito_n	u_nadh_m_n	NADH in neuronal mito.
4	QH2mito_n	u_q10h2_m_n	Reduced ubiquinol in neuronal mito. matrix

5	CytCredmito_n	u_focytC_m_n	Reduced cytochrome c in neuronal mito. matrix
6	O2_n	u_o2_c_n	Oxygen in neuronal cytosol
7	ATPmito_n	u_atp_m_n	Free ATP in neuronal mito. matrix
8	ADPmito_n	u_adp_m_n	Free ADP in neuronal mito. matrix
9	ATP_mx_n	u_notBigg_ATP_mx_m_n	Magnesium-bound ATP in neuronal mito. matrix
10	ADP_mx_n	u_notBigg_ADP_mx_m_n	Magnesium-bound ADP in neuronal mito. matrix
11	Pimito_n	u_pi_m_n	Phosphate in neuronal mito. matrix
12	ATP_i_n	u_atp_i_n	Free ATP in neuronal mito. IMS
13	ADP_i_n	u_adp_i_n	Free ADP in neuronal mito. IMS
14	ATP_mi_n	u_notBigg_ATP_mi_i_n	Magnesium-bound ATP in neuronal mito. IMS
15	ADP_mi_n	u_notBigg_ADP_mi_i_n	Magnesium-bound ADP in neuronal mito. IMS
16	Pi_i_n	u_pi_i_n	Phosphate in neuronal mito. IMS
17	MitoMembrPotent_n	u_notBigg_MitoMembrPotent_m_n	Neuronal mitochondrial membrane potential
18	ATP_n	u_atp_c_n	ATP in neuronal cytosol
19	FUMmito_n	u_fum_m_n	Fumarate in neuronal mito.
20	MALmito_n	u_mal_L_m_n	L-Malate in neuronal mito.
21	OXAmito_n	u_oaa_m_n	Oxaloacetate in neuronal mito.
22	SUCmito_n	u_succ_m_n	Succinate in neuronal mito.
23	SUCCOAmito_n	u_succoa_m_n	Succinyl-CoA in neuronal mito.
24	CoAmito_n	u_coa_m_n	Coenzyme A in neuronal mito.

25	AKGmito_n	u_akg_m_n	Alpha-ketoglutarate in neuronal mito.
26	ISOCITmito_n	u_icit_m_n	Isocitrate in neuronal mito.
27	CITmito_n	u_cit_m_n	Citrate in neuronal mito.
28	AcCoAmito_n	u_accoa_m_n	Acetyl-CoA in neuronal mito.
29	AcAc_n	u_acac_c_n	Acetoacetate in neuron (only mito., no cytosolic AcAc in the model)
30	AcAcCoA_n	u_aacoa_m_n	Acetoacetyl-CoA in neuronal mito.
31	PYRmito_n	u_pyr_m_n	Pyruvate in neuronal mito.
32	bHB_n	u_bhb_c_n	beta-Hydroxybutyrate in neuronal cytosol
33	bHB_ecs	u_bhb_e_e	beta-Hydroxybutyrate in extracellular space
34	bHB_b	u_bhb_b_b	beta-Hydroxybutyrate in capillaries
35	GLUmito_n	u_glu_L_m_n	L-Glutamate in neuronal mito.
36	GLU_n	u_glu_L_c_n	L-Glutamate in neuronal cytosol
37	NADH_n	u_nadh_c_n	NADH in neuronal cytosol
38	K_x_a	u_k_m_a	Potassium ion in astrocytic mito. matrix
39	Mg_x_a	u_mg2_m_a	Magnesium ion in astrocytic mito. matrix
40	NADHmito_a	u_nadh_m_a	NADH in astrocytic mito.
41	QH2mito_a	u_q10h2_m_a	Reduced ubiquinol in astrocytic mito. matrix
42	CytCredmito_a	u_focytC_m_a	Reduced cytochrome c in astrocytic mito. matrix
43	O2_a	u_o2_c_a	Oxygen in astrocytic cytosol

44	ATPmito_a	u_atp_m_a	Free ATP in astrocytic mito. matrix
45	ADPmito_a	u_adp_m_a	Free ADP in astrocytic mito. matrix
46	ATP_mx_a	u_notBigg_ATP_mx_m_a	Magnesium-bound ATP in astrocytic mito. matrix
47	ADP_mx_a	u_notBigg_ADP_mx_m_a	Magnesium-bound ADP in astrocytic mito. matrix
48	Pimito_a	u_pi_m_a	Phosphate in astrocytic mito. matrix
49	ATP_i_a	u_atp_i_a	Free ATP in astrocytic mito. IMS
50	ADP_i_a	u_adp_i_a	Free ADP in astrocytic mito. IMS
51	ATP_mi_a	u_notBigg_ATP_mi_i_a	Magnesium-bound ATP in astrocytic mito. IMS
52	ADP_mi_a	u_notBigg_ADP_mi_i_a	Magnesium-bound ADP in astrocytic mito. IMS
53	Pi_i_a	u_pi_i_a	Phosphate in astrocytic mito. IMS
54	MitoMembrPotent_a	u_notBigg_MitoMembrPotent_m_a	Astrocytic mitochondrial membrane potential
55	ATP_a	u_atp_c_a	ATP in astrocytic cytosol
56	FUMmito_a	u_fum_m_a	Fumarate in astrocytic mito.
57	MALmito_a	u_mal_L_m_a	L-Malate in astrocytic mito.
58	OXAmito_a	u_oaa_m_a	Oxaloacetate in astrocytic mito.
59	SUCmito_a	u_succ_m_a	Succinate in astrocytic mito.
60	SUCCOAmito_a	u_succoa_m_a	Succinyl-CoA in astrocytic mito.
61	CoAmito_a	u_coa_m_a	Coenzyme A in astrocytic mito.
62	AKGmito_a	u_akg_m_a	Alpha-ketoglutarate in astrocytic mito.

63	ISOCITmito_a	u_icit_m_a	Isocitrate in astrocytic mito.
64	CITmito_a	u_cit_m_a	Citrate in astrocytic mito.
65	AcCoAmito_a	u_accoa_m_a	Acetyl-CoA in astrocytic mito.
66	PYRmito_a	u_pyr_m_a	Pyruvate in astrocytic mito.
67	GLN_n	u_gln_L_c_n	Glutamine in neuron
68	GLN_out	u_gln_L_e_e	Glutamine in extracellular space
69	GLN_a	u_gln_L_c_a	Glutamine in astrocytic cytosol
70	GLUT_a	u_glu_L_c_a	Glutamate in astrocytic cytosol
71	Va	u_notBigg_Va_c_a	Astrocytic membrane potential
72	Na_a	u_na1_c_a	Sodium ion in astrocytic cytosol
73	K_a	u_k_c_a	Potassium ion in astrocytic cytosol
74	K_out	u_k_e_e	Potassium ion in extracellular space
75	GLUT_syn	u_glu_L_syn_syn	Synaptic glutamate
76	VNeu	u_notBigg_VNeu_c_n	Neuronal membrane potential
77	Na_n	u_na1_c_n	Sodium ion in neuronal cytosol
78	h	u_notBigg_hgate_c_n	Gating variable h of Hodgkin-Huxley model in neuron
79	n	u_notBigg_ngate_c_n	Gating variable n of Hodgkin-Huxley model in neuron
80	Ca_n	u_ca2_c_n	Calcium in neuronal cytosol
81	pgate	u_notBigg_pgate_c_n	Gating variable of M-current in neuron
82	nBK_a	u_notBigg_nBK_c_a	Gating variable of BK channels in astrocyte
83	mGluRboundRatio_a	u_notBigg_mGluRboundRatio_c_a	Ratio of bound metabotropic glutamate receptors in astrocyte

84	IP3_a	u_notBigg_IP3_c_a	IP3 in astrocytic cytosol
85	hIP3Ca_a	u_notBigg_hIP3Ca_c_a	Gating variable of IP3-dependent calcium flow in astrocytic cytosol
86	Ca_a	u_ca2_c_a	Calcium in astrocytic cytosol
87	sTRP_a	u_notBigg_sTRP_c_a	Astrocytic TRPV4 channel open probability
88	vV	u_notBigg_vV_b_b	Venous volume
89	EET_a	u_notBigg_EET_c_a	Epoxyeicosatrienoic acid
90	ddHb	u_notBigg_ddHb_b_b	Deoxyhemoglobin
91	O2cap	u_o2_b_b	Oxygen in capillaries
92	Glc_b	u_glc_D_b_b	D-Glucose in capillaries
93	Glc_t_t	u_glc_D_ecsEndothelium_ecsEndothelium	D-Glucose in endothelium
94	Glc_ecsBA	u_glc_D_ecsBA_ecsBA	D-Glucose in basal lamina
95	Glc_a	u_glc_D_c_a	D-Glucose in astrocytic cytosol
96	Glc_ecsAN	u_glc_D_ecsAN_ecsAN	D-Glucose in interstitial space
97	Glc_n	u_glc_D_c_n	D-Glucose in neuronal cytosol
98	G6P_n	u_g6p_c_n	D-Glucose 6-phosphate in neuronal cytosol
99	G6P_a	u_g6p_c_a	D-Glucose 6-phosphate in astrocytic cytosol
100	F6P_n	u_f6p_c_n	D-Fructose 6-phosphate in neuronal cytosol
101	F6P_a	u_f6p_c_a	D-Fructose 6-phosphate in astrocytic cytosol
102	FBP_n	u_fdp_c_n	D-Fructose 1,6-bisphosphate in neuronal cytosol
103	FBP_a	u_fdp_c_a	D-Fructose 1,6-bisphosphate in astrocytic cytosol

104	f26bp_a	u_f26bp_c_a	D-Fructose 2,6-bisphosphate in astrocytic cytosol
105	GLY_a	u_glycogen_c_a	Glycogen in astrocytic cytosol
106	G1P_a	u_g1p_c_a	D-Glucose 1-phosphate in astrocytic cytosol
107	GAP_n	u_g3p_c_n	Glyceraldehyde 3-phosphate in neuronal cytosol
108	GAP_a	u_g3p_c_a	Glyceraldehyde 3-phosphate in astrocytic cytosol
109	DHAP_n	u_dhap_c_n	Dihydroxyacetone phosphate in neuronal cytosol
110	DHAP_a	u_dhap_c_a	Dihydroxyacetone phosphate in astrocytic cytosol
111	BPG13_n	u_13dpg_c_n	3-Phospho-D-glyceroyl phosphate in neuronal cytosol
112	BPG13_a	u_13dpg_c_a	3-Phospho-D-glyceroyl phosphate in astrocytic cytosol
113	NADH_a	u_nadh_c_a	NADH in astrocytic cytosol
114	PG3_n	u_3pg_c_n	3-Phospho-D-glycerate in neuronal cytosol
115	PG3_a	u_3pg_c_a	3-Phospho-D-glycerate in astrocytic cytosol
116	PG2_n	u_2pg_c_n	D-Glycerate 2-phosphate in neuronal cytosol
117	PG2_a	u_2pg_c_a	D-Glycerate 2-phosphate in astrocytic cytosol
118	PEP_n	u_pep_c_n	Phosphoenolpyruvate in neuronal cytosol
119	PEP_a	u_pep_c_a	Phosphoenolpyruvate in astrocytic cytosol

120	Pyr_n	u_pyr_c_n	Pyruvate in neuronal cytosol
121	Pyr_a	u_pyr_c_a	Pyruvate in astrocytic cytosol
122	Lac_b	u_lac_L_b_b	L-Lactate in capillaries
123	Lac_ecs	u_lac_L_e_e	L-Lactate in extracellular space
124	Lac_a	u_lac_L_c_a	L-Lactate in astrocytic cytosol
125	Lac_n	u_lac_L_c_n	L-Lactate in neuronal cytosol
126	NADPH_n	u_nadph_c_n	NADPH in neuronal cytosol
127	NADPH_a	u_nadph_c_a	NADPH in astrocytic cytosol
128	GL6P_n	u_6pgl_c_n	6-phospho-D-glucono-1,5-lactone in neuronal cytosol
129	GL6P_a	u_6pgl_c_a	6-phospho-D-glucono-1,5-lactone in astrocytic cytosol
130	GO6P_n	u_6pgc_c_n	6-Phospho-D-gluconate in neuronal cytosol
131	GO6P_a	u_6pgc_c_a	6-Phospho-D-gluconate in astrocytic cytosol
132	RU5P_n	u_ru5p_D_c_n	D-Ribulose 5-phosphate in neuronal cytosol
133	RU5P_a	u_ru5p_D_c_a	D-Ribulose 5-phosphate in astrocytic cytosol
134	R5P_n	u_r5p_c_n	D-Ribose 5-phosphate in neuronal cytosol
135	R5P_a	u_r5p_c_a	D-Ribose 5-phosphate in astrocytic cytosol
136	X5P_n	u_xu5p_D_c_n	D-Xylulose 5-phosphate in neuronal cytosol
137	X5P_a	u_xu5p_D_c_a	D-Xylulose 5-phosphate in astrocytic cytosol

138	S7P_n	u_s7p_c_n	Sedoheptulose 7-phosphate in neuronal cytosol
139	S7P_a	u_s7p_c_a	Sedoheptulose 7-phosphate in astrocytic cytosol
140	E4P_n	u_e4p_c_n	D-Erythrose 4-phosphate in neuronal cytosol
141	E4P_a	u_e4p_c_a	D-Erythrose 4-phosphate in astrocytic cytosol
142	GSH_n	u_gthrd_c_n	Reduced glutathione in neuronal cytosol
143	GSH_a	u_gthrd_c_a	Reduced glutathione in astrocytic cytosol
144	GSSG_n	u_gthox_c_n	Oxidized glutathione in neuronal cytosol
145	GSSG_a	u_gthox_c_a	Oxidized glutathione in astrocytic cytosol
146	PCr_n	u_pcreat_c_n	Phosphocreatine in neuronal cytosol
147	PCr_a	u_pcreat_c_a	Phosphocreatine in astrocytic cytosol
148	cAMP_a	u_camp_c_a	Cyclic AMP in astrocytic cytosol
149	NE_neuromod	u_nrpphr_e_e	Norepinephrine in extracellular space
150	GPa_a	u_notBigg_GPa_c_a	Active glycogen phosphorylase in astrocytic cytosol
151	GPb_a	u_notBigg_GPb_c_a	Inactive glycogen phosphorylase in astrocytic cytosol

Supplementary Information File 8.

This information will be available after peer-reviewed publication.

References

Acevedo, A., Torres, F., Kiwi, M., Baeza-Lehnert, F., Barros, L. F., Lee-Liu, D., et al. (2023). Metabolic switch in the aging astrocyte supported via integrative approach comprising network and transcriptome analyses. *Aging* 15. doi: 10.18632/aging.204663.

Achanta, L. B., and Rae, C. D. (2017). β-Hydroxybutyrate in the Brain: One Molecule, Multiple Mechanisms. *Neurochem. Res.* 42, 35–49. doi: 10.1007/s11064-016-2099-2.

Anderson, P. J., and Wright, B. E. (1980). Kinetic models of glycogen metabolism in normal rat liver, morris Hepatom 7787 and host liver. *Int. J. Biochem.* 12, 361–369. doi: 10.1016/0020-711X(80)90115-9.

Anderson, R., and Prolla, T. (2009). PGC-1alpha in aging and anti-aging interventions. *Biochim. Biophys. Acta* 1790, 1059–1066. doi: 10.1016/j.bbagen.2009.04.005.

Antonenkov, V. D., Croes, K., Waelkens, E., Van Veldhoven, P. P., and Mannaerts, G. P. (2000). Identification, purification and characterization of an acetoacetyl-CoA thiolase from rat liver peroxisomes: Acetoacetyl-CoA thiolase from liver peroxisomes. *Eur. J. Biochem.* 267, 2981–2990. doi: 10.1046/j.1432-1033.2000.01314.x.

Arce-Molina, R., Cortés-Molina, F., Sandoval, P. Y., Galaz, A., Alegría, K., Schirmeier, S., et al. (2020). A highly responsive pyruvate sensor reveals pathway-regulatory role of the mitochondrial pyruvate carrier MPC. *eLife* 9, e53917. doi: 10.7554/eLife.53917.

Ashok, B. S., Ajith, T. A., and Sivanesan, S. (2017). Hypoxia-inducible factors as neuroprotective agent in Alzheimer's disease. *Clin. Exp. Pharmacol. Physiol.* 44, 327–334. doi: 10.1111/1440-1681.12717.

Atkinson, D. E. (1968). Energy charge of the adenylate pool as a regulatory parameter. Interaction with feedback modifiers. *Biochemistry* 7, 4030–4034. doi: 10.1021/bi00851a033.

Aubert, A., Costalat, R., and Valabrègue, R. (2001). Modelling of the coupling between brain electrical activity and metabolism. *Acta Biotheor.* 49, 301–326. doi: 10.1023/a:1014286728421.

Baeza-Lehnert, F., Saab, A. S., Gutiérrez, R., Larenas, V., Díaz, E., Horn, M., et al. (2019). Non-Canonical Control of Neuronal Energy Status by the Na+ Pump. *Cell Metab.* 29, 668-680.e4. doi: 10.1016/j.cmet.2018.11.005.

Barbagallo, M., Belvedere, M., and Dominguez, L. J. (2009). Magnesium homeostasis and aging. *Magnes. Res.* 22, 235–246. doi: 10.1684/mrh.2009.0187.

Barbagallo, M., and Dominguez, L. (2010). Magnesium and Aging. *Curr. Pharm. Des.* 16, 832–839. doi: 10.2174/138161210790883679.

Barbagallo, M., Veronese, N., and Dominguez, L. J. (2021). Magnesium in Aging, Health and Diseases. *Nutrients* 13, 463. doi: 10.3390/nu13020463.

Barden, R. E., Fung, C. H., Utter, M. F., and Scrutton, M. C. (1972). Pyruvate carboxylase from chicken liver. Steady state kinetic studies indicate a "two-site" ping-pong mechanism. *J. Biol. Chem.* 247, 1323–1333.

Barker, S. J., Raju, R. M., Milman, N. E. P., Wang, J., Davila-Velderrain, J., Gunter-Rahman, F., et al. (2021). MEF2 is a key regulator of cognitive potential and confers resilience to neurodegeneration. *Sci. Transl. Med.* 13, eabd7695. doi: 10.1126/scitranslmed.abd7695.

Barros, L. (2022). How expensive is the astrocyte? *J. Cereb. Blood Flow Metab.* 42, 738–745. doi: 10.1177/0271678X221077343.

Barros, L. F., Bittner, C. X., Loaiza, A., and Porras, O. H. (2007). A quantitative overview of glucose dynamics in the gliovascular unit. *Glia* 55, 1222–1237. doi: 10.1002/glia.20375.

Barros, L. F., San Martín, A., Ruminot, I., Sandoval, P. Y., Fernández-Moncada, I., Baeza-Lehnert, F., et al. (2017). Near-critical GLUT1 and Neurodegeneration: Glucose Transport and Neurodegeneration. *J. Neurosci. Res.* 95, 2267–2274. doi: 10.1002/jnr.23998.

Bélanger, M., Allaman, I., and Magistretti, P. J. (2011). Brain energy metabolism: focus on astrocyte-neuron metabolic cooperation. *Cell Metab.* 14, 724–738. doi: 10.1016/j.cmet.2011.08.016.

Bennett, M. R., Farnell, L., and Gibson, W. G. (2008). Origins of blood volume change due to glutamatergic synaptic activity at astrocytes abutting on arteriolar smooth muscle cells. *J. Theor. Biol.* 250, 172–185. doi: 10.1016/j.jtbi.2007.08.024.

Benton, D., Parker, P. Y., and Donohoe, R. T. (1996). The supply of glucose to the brain and cognitive functioning. *J. Biosoc. Sci.* 28, 463–479. doi: 10.1017/S0021932000022537.

Berndt, N., Bulik, S., and Holzhütter, H.-G. (2012). Kinetic Modeling of the Mitochondrial Energy Metabolism of Neuronal Cells: The Impact of Reduced α-Ketoglutarate Dehydrogenase Activities on ATP Production and Generation of Reactive Oxygen Species. *Int. J. Cell Biol.* 2012, 757594. doi: 10.1155/2012/757594.

Berndt, N., Bulik, S., Wallach, I., Wünsch, T., König, M., Stockmann, M., et al. (2018). HEPATOKIN1 is a biochemistry-based model of liver metabolism for applications in medicine and pharmacology. *Nat. Commun.* 9, 2386. doi: 10.1038/s41467-018-04720-9.

Berndt, N., Kann, O., and Holzhütter, H.-G. (2015). Physiology-Based Kinetic Modeling of Neuronal Energy Metabolism Unravels the Molecular Basis of NAD(P)H Fluorescence Transients. *J. Cereb. Blood Flow Metab.* 35, 1494–1506. doi: 10.1038/jcbfm.2015.70.

Bezanson, J., Edelman, A., Karpinski, S., and Shah, V. B. (2017). Julia: A Fresh Approach to Numerical Computing. *SIAM Rev.* 59, 65–98. doi: 10.1137/141000671.

Bishop, N. A., Lu, T., and Yankner, B. A. (2010). Neural mechanisms of ageing and cognitive decline. *Nature* 464, 529–535. doi: 10.1038/nature08983.

Błaszczyk, J. W. (2020). Energy Metabolism Decline in the Aging Brain—Pathogenesis of Neurodegenerative Disorders. *Metabolites* 10, 450. doi: 10.3390/metabo10110450.

Bonvento, G., and Bolaños, J. P. (2021). Astrocyte-neuron metabolic cooperation shapes brain activity. *Cell Metab.* 33, 1546–1564. doi: 10.1016/j.cmet.2021.07.006.

Borst, P. (2020). The malate–aspartate shuttle (Borst cycle): How it started and developed into a major metabolic pathway. *IUBMB Life* 72, 2241–2259. doi: 10.1002/iub.2367.

Botman, D., Tigchelaar, W., and Van Noorden, C. J. F. (2014). Determination of glutamate dehydrogenase activity and its kinetics in mouse tissues using metabolic mapping (quantitative enzyme histochemistry). *J. Histochem. Cytochem. Off. J. Histochem. Soc.* 62, 802–812. doi: 10.1369/0022155414549071.

Bouzier-Sore, A.-K., and Bolaños, J. P. (2015). Uncertainties in pentose-phosphate pathway flux assessment underestimate its contribution to neuronal glucose consumption: relevance for neurodegeneration and aging. *Front. Aging Neurosci.* 7. doi: 10.3389/fnagi.2015.00089.

Bouzier-Sore, A.-K., Voisin, P., Bouchaud, V., Bezancon, E., Franconi, J.-M., and Pellerin, L. (2006). Competition between glucose and lactate as oxidative energy substrates in both neurons and astrocytes: a comparative NMR study. *Eur. J. Neurosci.* 24, 1687–1694. doi: 10.1111/j.1460-9568.2006.05056.x.

Bradshaw, P. (2019). Cytoplasmic and Mitochondrial NADPH-Coupled Redox Systems in the Regulation of Aging. *Nutrients* 11, 504. doi: 10.3390/nu11030504.

Braidy, N., Poljak, A., Grant, R., Jayasena, T., Mansour, H., Chan-Ling, T., et al. (2014). Mapping NAD+ metabolism in the brain of ageing Wistar rats: potential targets for influencing brain senescence. *Biogerontology* 15, 177–198. doi: 10.1007/s10522-013-9489-5.

Breslin, K., Wade, J. J., Wong-Lin, K., Harkin, J., Flanagan, B., Van Zalinge, H., et al. (2018). Potassium and sodium microdomains in thin astroglial processes: A computational model study. *PLOS Comput. Biol.* 14, e1006151. doi: 10.1371/journal.pcbi.1006151.

Brilkova, M., Nigri, M., Kumar, H. S., Moore, J., Mantovani, M., Keller, C., et al. (2022). Error-prone

protein synthesis recapitulates early symptoms of Alzheimer disease in aging mice. *Cell Rep.* 40, 111433. doi: 10.1016/j.celrep.2022.111433.

Brocard, J. B., Tassetto, M., and Reynolds, I. J. (2001). Quantitative evaluation of mitochondrial calcium content in rat cortical neurones following a glutamate stimulus. *J. Physiol.* 531, 793–805. doi: 10.1111/j.1469-7793.2001.0793h.x.

Bröer, S., and Brookes, N. (2001). Transfer of glutamine between astrocytes and neurons: Glutamine transfer between astrocytes and neurons. *J. Neurochem.* 77, 705–719. doi: 10.1046/j.1471-4159.2001.00322.x.

Brunk, E., Sahoo, S., Zielinski, D. C., Altunkaya, A., Dräger, A., Mih, N., et al. (2018). Recon3D enables a three-dimensional view of gene variation in human metabolism. *Nat. Biotechnol.* 36, 272–281. doi: 10.1038/nbt.4072.

Burtscher, J., Mallet, R. T., Burtscher, M., and Millet, G. P. (2021). Hypoxia and brain aging: Neurodegeneration or neuroprotection? *Ageing Res. Rev.* 68, 101343. doi: 10.1016/j.arr.2021.101343.

Byrne, J. H., Heidelberger, R., and Waxham, M. N. eds. (2014). *From molecules to networks: an introduction to cellular and molecular neuroscience*. Third edition. Amsterdam ; Boston: Elsevier/AP, Academic Press is an imprint of Elsevier.

Cai, L., Sutter, B. M., Li, B., and Tu, B. P. (2011). Acetyl-CoA Induces Cell Growth and Proliferation by Promoting the Acetylation of Histones at Growth Genes. *Mol. Cell* 42, 426–437. doi: 10.1016/j.molcel.2011.05.004.

Calvetti, D., Capo Rangel, G., Gerardo Giorda, L., and Somersalo, E. (2018). A computational model integrating brain electrophysiology and metabolism highlights the key role of extracellular potassium and oxygen. *J. Theor. Biol.* 446, 238–258. doi: 10.1016/j.jtbi.2018.02.029.

Calvetti, D., and Somersalo, E. (2011). Dynamic activation model for a glutamatergic neurovascular unit. *J. Theor. Biol.* 274, 12–29. doi: 10.1016/j.jtbi.2010.12.007.

Campisi, J., Kapahi, P., Lithgow, G. J., Melov, S., Newman, J. C., and Verdin, E. (2019). From discoveries in ageing research to therapeutics for healthy ageing. *Nature* 571, 183–192. doi: 10.1038/s41586-019-1365-2.

Cantó, C., Gerhart-Hines, Z., Feige, J. N., Lagouge, M., Noriega, L., Milne, J. C., et al. (2009). AMPK regulates energy expenditure by modulating NAD+ metabolism and SIRT1 activity. *Nature* 458, 1056–1060. doi: 10.1038/nature07813.

Chakrabarti, A., Oehme, I., Witt, O., Oliveira, G., Sippl, W., Romier, C., et al. (2015). HDAC8: a multifaceted target for therapeutic interventions. *Trends Pharmacol. Sci.* 36, 481–492. doi: 10.1016/j.tips.2015.04.013.

Chang, A., Jeske, L., Ulbrich, S., Hofmann, J., Koblitz, J., Schomburg, I., et al. (2021). BRENDA, the ELIXIR core data resource in 2021: new developments and updates. *Nucleic Acids Res.* 49, D498–D508. doi: 10.1093/nar/gkaa1025.

Chaudhry, F. A., Reimer, R. J., Krizaj, D., Barber, D., Storm-Mathisen, J., Copenhagen, D. R., et al. (1999). Molecular Analysis of System N Suggests Novel Physiological Roles in Nitrogen Metabolism and Synaptic Transmission. *Cell* 99, 769–780. doi: 10.1016/S0092-8674(00)81674-8.

Choi, I.-Y., and Gruetter, R. eds. (2012). *Neural Metabolism In Vivo*. Boston, MA: Springer US doi: 10.1007/978-1-4614-1788-0.

Chowdhury, G. M., Jiang, L., Rothman, D. L., and Behar, K. L. (2014). The Contribution of Ketone Bodies to Basal and Activity-Dependent Neuronal Oxidation in Vivo. *J. Cereb. Blood Flow Metab.* 34, 1233–1242. doi: 10.1038/jcbfm.2014.77.

Cloutier, M., Bolger, F. B., Lowry, J. P., and Wellstead, P. (2009). An integrative dynamic model of brain energy metabolism using in vivo neurochemical measurements. *J. Comput. Neurosci.* 27, 391–414. doi: 10.1007/s10827-009-0152-8.

Coggan, J. S., Keller, D., Calì, C., Lehväslaiho, H., Markram, H., Schürmann, F., et al. (2018). Norepinephrine stimulates glycogenolysis in astrocytes to fuel neurons with lactate. *PLOS Comput. Biol.* 14, e1006392. doi: 10.1371/journal.pcbi.1006392.

Coggan, J. S., Keller, D., Markram, H., Schürmann, F., and Magistretti, P. J. (2020). Excitation states

of metabolic networks predict dose-response fingerprinting and ligand pulse phase signalling. *J. Theor. Biol.* 487, 110123. doi: 10.1016/j.jtbi.2019.110123.

Cox, M. F., Hascup, E. R., Bartke, A., and Hascup, K. N. (2022). Friend or Foe? Defining the Role of Glutamate in Aging and Alzheimer's Disease. *Front. Aging* 3, 929474. doi: 10.3389/fragi.2022.929474.

Cui, L., Jeong, H., Borovecki, F., Parkhurst, C. N., Tanese, N., and Krainc, D. (2006). Transcriptional repression of PGC-1alpha by mutant huntingtin leads to mitochondrial dysfunction and neurodegeneration. *Cell* 127, 59–69. doi: 10.1016/j.cell.2006.09.015.

Curtis, W. M., Seeds, W. A., Mattson, M. P., and Bradshaw, P. C. (2022). NADPH and Mitochondrial Quality Control as Targets for a Circadian-Based Fasting and Exercise Therapy for the Treatment of Parkinson's Disease. *Cells* 11, 2416. doi: 10.3390/cells11152416.

Datta, S., and Chakrabarti, N. (2018). Age related rise in lactate and its correlation with lactate dehydrogenase (LDH) status in post-mitochondrial fractions isolated from different regions of brain in mice. *Neurochem. Int.* 118, 23–33. doi: 10.1016/j.neuint.2018.04.007.

De Simone, G., di Masi, A., Polticelli, F., and Ascenzi, P. (2018). Human nitrobindin: the first example of an all-β-barrel ferric heme-protein that catalyzes peroxynitrite detoxification. *FEBS Open Bio* 8, 2002–2010. doi: 10.1002/2211-5463.12534.

Deczkowska, A., Matcovitch-Natan, O., Tsitsou-Kampeli, A., Ben-Hamo, S., Dvir-Szternfeld, R., Spinrad, A., et al. (2017). Mef2C restrains microglial inflammatory response and is lost in brain ageing in an IFN-I-dependent manner. *Nat. Commun.* 8, 717. doi: 10.1038/s41467-017-00769-0.

Dienel, G. A. (2012). Brain Lactate Metabolism: The Discoveries and the Controversies. *J. Cereb. Blood Flow Metab.* 32, 1107–1138. doi: 10.1038/jcbfm.2011.175.

DiNuzzo, M., Mangia, S., Maraviglia, B., and Giove, F. (2010). Glycogenolysis in astrocytes supports blood-borne glucose channeling not glycogen-derived lactate shuttling to neurons: evidence from mathematical modeling. *J. Cereb. Blood Flow Metab. Off. J. Int. Soc. Cereb. Blood Flow Metab.* 30, 1895–1904. doi: 10.1038/jcbfm.2010.151.

Disterhoft, J. F., and Oh, M. M. (2007). Alterations in intrinsic neuronal excitability during normal aging. *Aging Cell* 6, 327–336. doi: 10.1111/j.1474-9726.2007.00297.x.

Dombrowski, G. J., Cheung, G. P., and Swiatek, K. R. (1977). Evidence for the existence of enzymatic variants of β-hydroxybutyrate dehydrogenase from rat liver and brain mitochondria. *Life Sci.* 21, 1821–1829. doi: 10.1016/0024-3205(77)90164-3.

Dong, Y., and Brewer, G. J. (2019). Global Metabolic Shifts in Age and Alzheimer's Disease Mouse Brains Pivot at NAD+/NADH Redox Sites. *J. Alzheimers Dis.* 71, 119–140. doi: 10.3233/JAD-190408.

Duarte, J. M. N., and Gruetter, R. (2013). Glutamatergic and GABAergic energy metabolism measured in the rat brain by 13 C NMR spectroscopy at 14.1 T. *J. Neurochem.* 126, 579–590. doi: 10.1111/jnc.12333.

Dyson, F. (2004). A meeting with Enrico Fermi. *Nature* 427, 297–297. doi: 10.1038/427297a.

Eap, B., Nomura, M., Panda, O., Garcia, T. Y., King, C. D., Rose, J. P., et al. (2022). Ketone body metabolism declines with age in mice in a sex-dependent manner. Physiology doi: 10.1101/2022.10.05.511032.

Emmons, M. F., Bennett, R. L., Riva, A., Zhang, C., Macaulay, R., Dupéré-Richér, D., et al. (2022). HDAC8-mediated inhibition of EP300 drives a neural crest-like transcriptional state that increases melanoma brain metastasis. Cancer Biology doi: 10.1101/2022.10.12.511971.

Erecińska, M., and Silver, I. A. (1989). ATP and brain function. *J. Cereb. Blood Flow Metab. Off. J. Int. Soc. Cereb. Blood Flow Metab.* 9, 2–19. doi: 10.1038/jcbfm.1989.2.

Erecińska, M., and Silver, I. A. (1994). Ions and energy in mammalian brain. *Prog. Neurobiol.* 43, 37–71. doi: 10.1016/0301-0082(94)90015-9.

Fang, E. F., Lautrup, S., Hou, Y., Demarest, T. G., Croteau, D. L., Mattson, M. P., et al. (2017). NAD + in Aging: Molecular Mechanisms and Translational Implications. *Trends Mol. Med.* 23, 899–916. doi: 10.1016/j.molmed.2017.08.001.

Featherstone, D. E. (2010). Intercellular Glutamate Signaling in the Nervous System and Beyond. *ACS*

Chem. Neurosci. 1, 4–12. doi: 10.1021/cn900006n.

Fillenz, M., and Lowry, J. P. (1998). Studies of the source of glucose in the extracellular compartment of the rat brain. *Dev. Neurosci.* 20, 365–368. doi: 10.1159/000017332.

Fink, B. D., Bai, F., Yu, L., Sheldon, R. D., Sharma, A., Taylor, E. B., et al. (2018). Oxaloacetic acid mediates ADP-dependent inhibition of mitochondrial complex II–driven respiration. *J. Biol. Chem.* 293, 19932–19941. doi: 10.1074/jbc.RA118.005144.

Finkel, T., Deng, C.-X., and Mostoslavsky, R. (2009). Recent progress in the biology and physiology of sirtuins. *Nature* 460, 587–591. doi: 10.1038/nature08197.

Flanagan, B., McDaid, L., Wade, J., Wong-Lin, K., and Harkin, J. (2018). A computational study of astrocytic glutamate influence on post-synaptic neuronal excitability. *PLoS Comput. Biol.* 14, e1006040. doi: 10.1371/journal.pcbi.1006040.

Fraser, C. L., and Arieff, A. I. (2001). Na-K-ATPase activity decreases with aging in female rat brain synaptosomes. *Am. J. Physiol. Renal Physiol.* 281, F674-678. doi: 10.1152/ajprenal.2001.281.4.F674.

Frezza, C. (2017). Mitochondrial metabolites: undercover signalling molecules. *Interface Focus* 7, 20160100. doi: 10.1098/rsfs.2016.0100.

Gaitonde, M. K., Murray, E., and Cunningham, V. J. (1989). Effect of 6-phosphogluconate on phosphoglucose isomerase in rat brain in vitro and in vivo. *J. Neurochem.* 52, 1348–1352. doi: 10.1111/j.1471-4159.1989.tb09178.x.

Garcia, S., Nissanka, N., Mareco, E. A., Rossi, S., Peralta, S., Diaz, F., et al. (2018). Overexpression of PGC-1α in aging muscle enhances a subset of young-like molecular patterns. *Aging Cell* 17, e12707. doi: 10.1111/acel.12707.

Garrett, R., and Grisham, C. M. (2013). *Biochemistry*. 5th ed. Belmont, CA: Brooks/Cole, Cengage Learning.

Ge, I., Kirschen, G. W., and Wang, X. (2021). Shifted Dynamics of Glucose Metabolism in the Hippocampus During Aging. *Front. Aging Neurosci.* 13, 700306. doi: 10.3389/fnagi.2021.700306.

Ghosh, D., Levault, K. R., and Brewer, G. J. (2014). Relative importance of redox buffers GSH and NAD(P)H in age‐related neurodegeneration and Alzheimer disease‐like mouse neurons. *Aging Cell* 13, 631–640. doi: 10.1111/acel.12216.

Gilbert, H. F., Lennox, B. J., Mossman, C. D., and Carle, W. C. (1981). The relation of acyl transfer to the overall reaction of thiolase I from porcine heart. *J. Biol. Chem.* 256, 7371–7377.

Grimm, A., and Eckert, A. (2017). Brain aging and neurodegeneration: from a mitochondrial point of view. *J. Neurochem.* 143, 418–431. doi: 10.1111/jnc.14037.

Guarente, L. (2006). Sirtuins as potential targets for metabolic syndrome. *Nature* 444, 868–874. doi: 10.1038/nature05486.

Gut, P., and Verdin, E. (2013). The nexus of chromatin regulation and intermediary metabolism. *Nature* 502, 489–498. doi: 10.1038/nature12752.

Hädel, S., Wirth, C., Rapp, M., Gallinat, J., and Schubert, F. (2013). Effects of age and sex on the concentrations of glutamate and glutamine in the human brain: Brain Glutamate and Glutamine With Age and Sex. *J. Magn. Reson. Imaging* 38, 1480–1487. doi: 10.1002/jmri.24123.

Hagberg, A. A., Schult, D. A., and Swart, P. J. (2008). Exploring Network Structure, Dynamics, and Function using NetworkX. in *Proceedings of the 7th Python in Science Conference*, eds. G. Varoquaux, T. Vaught, and J. Millman (Pasadena, CA USA), 11–15.

Halestrap, A. P., and Denton, R. M. (1974). Specific inhibition of pyruvate transport in rat liver mitochondria and human erythrocytes by α-cyano-4-hydroxycinnamate (Short Communication). *Biochem. J.* 138, 313–316. doi: 10.1042/bj1380313.

Hersh, L. B., and Jencks, W. P. (1967). Isolation of an enzyme-coenzyme A intermediate from succinyl coenzyme A-acetoacetate coenzyme A transferase. *J. Biol. Chem.* 242, 339–340.

Hertz, L., and Rothman, D. (2017). Glutamine-Glutamate Cycle Flux Is Similar in Cultured Astrocytes and Brain and Both Glutamate Production and Oxidation Are Mainly Catalyzed by Aspartate Aminotransferase. *Biology* 6, 17. doi: 10.3390/biology6010017.

Hosseini, L., Majdi, A., Sadigh-Eteghad, S., Farajdokht, F., Ziaee, M., Rahigh Aghsan, S., et al.

(2022). Coenzyme Q10 ameliorates aging-induced memory deficits via modulation of apoptosis, oxidative stress, and mitophagy in aged rats. *Exp. Gerontol.* 168, 111950. doi: 10.1016/j.exger.2022.111950.

Hou, Y., Dan, X., Babbar, M., Wei, Y., Hasselbalch, S. G., Croteau, D. L., et al. (2019). Ageing as a risk factor for neurodegenerative disease. *Nat. Rev. Neurol.* 15, 565–581. doi: 10.1038/s41582-019-0244-7.

Howarth, C., Gleeson, P., and Attwell, D. (2012). Updated Energy Budgets for Neural Computation in the Neocortex and Cerebellum. *J. Cereb. Blood Flow Metab.* 32, 1222–1232. doi: 10.1038/jcbfm.2012.35.

Huang, C.-Y., Oka, S.-I., Xu, X., Chen, C.-F., Tung, C.-Y., Chang, Y.-Y., et al. (2022). PERM1 regulates genes involved in fatty acid metabolism in the heart by interacting with PPARα and PGC-1α. *Sci. Rep.* 12, 14576. doi: 10.1038/s41598-022-18885-3.

Huang, H., Zhou, F., Zhou, S., and Qiu, M. (2021). MYRF: A Mysterious Membrane-Bound Transcription Factor Involved in Myelin Development and Human Diseases. *Neurosci. Bull.* 37, 881–884. doi: 10.1007/s12264-021-00678-9.

Hupfeld, K. E., Hyatt, H. W., Alvarez Jerez, P., Mikkelsen, M., Hass, C. J., Edden, R. A. E., et al. (2021). In Vivo Brain Glutathione is Higher in Older Age and Correlates with Mobility. *Cereb. Cortex* 31, 4576–4594. doi: 10.1093/cercor/bhab107.

Huth, W., and Menke, R. (1982). Regulation of ketogenesis. Mitochondrial acetyl-CoA acetyltransferase from rat liver: initial-rate kinetics in the presence of the product CoASH reveal intermediary plateau regions. *Eur. J. Biochem.* 128, 413–419.

Huynh, Q. K., Sakakibara, R., Watanabe, T., and Wada, H. (1980). Glutamic oxaloacetic transaminase isozymes from rat liver. Purification and physicochemical characterization. *J. Biochem. (Tokyo)* 88, 231–239.

Iskusnykh, I. Y., Zakharova, A. A., and Pathak, D. (2022). Glutathione in Brain Disorders and Aging. *Mol. Basel Switz.* 27, 324. doi: 10.3390/molecules27010324.

Ivanisevic, J., Stauch, K., Petrascheck, M., Benton, H., Epstein, A., Fang, M., et al. (2016). Metabolic drift in the aging brain. *Aging* 8, 1000–1020. doi: 10.18632/aging.100961.

Izzo, A., Manco, R., Bonfiglio, F., Calì, G., De Cristofaro, T., Patergnani, S., et al. (2014). NRIP1/RIP140 siRNA-mediated attenuation counteracts mitochondrial dysfunction in Down syndrome. *Hum. Mol. Genet.* 23, 4406–4419. doi: 10.1093/hmg/ddu157.

Jolivet, R., Allaman, I., Pellerin, L., Magistretti, P. J., and Weber, B. (2010). Comment on Recent Modeling Studies of Astrocyte–Neuron Metabolic Interactions. *J. Cereb. Blood Flow Metab.* 30, 1982–1986. doi: 10.1038/jcbfm.2010.132.

Jolivet, R., Coggan, J. S., Allaman, I., and Magistretti, P. J. (2015). Multi-timescale Modeling of Activity-Dependent Metabolic Coupling in the Neuron-Glia-Vasculature Ensemble. *PLOS Comput. Biol.* 11, e1004036. doi: 10.1371/journal.pcbi.1004036.

Jones, T. T., and Brewer, G. J. (2009). Critical age-related loss of cofactors of neuron cytochrome C oxidase reversed by estrogen. *Exp. Neurol.* 215, 212–219. doi: 10.1016/j.expneurol.2008.09.011.

Jung, W. B., Im, G. H., Jiang, H., and Kim, S.-G. (2021). Early fMRI responses to somatosensory and optogenetic stimulation reflect neural information flow. *Proc. Natl. Acad. Sci.* 118, e2023265118. doi: 10.1073/pnas.2023265118.

Kaiser, L. G., Schuff, N., Cashdollar, N., and Weiner, M. W. (2005). Age-related glutamate and glutamine concentration changes in normal human brain: 1H MR spectroscopy study at 4 T. *Neurobiol. Aging* 26, 665–672. doi: 10.1016/j.neurobiolaging.2004.07.001.

Kang, I., Chu, C. T., and Kaufman, B. A. (2018). The mitochondrial transcription factor TFAM in neurodegeneration: emerging evidence and mechanisms. *FEBS Lett.* 592, 793–811. doi: 10.1002/1873-3468.12989.

Katsyuba, E., Mottis, A., Zietak, M., De Franco, F., van der Velpen, V., Gariani, K., et al. (2018). De novo NAD+ synthesis enhances mitochondrial function and improves health. *Nature* 563, 354–359. doi: 10.1038/s41586-018-0645-6.

Kauffman, F. C., Brown, J. G., Passonneau, J. V., and Lowry, O. H. (1969). Effects of changes in brain

metabolism on levels of pentose phosphate pathway intermediates. *J. Biol. Chem.* 244, 3647–3653.

Keenan, A. B., Torre, D., Lachmann, A., Leong, A. K., Wojciechowicz, M. L., Utti, V., et al. (2019). ChEA3: transcription factor enrichment analysis by orthogonal omics integration. *Nucleic Acids Res.* 47, W212–W224. doi: 10.1093/nar/gkz446.

Kelly, M. P. (2018). Cyclic nucleotide signaling changes associated with normal aging and age-related diseases of the brain. *Cell. Signal.* 42, 281–291. doi: 10.1016/j.cellsig.2017.11.004.

Kety, S. S. (1957). "The general metabolism of the brain in vivo," in *Metabolism of the nervous system* (Elsevier), 221–237.

Kim, S. Y., Yang, C.-S., Lee, H.-M., Kim, J. K., Kim, Y.-S., Kim, Y.-R., et al. (2018). ESRRA (estrogen-related receptor α) is a key coordinator of transcriptional and post-translational activation of autophagy to promote innate host defense. *Autophagy* 14, 152–168. doi: 10.1080/15548627.2017.1339001.

King, Z. A., Lu, J., Dräger, A., Miller, P., Federowicz, S., Lerman, J. A., et al. (2016). BiGG Models: A platform for integrating, standardizing and sharing genome-scale models. *Nucleic Acids Res.* 44, D515–D522. doi: 10.1093/nar/gkv1049.

Kiyatkin, E. A., and Lenoir, M. (2012). Rapid fluctuations in extracellular brain glucose levels induced by natural arousing stimuli and intravenous cocaine: fueling the brain during neural activation. *J. Neurophysiol.* 108, 1669–1684. doi: 10.1152/jn.00521.2012.

Koga, M., Serritella, A. V., Messmer, M. M., Hayashi-Takagi, A., Hester, L. D., Snyder, S. H., et al. (2011). Glutathione is a physiologic reservoir of neuronal glutamate. *Biochem. Biophys. Res. Commun.* 409, 596–602. doi: 10.1016/j.bbrc.2011.04.087.

Köhler, S., Schmidt, H., Fülle, P., Hirrlinger, J., and Winkler, U. (2020). A Dual Nanosensor Approach to Determine the Cytosolic Concentration of ATP in Astrocytes. *Front. Cell. Neurosci.* 14, 565921. doi: 10.3389/fncel.2020.565921.

Krishnan, G. P., Filatov, G., Shilnikov, A., and Bazhenov, M. (2015). Electrogenic properties of the Na+/K + ATPase control transitions between normal and pathological brain states. *J. Neurophysiol.* 113, 3356–3374. doi: 10.1152/jn.00460.2014.

Kulkarni, A. S., Gubbi, S., and Barzilai, N. (2020). Benefits of Metformin in Attenuating the Hallmarks of Aging. *Cell Metab.* 32, 15–30. doi: 10.1016/j.cmet.2020.04.001.

Kumar, A., and Foster, T. C. (2007). "Neurophysiology of Old Neurons and Synapses," in *Brain Aging: Models, Methods, and Mechanisms* Frontiers in Neuroscience., ed. D. R. Riddle (Boca Raton (FL): CRC Press/Taylor & Francis). Available at: http://www.ncbi.nlm.nih.gov/books/NBK3882/ [Accessed June 28, 2023].

Kuroda, T., Yasuda, S., Tachi, S., Matsuyama, S., Kusakawa, S., Tano, K., et al. (2019). SALL3 expression balance underlies lineage biases in human induced pluripotent stem cell differentiation. *Nat. Commun.* 10, 2175. doi: 10.1038/s41467-019-09511-4.

Lajtha, A., and Reith, M. E. A. eds. (2007). *Handbook of Neurochemistry and Molecular Neurobiology*. Boston, MA: Springer US doi: 10.1007/978-0-387-30380-2.

Lambeth, M. J., and Kushmerick, M. J. (2002). A computational model for glycogenolysis in skeletal muscle. *Ann. Biomed. Eng.* 30, 808–827.

Ledford, H. (2010). Ageing: Much ado about ageing. *Nature* 464, 480–481. doi: 10.1038/464480a.

Lee, C. S., Lee, C., Hu, T., Nguyen, J. M., Zhang, J., Martin, M. V., et al. (2011). Loss of nuclear factor E2-related factor 1 in the brain leads to dysregulation of proteasome gene expression and neurodegeneration. *Proc. Natl. Acad. Sci. U. S. A.* 108, 8408–8413. doi: 10.1073/pnas.1019209108.

Lee, J. V., Carrer, A., Shah, S., Snyder, N. W., Wei, S., Venneti, S., et al. (2014). Akt-dependent metabolic reprogramming regulates tumor cell histone acetylation. *Cell Metab.* 20, 306–319. doi: 10.1016/j.cmet.2014.06.004.

Lee, J. W., Ko, J., Ju, C., and Eltzschig, H. K. (2019). Hypoxia signaling in human diseases and therapeutic targets. *Exp. Mol. Med.* 51, 1–13. doi: 10.1038/s12276-019-0235-1.

Lee, S., Devanney, N. A., Golden, L. R., Smith, C. T., Schwartz, J. L., Walsh, A. E., et al. (2023). APOE modulates microglial immunometabolism in response to age, amyloid pathology, and

inflammatory challenge. *Cell Rep.* 42, 112196. doi: 10.1016/j.celrep.2023.112196.

Lerchundi, R., Fernández-Moncada, I., Contreras-Baeza, Y., Sotelo-Hitschfeld, T., Mächler, P., Wyss, M. T., et al. (2015). NH4+ triggers the release of astrocytic lactate via mitochondrial pyruvate shunting. *Proc. Natl. Acad. Sci.* 112, 11090–11095. doi: 10.1073/pnas.1508259112.

Li, L.-Z., Zhao, Y.-W., Pan, H.-X., Xiang, Y.-Q., Wang, Y.-G., Xu, Q., et al. (2022). Association of rare PPARGC1A variants with Parkinson's disease risk. *J. Hum. Genet.* 67, 687–690. doi: 10.1038/s10038-022-01074-5.

Li, W., Yu, J., Liu, Y., Huang, X., Abumaria, N., Zhu, Y., et al. (2014). Elevation of brain magnesium prevents synaptic loss and reverses cognitive deficits in Alzheimer's disease mouse model. *Mol. Brain* 7, 65. doi: 10.1186/s13041-014-0065-y.

Listrom, D. C., Morizono, H., Rajagopal, S. B., McCANN, T. M., Tuchman, M., and Allewell, M. N. (1997). Expression, purification, and characterization of recombinant human glutamine synthetase. *Biochem. J.* 328, 159–163. doi: 10.1042/bj3280159.

López-Otín, C., Blasco, M. A., Partridge, L., Serrano, M., and Kroemer, G. (2013). The Hallmarks of Aging. *Cell* 153, 1194–1217. doi: 10.1016/j.cell.2013.05.039.

López-Otín, C., Blasco, M. A., Partridge, L., Serrano, M., and Kroemer, G. (2023). Hallmarks of aging: An expanding universe. *Cell* 186, 243–278. doi: 10.1016/j.cell.2022.11.001.

Luder, A. S., Parks, J. K., Frerman, F., and Parker, W. D. (1990). Inactivation of beef brain alpha-ketoglutarate dehydrogenase complex by valproic acid and valproic acid metabolites. Possible mechanism of anticonvulsant and toxic actions. *J. Clin. Invest.* 86, 1574–1581. doi: 10.1172/JCI114877.

Luo, Z., Tian, M., Yang, G., Tan, Q., Chen, Y., Li, G., et al. (2022). Hypoxia signaling in human health and diseases: implications and prospects for therapeutics. *Signal Transduct. Target. Ther.* 7, 218. doi: 10.1038/s41392-022-01080-1.

Mächler, P., Wyss, M. T., Elsayed, M., Stobart, J., Gutierrez, R., von Faber-Castell, A., et al. (2016). In Vivo Evidence for a Lactate Gradient from Astrocytes to Neurons. *Cell Metab.* 23, 94–102. doi: 10.1016/j.cmet.2015.10.010.

Mahan, D. E., Mushahwar, I. K., and Koeppe, R. E. (1975). Purification and properties of rat brain pyruvate carboxylase. *Biochem. J.* 145, 25–35. doi: 10.1042/bj1450025.

Mahmoud, S., Gharagozloo, M., Simard, C., and Gris, D. (2019). Astrocytes Maintain Glutamate Homeostasis in the CNS by Controlling the Balance between Glutamate Uptake and Release. *Cells* 8, 184. doi: 10.3390/cells8020184.

Majmundar, A. J., Wong, W. J., and Simon, M. C. (2010). Hypoxia-inducible factors and the response to hypoxic stress. *Mol. Cell* 40, 294–309. doi: 10.1016/j.molcel.2010.09.022.

Maletic-Savatic, M., Vingara, L. K., Manganas, L. N., Li, Y., Zhang, S., Sierra, A., et al. (2008). Metabolomics of Neural Progenitor Cells: A Novel Approach to Biomarker Discovery. *Cold Spring Harb. Symp. Quant. Biol.* 73, 389–401. doi: 10.1101/sqb.2008.73.021.

Mann, K., Deny, S., Ganguli, S., and Clandinin, T. R. (2021). Coupling of activity, metabolism and behaviour across the Drosophila brain. *Nature* 593, 244–248. doi: 10.1038/s41586-021-03497-0.

Mantle, D., Heaton, R. A., and Hargreaves, I. P. (2021). Coenzyme Q10, Ageing and the Nervous System: An Overview. *Antioxidants* 11, 2. doi: 10.3390/antiox11010002.

March-Diaz, R., Lara-Ureña, N., Romero-Molina, C., Heras-Garvin, A., Ortega-de San Luis, C., Alvarez-Vergara, M. I., et al. (2021). Hypoxia compromises the mitochondrial metabolism of Alzheimer's disease microglia via HIF1. *Nat. Aging* 1, 385–399. doi: 10.1038/s43587-021-00054-2.

Mattson, M. P., and Arumugam, T. V. (2018). Hallmarks of Brain Aging: Adaptive and Pathological Modification by Metabolic States. *Cell Metab.* 27, 1176–1199. doi: 10.1016/j.cmet.2018.05.011.

McBean, G. (2017). Cysteine, Glutathione, and Thiol Redox Balance in Astrocytes. *Antioxidants* 6, 62. doi: 10.3390/antiox6030062.

McCormack, J. G., and Denton, R. M. (1979). The effects of calcium ions and adenine nucleotides on the activity of pig heart 2-oxoglutarate dehydrogenase complex. *Biochem. J.* 180, 533–544.

doi: 10.1042/bj1800533.

McGettrick, A. F., and O'Neill, L. A. J. (2020). The Role of HIF in Immunity and Inflammation. *Cell Metab.* 32, 524–536. doi: 10.1016/j.cmet.2020.08.002.

Menahan, L. A., Hron, W. T., Hinkelman, D. G., and Miziorko, H. M. (1981). Interrelationships between 3-Hydroxy-3-Methylglutaryl-CoA Synthase, Acetoacetyl-CoA and Ketogenesis. *Eur. J. Biochem.* 119, 287–294. doi: 10.1111/j.1432-1033.1981.tb05606.x.

Meyer, D. J., Díaz-García, C. M., Nathwani, N., Rahman, M., and Yellen, G. (2022). The Na+/K+ pump dominates control of glycolysis in hippocampal dentate granule cells. *eLife* 11, e81645. doi: 10.7554/eLife.81645.

Milne, J. C., Lambert, P. D., Schenk, S., Carney, D. P., Smith, J. J., Gagne, D. J., et al. (2007). Small molecule activators of SIRT1 as therapeutics for the treatment of type 2 diabetes. *Nature* 450, 712–716. doi: 10.1038/nature06261.

Mink, J. W., Blumenschine, R. J., and Adams, D. B. (1981). Ratio of central nervous system to body metabolism in vertebrates: its constancy and functional basis. *Am. J. Physiol.* 241, R203-212. doi: 10.1152/ajpregu.1981.241.3.R203.

Mironov, S. L. (2007). ADP Regulates Movements of Mitochondria in Neurons. *Biophys. J.* 92, 2944–2952. doi: 10.1529/biophysj.106.092981.

Mogilevskaya, E., Demin, O., and Goryanin, I. (2006). Kinetic model of mitochondrial Krebs cycle: unraveling the mechanism of salicylate hepatotoxic effects. *J. Biol. Phys.* 32, 245–271. doi: 10.1007/s10867-006-9015-y.

Mongeon, R., Venkatachalam, V., and Yellen, G. (2016). Cytosolic NADH-NAD+ Redox Visualized in Brain Slices by Two-Photon Fluorescence Lifetime Biosensor Imaging. *Antioxid. Redox Signal.* 25, 553–563. doi: 10.1089/ars.2015.6593.

Mormino, A., Cocozza, G., Fontemaggi, G., Valente, S., Esposito, V., Santoro, A., et al. (2021). Histone-deacetylase 8 drives the immune response and the growth of glioma. *Glia* 69, 2682–2698. doi: 10.1002/glia.24065.

Mueggler, P. A., and Wolfe, R. G. (1978). Malate dehydrogenase. Kinetic studies of substrate activation of supernatant enzyme by L-malate. *Biochemistry* 17, 4615–4620. doi: 10.1021/bi00615a006.

Mulukutla, B. C., Yongky, A., Daoutidis, P., and Hu, W.-S. (2014). Bistability in Glycolysis Pathway as a Physiological Switch in Energy Metabolism. *PLoS ONE* 9, e98756. doi: 10.1371/journal.pone.0098756.

Mulukutla, B. C., Yongky, A., Grimm, S., Daoutidis, P., and Hu, W.-S. (2015). Multiplicity of Steady States in Glycolysis and Shift of Metabolic State in Cultured Mammalian Cells. *PLOS ONE* 10, e0121561. doi: 10.1371/journal.pone.0121561.

Muraleedharan, R., Gawali, M. V., Tiwari, D., Sukumaran, A., Oatman, N., Anderson, J., et al. (2020). AMPK-Regulated Astrocytic Lactate Shuttle Plays a Non-Cell-Autonomous Role in Neuronal Survival. *Cell Rep.* 32, 108092. doi: 10.1016/j.celrep.2020.108092.

Nazaret, C., Heiske, M., Thurley, K., and Mazat, J.-P. (2009). Mitochondrial energetic metabolism: A simplified model of TCA cycle with ATP production. *J. Theor. Biol.* 258, 455–464. doi: 10.1016/j.jtbi.2008.09.037.

Nehlig, A. (2004). Brain uptake and metabolism of ketone bodies in animal models. *Prostaglandins Leukot. Essent. Fatty Acids* 70, 265–275. doi: 10.1016/j.plefa.2003.07.006.

Neves, A., Costalat, R., and Pellerin, L. (2012). Determinants of brain cell metabolic phenotypes and energy substrate utilization unraveled with a modeling approach. *PLoS Comput. Biol.* 8, e1002686. doi: 10.1371/journal.pcbi.1002686.

Neves, S. R. (2011). Obtaining and Estimating Kinetic Parameters from the Literature. *Sci. Signal.* 4. doi: 10.1126/scisignal.2001988.

Ng, F., Wijaya, L., and Tang, B. L. (2015). SIRT1 in the brain-connections with aging-associated disorders and lifespan. *Front. Cell. Neurosci.* 9, 64. doi: 10.3389/fncel.2015.00064.

Niccoli, T., and Partridge, L. (2012). Ageing as a Risk Factor for Disease. *Curr. Biol.* 22, R741–R752. doi: 10.1016/j.cub.2012.07.024.

Nielsen, N. C., Zahler, W. L., and Fleischer, S. (1973). Mitochondrial D- -hydroxybutyrate

dehydrogenase. IV. Kinetic analysis of reaction mechanism. *J. Biol. Chem.* 248, 2556–2562.

Nishihara, E., Moriya, T., and Shinohara, K. (2007). Expression of steroid receptor coactivator-1 is elevated during neuronal differentiation of murine neural stem cells. *Brain Res.* 1135, 22–30. doi: 10.1016/j.brainres.2006.12.026.

Niven, J. E. (2016). Neuronal energy consumption: biophysics, efficiency and evolution. *Curr. Opin. Neurobiol.* 41, 129–135. doi: 10.1016/j.conb.2016.09.004.

Oka, M., Suzuki, E., Asada, A., Saito, T., Iijima, K. M., and Ando, K. (2021). Increasing neuronal glucose uptake attenuates brain aging and promotes life span under dietary restriction in Drosophila. *iScience* 24, 101979. doi: 10.1016/j.isci.2020.101979.

O'Neill, L. A. J., and Hardie, D. G. (2013). Metabolism of inflammation limited by AMPK and pseudo-starvation. *Nature* 493, 346–355. doi: 10.1038/nature11862.

Orosz, F., Wágner, G., Ortega, F., Cascante, M., and Ovádi, J. (2003). Glucose conversion by multiple pathways in brain extract: theoretical and experimental analysis. *Biochem. Biophys. Res. Commun.* 309, 792–797. doi: 10.1016/j.bbrc.2003.08.072.

Øyehaug, L., Østby, I., Lloyd, C. M., Omholt, S. W., and Einevoll, G. T. (2012). Dependence of spontaneous neuronal firing and depolarisation block on astroglial membrane transport mechanisms. *J. Comput. Neurosci.* 32, 147–165. doi: 10.1007/s10827-011-0345-9.

Palla, A. R., Ravichandran, M., Wang, Y. X., Alexandrova, L., Yang, A. V., Kraft, P., et al. (2021). Inhibition of prostaglandin-degrading enzyme 15-PGDH rejuvenates aged muscle mass and strength. *Science* 371, eabc8059. doi: 10.1126/science.abc8059.

Pamiljans, V., Krishnaswamy, P. R., Dumville, G., and Meister, A. (1962). Studies on the Mechanism of Glutamine Synthesis; Isolation and Properties of the Enzyme from Sheep Brain. *Biochemistry* 1, 153–158. doi: 10.1021/bi00907a023.

Park, J. O., Rubin, S. A., Xu, Y.-F., Amador-Noguez, D., Fan, J., Shlomi, T., et al. (2016). Metabolite concentrations, fluxes and free energies imply efficient enzyme usage. *Nat. Chem. Biol.* 12, 482–489. doi: 10.1038/nchembio.2077.

Park, S.-J., Ahmad, F., Philp, A., Baar, K., Williams, T., Luo, H., et al. (2012). Resveratrol ameliorates aging-related metabolic phenotypes by inhibiting cAMP phosphodiesterases. *Cell* 148, 421–433. doi: 10.1016/j.cell.2012.01.017.

Pathak, D., Shields, L. Y., Mendelsohn, B. A., Haddad, D., Lin, W., Gerencser, A. A., et al. (2015). The Role of Mitochondrially Derived ATP in Synaptic Vesicle Recycling. *J. Biol. Chem.* 290, 22325–22336. doi: 10.1074/jbc.M115.656405.

Pérez-Escuredo, J., Van Hée, V. F., Sboarina, M., Falces, J., Payen, V. L., Pellerin, L., et al. (2016). Monocarboxylate transporters in the brain and in cancer. *Biochim. Biophys. Acta BBA - Mol. Cell Res.* 1863, 2481–2497. doi: 10.1016/j.bbamcr.2016.03.013.

Pochini, L., Scalise, M., Galluccio, M., and Indiveri, C. (2014). Membrane transporters for the special amino acid glutamine: structure/function relationships and relevance to human health. *Front. Chem.* 2. doi: 10.3389/fchem.2014.00061.

Poliquin, P. O., Chen, J., Cloutier, M., Trudeau, L.-É., and Jolicoeur, M. (2013). Metabolomics and In-Silico Analysis Reveal Critical Energy Deregulations in Animal Models of Parkinson's Disease. *PLoS ONE* 8, e69146. doi: 10.1371/journal.pone.0069146.

Pospischil, M., Toledo-Rodriguez, M., Monier, C., Piwkowska, Z., Bal, T., Frégnac, Y., et al. (2008). Minimal Hodgkin–Huxley type models for different classes of cortical and thalamic neurons. *Biol. Cybern.* 99, 427–441. doi: 10.1007/s00422-008-0263-8.

Power, J. M., Wu, W. W., Sametsky, E., Oh, M. M., and Disterhoft, J. F. (2002). Age-related enhancement of the slow outward calcium-activated potassium current in hippocampal CA1 pyramidal neurons in vitro. *J. Neurosci. Off. J. Soc. Neurosci.* 22, 7234–7243. doi: 10.1523/JNEUROSCI.22-16-07234.2002.

Pritchard, J. B. (1995). Intracellular alpha-ketoglutarate controls the efficacy of renal organic anion transport. *J. Pharmacol. Exp. Ther.* 274, 1278–1284.

Rackauckas, C., and Nie, Q. (2017). DifferentialEquations.jl – A Performant and Feature-Rich Ecosystem for Solving Differential Equations in Julia. *J. Open Res. Softw.* 5, 15. doi: 10.5334/jors.151.

Recasens, M., Benezra, R., Basset, P., and Mandel, P. (1980). Cysteine sulfinate aminotransferase and aspartate aminotransferase isoenzymes of rat brain. Purification, characterization, and further evidence for identity. *Biochemistry* 19, 4583–4589. doi: 10.1021/bi00561a007.

Riddle, D. R. ed. (2007). *Brain Aging: Models, Methods, and Mechanisms*. Boca Raton (FL): CRC Press/Taylor & Francis Available at: http://www.ncbi.nlm.nih.gov/books/NBK1834/ [Accessed August 29, 2023].

Rizzo, V., Richman, J., and Puthanveettil, S. V. (2015). Dissecting mechanisms of brain aging by studying the intrinsic excitability of neurons. *Front. Aging Neurosci.* 6. doi: 10.3389/fnagi.2014.00337.

Roberg, B., Torgner, I. A., and Kvamme, E. (1999). Inhibition of glutamine transport in rat brain mitochondria by some amino acids and tricarboxylic acid cycle intermediates. *Neurochem. Res.* 24, 809–814. doi: 10.1023/a:1020941510764.

Robinson, M. B., and Jackson, J. G. (2016). Astroglial glutamate transporters coordinate excitatory signaling and brain energetics. *Neurochem. Int.* 98, 56–71. doi: 10.1016/j.neuint.2016.03.014.

Rock, C. O., Calder, R. B., Karim, M. A., and Jackowski, S. (2000). Pantothenate Kinase Regulation of the Intracellular Concentration of Coenzyme A. *J. Biol. Chem.* 275, 1377–1383. doi: 10.1074/jbc.275.2.1377.

Rodgers, J. T., Lerin, C., Haas, W., Gygi, S. P., Spiegelman, B. M., and Puigserver, P. (2005). Nutrient control of glucose homeostasis through a complex of PGC-1alpha and SIRT1. *Nature* 434, 113–118. doi: 10.1038/nature03354.

Roeder, L. M., Poduslo, S. E., and Tildon, J. T. (1982). Utilization of ketone bodies and glucose by established neural cell lines. *J. Neurosci. Res.* 8, 671–682. doi: 10.1002/jnr.490080412.

Rolfe, D. F., and Brown, G. C. (1997). Cellular energy utilization and molecular origin of standard metabolic rate in mammals. *Physiol. Rev.* 77, 731–758. doi: 10.1152/physrev.1997.77.3.731.

Ronowska, A., Szutowicz, A., Bielarczyk, H., Gul-Hinc, S., Klimaszewska-Łata, J., Dyś, A., et al. (2018). The Regulatory Effects of Acetyl-CoA Distribution in the Healthy and Diseased Brain. *Front. Cell. Neurosci.* 12. doi: 10.3389/fncel.2018.00169.

Ross, J. M., Oberg, J., Brene, S., Coppotelli, G., Terzioglu, M., Pernold, K., et al. (2010). High brain lactate is a hallmark of aging and caused by a shift in the lactate dehydrogenase A/B ratio. *Proc. Natl. Acad. Sci.* 107, 20087–20092. doi: 10.1073/pnas.1008189107.

Rybalkin, S. D., Hinds, T. R., and Beavo, J. A. (2013). "Enzyme Assays for cGMP Hydrolyzing Phosphodiesterases," in *Guanylate Cyclase and Cyclic GMP* Methods in Molecular Biology., eds. T. Krieg and R. Lukowski (Totowa, NJ: Humana Press), 51–62. doi: 10.1007/978-1-62703-459-3_3.

Santos, M. A., Franco, F. N., Caldeira, C. A., de Araújo, G. R., Vieira, A., Chaves, M. M., et al. (2021). Antioxidant effect of Resveratrol: Change in MAPK cell signaling pathway during the aging process. *Arch. Gerontol. Geriatr.* 92, 104266. doi: 10.1016/j.archger.2020.104266.

Satoh, A., Imai, S., and Guarente, L. (2017). The brain, sirtuins, and ageing. *Nat. Rev. Neurosci.* 18, 362–374. doi: 10.1038/nrn.2017.42.

Savtchenko, L. P., Bard, L., Jensen, T. P., Reynolds, J. P., Kraev, I., Medvedev, N., et al. (2018). Disentangling astroglial physiology with a realistic cell model in silico. *Nat. Commun.* 9. doi: 10.1038/s41467-018-05896-w.

Schaum, N., Lehallier, B., Hahn, O., Pálovics, R., Hosseinzadeh, S., Lee, S. E., et al. (2020). Ageing hallmarks exhibit organ-specific temporal signatures. *Nature* 583, 596–602. doi: 10.1038/s41586-020-2499-y.

Schousboe, A., Waagepetersen, H. S., and Sonnewald, U. (2019). Astrocytic pyruvate carboxylation: Status after 35 years. *J. Neurosci. Res.* 97, 890–896. doi: 10.1002/jnr.24402.

Sedlak, T. W., Paul, B. D., Parker, G. M., Hester, L. D., Snowman, A. M., Taniguchi, Y., et al. (2019). The glutathione cycle shapes synaptic glutamate activity. *Proc. Natl. Acad. Sci.* 116, 2701–2706. doi: 10.1073/pnas.1817885116.

Seelig, M. S., and Preuss, H. G. (1994). Magnesium metabolism and perturbations in the elderly. *Geriatr. Nephrol. Urol.* 4, 101–111. doi: 10.1007/BF01436050.

Sharma, H. K., and Rothstein, M. (1984). Altered brain phosphoglycerate kinase from aging rats.

Mech. Ageing Dev. 25, 285–296. doi: 10.1016/0047-6374(84)90002-2.

Shen, P., Xu, A., Hou, Y., Wang, H., Gao, C., He, F., et al. (2021). Conserved paradoxical relationships among the evolutionary, structural and expressional features of KRAB zinc-finger proteins reveal their special functional characteristics. *BMC Mol. Cell Biol.* 22, 7. doi: 10.1186/s12860-021-00346-w.

Shestov, A. A., Valette, J., Uğurbil, K., and Henry, P.-G. (2007). On the reliability of13C metabolic modeling with two-compartment neuronal-glial models. *J. Neurosci. Res.* 85, 3294–3303. doi: 10.1002/jnr.21269.

Shichkova, P., Coggan, J. S., Markram, H., and Keller, D. (2021). A Standardized Brain Molecular Atlas: A Resource for Systems Modeling and Simulation. *Front. Mol. Neurosci.* 14, 604559. doi: 10.3389/fnmol.2021.604559.

Shin, H.-J. R., Kim, H., Oh, S., Lee, J.-G., Kee, M., Ko, H.-J., et al. (2016). AMPK-SKP2-CARM1 signalling cascade in transcriptional regulation of autophagy. *Nature* 534, 553–557. doi: 10.1038/nature18014.

Simpson, I. A., Carruthers, A., and Vannucci, S. J. (2007). Supply and Demand in Cerebral Energy Metabolism: The Role of Nutrient Transporters. *J. Cereb. Blood Flow Metab.* 27, 1766–1791. doi: 10.1038/sj.jcbfm.9600521.

Smith, C. M., Bryla, J., and Williamson, J. R. (1974). Regulation of mitochondrial alpha-ketoglutarate metabolism by product inhibition at alpha-ketoglutarate dehydrogenase. *J. Biol. Chem.* 249, 1497–1505.

Smith, R. N., Agharkar, A. S., and Gonzales, E. B. (2014). A review of creatine supplementation in age-related diseases: more than a supplement for athletes. *F1000Research* 3, 222. doi: 10.12688/f1000research.5218.1.

Smithers, H. E., Terry, J. R., Brown, J. T., and Randall, A. D. (2017). Aging-Associated Changes to Intrinsic Neuronal Excitability in the Bed Nucleus of the Stria Terminalis Is Cell Type-Dependent. *Front. Aging Neurosci.* 9, 424. doi: 10.3389/fnagi.2017.00424.

Sokoloff, L. (1996). "Cerebral Metabolism and Visualization of Cerebral Activity," in *Comprehensive Human Physiology*, eds. R. Greger and U. Windhorst (Berlin, Heidelberg: Springer Berlin Heidelberg), 579–602. doi: 10.1007/978-3-642-60946-6_30.

Sugrue, M. M., and Tatton, W. G. (2001). Mitochondrial Membrane Potential in Aging Cells. *Neurosignals* 10, 176–188. doi: 10.1159/000046886.

Sun, X., He, G., Qing, H., Zhou, W., Dobie, F., Cai, F., et al. (2006). Hypoxia facilitates Alzheimer's disease pathogenesis by up-regulating BACE1 gene expression. *Proc. Natl. Acad. Sci. U. S. A.* 103, 18727–18732. doi: 10.1073/pnas.0606298103.

Sun, Z., and Xu, Y. (2020). Nuclear Receptor Coactivators (NCOAs) and Corepressors (NCORs) in the Brain. *Endocrinology* 161, bqaa083. doi: 10.1210/endocr/bqaa083.

Suresh, S. N., Chavalmane, A. K., Pillai, M., Ammanathan, V., Vidyadhara, D. J., Yarreiphang, H., et al. (2018). Modulation of Autophagy by a Small Molecule Inverse Agonist of ERRα Is Neuroprotective. *Front. Mol. Neurosci.* 11, 109. doi: 10.3389/fnmol.2018.00109.

Szklarczyk, D., Gable, A. L., Lyon, D., Junge, A., Wyder, S., Huerta-Cepas, J., et al. (2019). STRING v11: protein–protein association networks with increased coverage, supporting functional discovery in genome-wide experimental datasets. *Nucleic Acids Res.* 47, D607–D613. doi: 10.1093/nar/gky1131.

Takahashi, H., Manaka, S., and Sano, K. (1981). Changes in extracellular potassium concentration in cortex and brain stem during the acute phase of experimental closed head injury. *J. Neurosurg.* 55, 708–717. doi: 10.3171/jns.1981.55.5.0708.

Takeda, M., Briggs, L. E., Wakimoto, H., Marks, M. H., Warren, S. A., Lu, J. T., et al. (2009). Slow progressive conduction and contraction defects in loss of Nkx2-5 mice after cardiomyocyte terminal differentiation. *Lab. Investig. J. Tech. Methods Pathol.* 89, 983–993. doi: 10.1038/labinvest.2009.59.

Tantama, M., Martínez-François, J. R., Mongeon, R., and Yellen, G. (2013). Imaging energy status in live cells with a fluorescent biosensor of the intracellular ATP-to-ADP ratio. *Nat. Commun.* 4, 2550. doi: 10.1038/ncomms3550.

Taylor, C. T., and Scholz, C. C. (2022). The effect of HIF on metabolism and immunity. *Nat. Rev. Nephrol.* 18, 573–587. doi: 10.1038/s41581-022-00587-8.

Theurey, P., Connolly, N. M. C., Fortunati, I., Basso, E., Lauwen, S., Ferrante, C., et al. (2019). Systems biology identifies preserved integrity but impaired metabolism of mitochondria due to a glycolytic defect in Alzheimer's disease neurons. *Aging Cell* 18, e12924. doi: 10.1111/acel.12924.

Thibonnier, M., Esau, C., Ghosh, S., Wargent, E., and Stocker, C. (2020). Metabolic and energetic benefits of microRNA-22 inhibition. *BMJ Open Diabetes Res. Care* 8, e001478. doi: 10.1136/bmjdrc-2020-001478.

Thiepold, A.-L., Lorenz, N. I., Foltyn, M., Engel, A. L., Divé, I., Urban, H., et al. (2017). Mammalian target of rapamycin complex 1 activation sensitizes human glioma cells to hypoxia-induced cell death. *Brain J. Neurol.* 140, 2623–2638. doi: 10.1093/brain/awx196.

Tiveci, S., Akın, A., Çakır, T., Saybaşılı, H., and Ülgen, K. (2005). Modelling of calcium dynamics in brain energy metabolism and Alzheimer's disease. *Comput. Biol. Chem.* 29, 151–162. doi: 10.1016/j.compbiolchem.2005.03.002.

Tong, J., Fitzmaurice, P. S., Moszczynska, A., Mattina, K., Ang, L.-C., Boileau, I., et al. (2016). Do glutathione levels decline in aging human brain? *Free Radic. Biol. Med.* 93, 110–117. doi: 10.1016/j.freeradbiomed.2016.01.029.

Tretter, L., Patocs, A., and Chinopoulos, C. (2016). Succinate, an intermediate in metabolism, signal transduction, ROS, hypoxia, and tumorigenesis. *Biochim. Biophys. Acta* 1857, 1086–1101. doi: 10.1016/j.bbabio.2016.03.012.

Tripathi, M., Yen, P. M., and Singh, B. K. (2020). Estrogen-Related Receptor Alpha: An Under-Appreciated Potential Target for the Treatment of Metabolic Diseases. *Int. J. Mol. Sci.* 21, 1645. doi: 10.3390/ijms21051645.

Tsuboi, K. K., Fukunaga, K., and Petricciani, J. C. (1969). Purification and specific kinetic properties of erythrocyte uridine diphosphate glucose pyrophosphorylase. *J. Biol. Chem.* 244, 1008–1015.

Vali, S., Mythri, R. B., Jagatha, B., Padiadpu, J., Ramanujan, K. S., Andersen, J. K., et al. (2007). Integrating glutathione metabolism and mitochondrial dysfunction with implications for Parkinson's disease: a dynamic model. *Neuroscience* 149, 917–930. doi: 10.1016/j.neuroscience.2007.08.028.

Verkhratsky, A., and Nedergaard, M. (2018). Physiology of Astroglia. *Physiol. Rev.* 98, 239–389. doi: 10.1152/physrev.00042.2016.

Vitale, P., Salgueiro-Pereira, A. R., Lupascu, C. A., Willem, M., Migliore, R., Migliore, M., et al. (2021). Analysis of Age-Dependent Alterations in Excitability Properties of CA1 Pyramidal Neurons in an APPPS1 Model of Alzheimer's Disease. *Front. Aging Neurosci.* 13, 668948. doi: 10.3389/fnagi.2021.668948.

Volkova, M., Garg, R., Dick, S., and Boheler, K. R. (2005). Aging-associated changes in cardiac gene expression. *Cardiovasc. Res.* 66, 194–204. doi: 10.1016/j.cardiores.2004.11.016.

Waitt, A. E., Reed, L., Ransom, B. R., and Brown, A. M. (2017). Emerging Roles for Glycogen in the CNS. *Front. Mol. Neurosci.* 10. doi: 10.3389/fnmol.2017.00073.

Weber, B., and Barros, L. F. (2015). The Astrocyte: Powerhouse and Recycling Center. *Cold Spring Harb. Perspect. Biol.* 7, a020396. doi: 10.1101/cshperspect.a020396.

White, H., and Jencks, W. P. (1976). Mechanism and specificity of succinyl-CoA:3-ketoacid coenzyme A transferase. *J. Biol. Chem.* 251, 1688–1699.

Wilcock, A. R., Sharpe, D. M., and Goldberg, D. M. (1973). Kinetic similarity of enzymes in human blood serum and cerebrospinal fluid: Aspartate aminotransferase and lactate dehydrogenase. *J. Neurol. Sci.* 20, 97–101. doi: 10.1016/0022-510X(73)90121-4.

Williamson, D., Lund, P., and Krebs, H. (1967). The redox state of free nicotinamide-adenine dinucleotide in the cytoplasm and mitochondria of rat liver. *Biochem. J.* 103, 514–527. doi: 10.1042/bj1030514.

Winter, F., Bludszuweit-Philipp, C., and Wolkenhauer, O. (2018). Mathematical analysis of the influence of brain metabolism on the BOLD signal in Alzheimer's disease. *J. Cereb. Blood Flow Metab.* 38, 304–316. doi: 10.1177/0271678X17693024.

Witthoft, A., Filosa, J. A., and Karniadakis, G. E. (2013). Potassium Buffering in the Neurovascular Unit: Models and Sensitivity Analysis. *Biophys. J.* 105, 2046–2054. doi: 10.1016/j.bpj.2013.09.012.

Wittig, U., Rey, M., Weidemann, A., Kania, R., and Müller, W. (2018). SABIO-RK: an updated resource for manually curated biochemical reaction kinetics. *Nucleic Acids Res.* 46, D656–D660. doi: 10.1093/nar/gkx1065.

Wu, F., Yang, F., Vinnakota, K. C., and Beard, D. A. (2007). Computer modeling of mitochondrial tricarboxylic acid cycle, oxidative phosphorylation, metabolite transport, and electrophysiology. *J. Biol. Chem.* 282, 24525–24537. doi: 10.1074/jbc.M701024200.

Xu, K., Morgan, K. T., Todd Gehris, A., Elston, T. C., and Gomez, S. M. (2011). A Whole-Body Model for Glycogen Regulation Reveals a Critical Role for Substrate Cycling in Maintaining Blood Glucose Homeostasis. *PLoS Comput. Biol.* 7, e1002272. doi: 10.1371/journal.pcbi.1002272.

Yamashita, D., Moriuchi, T., Osumi, T., and Hirose, F. (2016). Transcription Factor hDREF Is a Novel SUMO E3 Ligase of Mi2α. *J. Biol. Chem.* 291, 11619–11634. doi: 10.1074/jbc.M115.713370.

Yang, J.-S., Hsu, J.-W., Park, S.-Y., Li, J., Oldham, W. M., Beznoussenko, G. V., et al. (2018). GAPDH inhibits intracellular pathways during starvation for cellular energy homeostasis. *Nature* 561, 263–267. doi: 10.1038/s41586-018-0475-6.

Yang, Q., Zhao, W., Xing, Y., Li, P., Zhou, X., Ning, H., et al. (2021). Dysfunction of an energy sensor NFE2L1 triggers uncontrollable AMPK signal and glucose metabolism reprogramming. Molecular Biology doi: 10.1101/2021.09.07.459348.

Yang, S. Y., He, X. Y., and Schulz, H. (1987). Fatty acid oxidation in rat brain is limited by the low activity of 3-ketoacyl-coenzyme A thiolase. *J. Biol. Chem.* 262, 13027–13032.

Yi, G., and Grill, W. M. (2019). Average firing rate rather than temporal pattern determines metabolic cost of activity in thalamocortical relay neurons. *Sci. Rep.* 9. doi: 10.1038/s41598-019-43460-8.

Yuk, J.-M., Kim, T. S., Kim, S. Y., Lee, H.-M., Han, J., Dufour, C. R., et al. (2015). Orphan Nuclear Receptor ERRα Controls Macrophage Metabolic Signaling and A20 Expression to Negatively Regulate TLR-Induced Inflammation. *Immunity* 43, 80–91. doi: 10.1016/j.immuni.2015.07.003.

Zhang, M. J., Pisco, A. O., Darmanis, S., and Zou, J. (2021a). Mouse aging cell atlas analysis reveals global and cell type-specific aging signatures. *eLife* 10, e62293. doi: 10.7554/eLife.62293.

Zhang, P., Qu, H.-Y., Wu, Z., Na, H., Hourihan, J., Zhang, F., et al. (2021b). ERK signaling licenses SKN-1A/NRF1 for proteasome production and proteasomal stress resistance. Cell Biology doi: 10.1101/2021.01.04.425272.

Zhang, X., Dash, R. K., Jacobs, E. R., Camara, A. K. S., Clough, A. V., and Audi, S. H. (2018). Integrated computational model of the bioenergetics of isolated lung mitochondria. *PloS One* 13, e0197921. doi: 10.1371/journal.pone.0197921.

Zhao, T., Kee, H. J., Bai, L., Kim, M.-K., Kee, S.-J., and Jeong, M. H. (2021). Selective HDAC8 Inhibition Attenuates Isoproterenol-Induced Cardiac Hypertrophy and Fibrosis via p38 MAPK Pathway. *Front. Pharmacol.* 12, 677757. doi: 10.3389/fphar.2021.677757.

Zhou, M., Xia, X., Yan, H., Li, S., Bian, S., Sha, X., et al. (2019). The Model of Aging Acceleration Network Reveals the Correlation of Alzheimer's Disease and Aging at System Level. *BioMed Res. Int.* 2019, 4273108. doi: 10.1155/2019/4273108.

Zhu, F., Wang, R., Pan, X., and Zhu, Z. (2019). Energy expenditure computation of a single bursting neuron. *Cogn. Neurodyn.* 13, 75–87. doi: 10.1007/s11571-018-9503-3.